Thesis for the degree of Philosophiae Doctor

The forcing and climate response of black carbon aerosols

Maria Sand

Meteorology and Oceanography Section
Department of Geosciences
Faculty of Mathematics and Natural Sciences
University of Oslo

2013

Series of dissertations submitted to the
Faculty of Mathematics and Natural Sciences, University of Oslo
No. 1442

ISSN 1501-7710

Cover: Inger Sandved Anfinsen.
Printed in Norway: AIT Oslo AS.

Produced in co-operation with Akademika Publishing.
The thesis is produced by Akademika Publishing merely in connection with the thesis defence. Kindly direct all inquiries regarding the thesis to the copyright holder or the unit which grants the doctorate.

Takk!

Det er nesten ikke til å tro at jeg sitter her og skal skrive forord til doktorgradsavhandlingen min. Åh lykke! Det har vært en lang, lang prosess og jeg har mer én gang vurdert om dette virkelig er noe jeg vil klare å gjennomføre. Så nå er jeg her da, og har gjort mitt beste, og jeg angrer absolutt ikke på at jeg beit tennene sammen på slutten og skrev ferdig alt sammen. I starten av doktorgraden, på de første møtene i Resclim (forskerskole i klimadynamikk som fortjener en stor takk!), hørte jeg om doktorgradsstudenter som fortalte at de hadde lært å reise seg opp igjen etter nesten å ha gitt opp, og jeg trodde jeg skjønte hva de mente. Men det er først nå, etter det beryktede sisteåret på doktorgraden at jeg virkelig skjønner hva de snakket om. For det er jo slik at de første 3 årene av en doktorgrad en dans på roser (!), men at det er det siste året hvor man virkelig må sette alle kluter til. Når jeg nå ser tilbake på alle årene er jeg svært takknemlig for alt jeg har lært og for at jeg har fått reist verden rundt på konferanser og møtt spennende mennesker og havnet oppe i rare situasjoner. Som verdens nordligste jazzucci i Ny-Ålesund i snøfokk iført bikini, pelslue og frosset mach-øl. Eller kurs i presentasjonsteknikk på Hurtigruta i sterk kuling utenfor Stadt. Og det var under doktorgraden at mitt store kjærlighetsforhold til byen Boulder i Colorado startet. Det var her jeg lærte å trene 5 ganger i uka, sykle til jobb uansett avstand, jobbe slik amerikanere gjør, og at fritert mozzarella kan spises til alle måltider. Jeg er så utrolig glad for at jeg fikk anledning til dra på et forskningsopphold i et halvt år til Boulder og jeg blir vel aldri den samme igjen (and a big thanks to Jean-Francois Lamarque for hosting me!).

Det er mange mennesker som fortjener en stor takk og jeg hadde aldri klart dette uten mye, mye, mye hjelp. Først ut vil jeg takke hovedveilederen min Terje Berntsen. Takk for mange spennende diskusjoner rundt resultater og din utømmelige kilde til fakta om black carbon. Jeg vil også takke for din det-går-så-bra-så-holdning! Hver gang jeg kommer lutrygget og små-deprimert inn på kontoret ditt, går jeg alltid ut igjen med følelsen at dette kan fikses og at verden går videre tross alt. En stor takk til medveilederne mine Trond Iversen (som frivillig ble med på skuta videre fra masteroppgaven) og Øyvind Seland. Øyvind; jeg håper jeg ikke har flydd ned kontoret ditt for mye. Dere har begge to lært meg utrolig mye om NorESM-modellen og klimadynamikk. Tusen takk! Jeg vil også takke Alf Kirkevåg for hjelp, diskusjon og god NorESM support og Gunnar og Kjell for uvurderlig data-fiksing. En stor takk til Ivar Seierstad for gode diskusjoner og hjelp, og til evnen å finne forståelige tilnærminger på komplekse problemer. Jeg vil også takke Jón

Egill Kristjánsson for bunnløs sky-kunnskap, men mest av alt for stor entusiasme rundt forskningen min. Jeg vil også takke for at du reddet meg de siste månedene i doktorgraden og for økonomisk støtte til forskningsoppholdet mitt.

Jeg har overlevd flere kontorsammensetninger på Metos, på 'Kontoret'. Først vil jeg takke kontorsammensetning nr. 1: Karianne, Ivan og Ole Kristian. Så vil jeg takke kontorsammensetning nr. 2: Johanne, Anna og Habiba. Takk for at jeg har fått bråke, klage og gapskratte. Og beklager til nabokontoret for eventuelle forstyrrelser. For 4 (3?) år siden startet vi doktorgradsstudentene og post-doc'ene på metos en klubb, 'metos-pop'. Jeg må si at doktorgraden hadde vært svært kjedelig uten alle dere fantastiske medstudenter/medfanger. Takk for alle hytteturer, skiturer og fylleturer. Og de gode faglige diskusjonene så klart. Litt færre av de kanskje, men.. ;)

Til slutt vil jeg takke familien min og vennene mine. Takk spesielt for stor forståelse for at jeg ble litt smårar/fraværende/ekstra distré den siste tiden. Dere er de beste!

Table of contents

The work presented has been carried out at the Department of Geosciences, Section of Meteorology and Oceanography at the University of Oslo. This study was partly funded by the Research Council in Norway through the Earthclim project and the Norwegian research Council's Programme for supercomputing (NOTUR) through a grant for computing time.

Chapter 1 General introduction

During the last decade the Arctic region has been warmer than any other period of the observational record [*IPCC* 2007]. Since 1980 the increase in surface temperatures in the Arctic has been twice as high as the global average. The Arctic warming has been enhanced by feedbacks in the sea-ice and snow cover [*AMAP* 2012]. The largest warming is observed during autumn, in regions where the sea-ice has disappeared during summer. As the open water and bare ground absorb more solar radiation, more heat can be released to the atmosphere. The number of snow-covered days in spring has decreased, and an earlier snow melt is promoted by the reduced surface albedo.

The potential for black carbon (BC) aerosols to considerably impact the climate over the high-albedo surfaces in the Arctic during spring was noted already by [*Warren and Wiscombe* 1980, *Valero et al.* 1984, *Blanchet* 1989]. This was documented in many papers around 1980 and later during several observational campaigns [*Rosen et al.* 1981, *Hansen et al.* 1982, *Clarke et al.* 1984, *Hansen and Rosen* 1984, *Rosen and Hansen* 1984, *Sheridan* 1989]. In 2000, two papers suggested that BC might presently warm the atmosphere by 1/3 of that of CO_2 [*Hansen et al.* 2000, *Jacobson* 2000]. Since BC concentrations will respond quickly to emission reductions due to its short atmospheric lifetime, BC was pointed to as a short-term mitigation option to delay global warming, in particular the rapid warming in the Arctic [*Jacobson* 2002, *Quinn et al.* 2008, *Jacobson* 2010, *Shindell et al.* 2012]. Since then, BC aerosols in the Arctic have received particular attention [*Hansen and Nazarenko* 2004, *Jacobson* 2004, *Koch and Hansen* 2005, *Flanner et al.* 2007, *Koch et al.* 2009b, *Doherty et al.* 2010]. Hansen et al. [2005] and Flanner et al. [2007] suggested that the BC/snow forcing is more effective than forcing by CO_2 in changing the surface temperatures (higher climate efficacy), consistent with Hansen and Nazarenko [2004].

Compared to other aerosols in the atmosphere, the amount of BC mass is small. What makes BC special among the aerosols is the fact that BC strongly absorbs visible light [*Bond and Bergstrom* 2006]. Even a small amount of BC in the Arctic atmosphere can change the energy budget, since BC absorbs a high fraction of the sunlight that is reflected at the surface [*Pueschel and Kinne* 1995]. In addition, BC can significantly reduce the surface albedo and promote snowmelt when it is deposited in the snow

[*Warren and Wiscombe* 1980, *Clarke and Noone* 1985]. The enhanced snowmelt leads to earlier exposure of the bare ground surface, which has a considerably lower albedo than snow. Due to positive feedback mechanisms in the snow, even a small initial BC forcing may give a relatively large temperature response. For example the increased warming may increase the snow grain size, and the solar radiation can penetrate deeper in the snow, increasing the absorption further. A further description of the different climate effect of BC is given in chapter 2.

For the past few years, BC has received policy attention at higher levels. In 2009, the Arctic Council asked the Arctic Monitoring and Assessment Programme (AMAP) to establish an expert group on short-lived climate forcers (SLCFs) to improve the state of knowledge and its application to policy-making. The expert group was also to provide scientific advice regarding the assessment of the Arctic climate benefits of different mitigation strategies. The mitigation strategies were suggested by the Task Force on SLCFs established by the Arctic Council. Some of the recommended mitigation strategies regarding air quality have already been implemented, e.g. diesel particle filters in private cars. This mitigation option focused on air quality and health effects, in particular. The United Nations organized a team of more than 50 experts to provide decision makers with an assessment report of black carbon and tropospheric ozone. The report was published in 2011 and concluded that reductions of concentrations of BC and tropospheric ozone will lead to considerable benefits for human well-being (http://www.unep.org/dewa/Portals/67/pdf/Black_Carbon.pdf). The Climate and Clean Air Coalition was formally launched in 2012 as part of the United Nations with the objective to 'reduce short-lived climate pollutants' (http://www.unep.org/ccac/). In the same year the Executive Body for the UN Economic Commission for Europe (UNECE) Convention on Long-range Transboundary Air Pollution (LRTAP) adopted national emission reduction commitments to be achieved by 2020 and beyond, and addressed, for the first time, particulate matter, including BC. UNECE notes that '*black carbon, as a short-lived climate forcer, has a stronger warming effect than carbon dioxide as it is 680 times more powerful but is less persistent in the atmosphere. Its reduction is thus expected to slow glacial melting, the reduction in polar ice mass, and associated effects such as sea-level rise*' http://climate-l.iisd.org/news/unece-meeting-on-long-range-transboundary-air-pollution-amends-gothenburg-protocol/**.** These days the Norwegian Environmental Agency is working on an action plan on SLCFs. It is worth noting that all

of the initiatives state that immediate reductions of carbon dioxide are required to in order to protect the climate in a long-term.

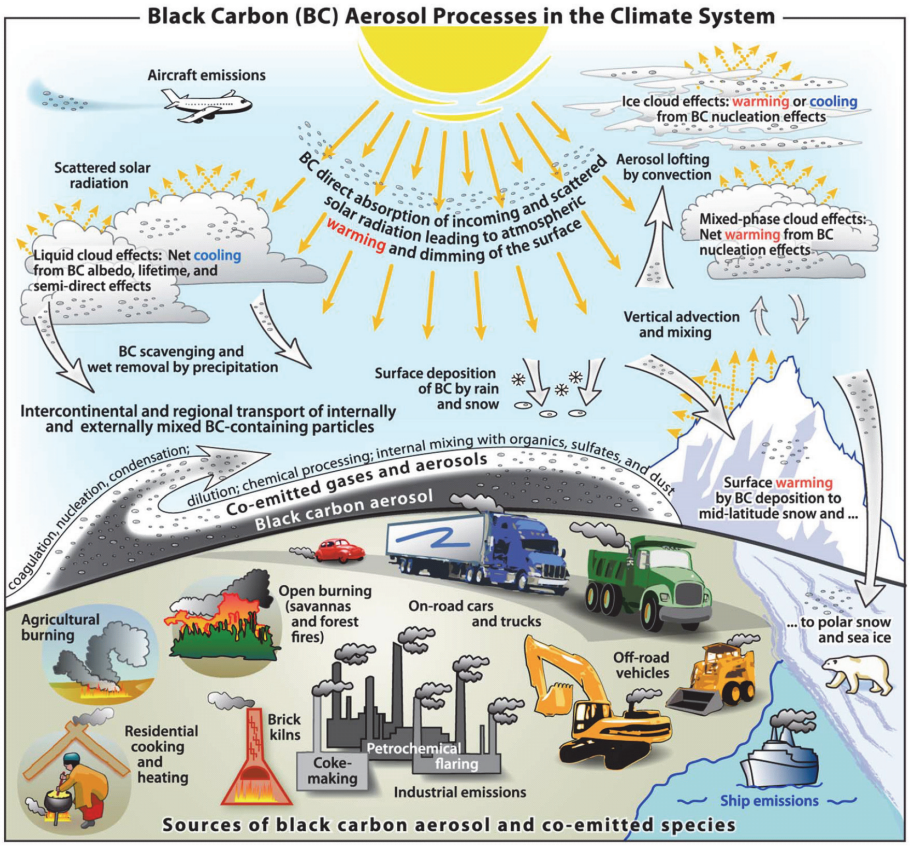

Figure 1: Schematic of the sources of BC and the different mechanisms in which BC can influence the climate. From Bond et al. [2013].

BC influence the climate in many ways; by absorbing solar radiation, promoting melting of snow cover and sea-ice, and changing the properties and distribution of clouds (Figure 1). By absorbing solar radiation, BC exerts a positive perturbation at the TOA radiative budget, as more SW radiation is 'trapped' in the atmosphere. The term *radiative forcing* (RF) is commonly defined as the change in the net radiation at the top-of-the-atmosphere (TOA) caused by a particular constituent or process with temperatures kept fixed [*Hansen et al.* 1997]. When studying global surface temperature change, it is often sufficient to look at the radiative fluxes at TOA, because these fluxes give a measure on the climate

response as a whole, and because the feedbacks are relatively equal for all the forcings. This instantaneous forcing occurs before any rapid adjustments or fast responses in the troposphere, stratosphere and land surface. As BC heats the air and changes clouds, it causes rapid adjustments in the climate system. These rapid adjustments, or 'adjusted forcing', change the radiative budget at TOA. The term 'radiative forcing' used by IPCC, is slightly different compared to what have used in this thesis, as this forcing is calculated after the temperatures in the stratosphere have adjusted.

For spatially and temporally varying climate forcers, the spatial pattern of the surface temperature change can be quite different from the spatial pattern of the forcing. Boer and Yu [2003] showed that there is not a simple relationship between the RF and temperature in a given region. For example, there have been strong indications that BC over China has led to regional surface cooling and decreased convection and thereby precipitation [*Menon et al.* 2002]. This is linked to reduced evaporation due to less downwelling solar radiation at the surface, and cannot be explained by TOA RF. TOA radiative forcing is therefore not adequate to understand regional effects at the surface. The temperature response to BC is a combination of a regional response and a large-scale response, with amplification over land surfaces and in the polar regions [*Bond et al.* 2013].

To study the different impacts of regional RF caused by different gases and aerosols, Shindell and Faluvegi [2009] applied forcings from a number of SLCFs and CO_2 in different latitude bands (the Arctic, mid-latitudes, the tropics, and the southern hemisphere) and looked at the corresponding surface temperature response, using the GISS global climate model. They found that the regional climate response depends on the location of the forcing. Figure 2 shows the climate sensitivity in each different latitude band for each forcing from their study. For the Arctic region we notice that the surface temperature response is negative for BC forcing located in the Arctic and positive for BC located outside Arctic. At first these results seem counter-intuitive. Does this mean that BC in the Arctic does not lead to a warming of the Arctic climate? And is it policy relevant? Are the results model-dependent or could they be reproduced by another model? In paper I, we duplicated this particular experiment in a different climate model, by perturbing the present-day distribution of BC in the Arctic and the mid-latitudes, respectively. We reproduced the results found by Shindell and Faluvegi [2009], but found that the results might be misleading for policy making. The study perturbs a number of

forcings at different locations to see how sensitive regional climate is to the location of the forcing. However, as the study perturbs BC concentrations (and not emissions) and does not include the BC snow albedo effect, the results cannot be used to analyse BC mitigation options. Thus, in paper II we investigated how increased emissions of BC in the Arctic itself and in the mid-latitudes influence the Arctic climate.

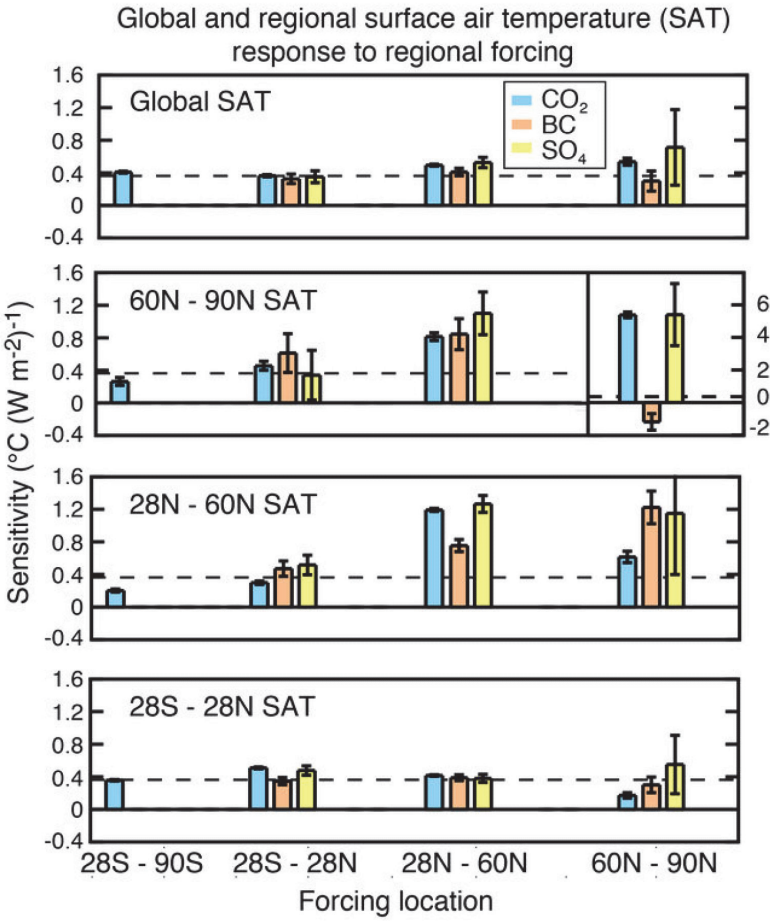

Figure 2: Surface air temperature sensitivity to different forcing locations for BC (pink), SO_4 (yellow) and CO_2 (blue). The forcing locations are given on the x-axis. From Shindell and Faluvegi [2009]. Adapted figure from Bond et al. [2013].

1.1 Objectives

The overall objective in this thesis is to improve the understanding of the climate response to absorbing aerosols with special focus on the high northern latitudes.

Some key questions:

- **Are forcing estimates of BC representative for the climate response in the Arctic?**
- **How sensitive is the Arctic climate to BC emissions within the region compared to mid-latitudes?**
- **How important is the BC snow/albedo effect in the total climate response to BC?**
- **How does the natural variability modulate the way BC influences climate?**

The rest of this thesis is structured as follows; chapter 2 gives a scientific background on the definition of BC aerosols, emissions, measurements and the different ways that BC perturbs climate. Chapter 3 describes the climate model used in this thesis with focus on the aerosol treatment. Chapter 4 gives the aim and key findings of the four papers in this thesis, and a summary and conclusion is given in Chapter 5.

Chapter 2 Scientific background

2.1 What is black carbon?

BC aerosols are tiny dark particles that are formed in flames through incomplete combustion of carbon-based fuels and from open biomass burning. When BC is emitted, it consists of tiny clustered spheres that are insoluble in water. Inside closed combustion chambers and exhaust pipes, very high number concentrations of ~1 nm BC particles can be nucleated, and in the high temperatures and pressures these may even further quickly grow to highly irregular accumulation-mode particles which are agglomerates of the (~1 nm) nucleation-mode BC particles [*Sheridan* 1989, *Ström et al.* 1992]. BC from open air biomass burning on the other hand (e.g. forest fires), is produced in very turbulent fire plumes which may reach a few km vertically [*Liousse et al.* 1996].

Quickly after BC is emitted, it becomes mixed with other co-emitted species like organic carbon and sulphate [*Lee et al*. 2002]. The different aerosol components then exist together within a single particle that is 'internally mixed' or 'coated'. Major emission sources of BC include open burning of forests and savannahs, residential fuel like coal and biomass, diesel engines, and industry. The total global BC emissions for the year 2000 are estimated to be 7500 Gg BC per year [*Bond et al.* 2013]. The largest single source of BC is open biomass burning, which accounts for about 40 % of the total emissions. Emissions from diesel engines account for 20 % of the total and have the lowest fraction of co-emitted species. Heating and cooking in homes using coal and wood, accounts for 25 % of the total emissions.

Figure 3 shows how different BC emissions sectors are distributed per latitude. 80 % of open burning is in the Tropics, while emissions from diesel engines peak in Europe and North America.

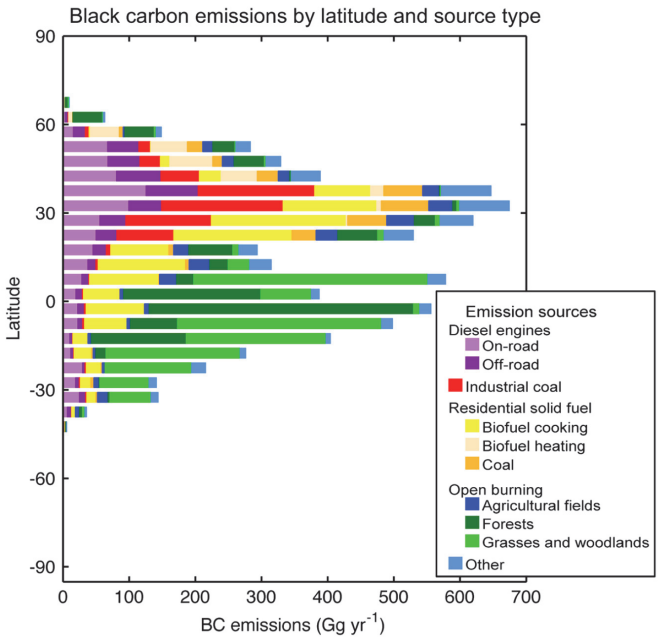

Figure 3: 2000 BC emissions sorted by latitude and source type. Emissions datasets are SPEW [*Lamarque et al.* 2010], GAINS [UNEP/WMO 2011] and RETRO [*Schultz et al.* 2008]. Figure from [*Bond et al.* 2013].

About 60 % of the total emissions are from sources related to energy use. Since 1950, the total anthropogenic BC emissions have increased by a factor of 9, but the trend varies with location. In general, emissions have increased as population and economy have risen, and decreased as cleaner technology has been implemented. During the last decades, the emissions of BC have declined both in North America and Europe, while an increase in emissions are found in places with rapid growth in Asia, specially India and China. In these countries, the anthropogenic emissions have increased by 40 % since 2000 [*Lu et al.* 2011].

Figure 4 shows measurement of BC from an ice core in Greenland spanning the years 1788-2002 [*McConnell et al.* 2007]. The BC concentrations show high seasonal variations with a maximum around the years ~1910-1920 and a steady decline to near pre-1850 levels. Using back-trajectory models, United Stated and Canada are suggested as the main source regions for BC in snow in Greenland. The decrease after ~1910 is linked to improvements in combustion and a transition from coal to oil and gas, and air pollution controls. The measurements are not necessary representative for the Arctic as a whole, as other source areas are important outside Greenland [*Hirdman et al.* 2010].

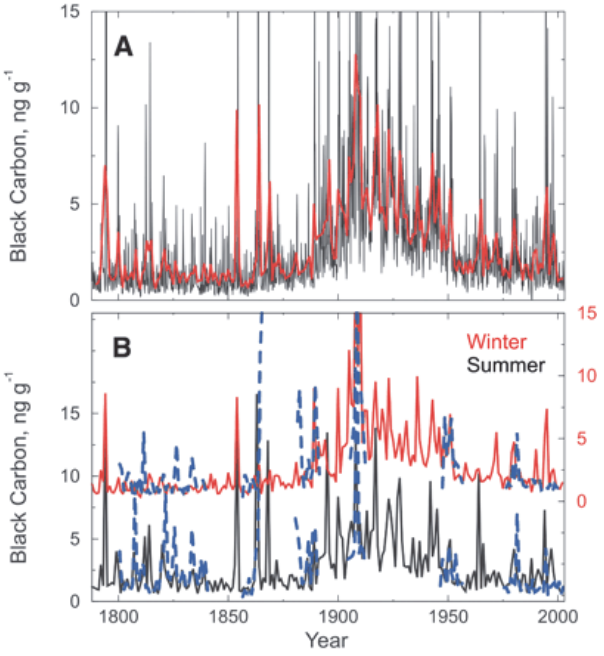

Figure 4: Measured monthly (black) and annual (red) BC concentrations from 1788-2002 ice core at Greenland (A). Measured winter (red) and summer (black) BC concentrations from an ice core located approx. 350 km south from the first ice core (B). From McConnell et al. [2007].

BC aging and transport

The internally mixed BC particles have different optical properties compared to the freshly emitted externally mixed particles. When sulphate or organic matter condenses on the BC particle, the absorption coefficient increases and the aerosol becomes hydrophilic [*Ackerman and Toon* 1981, *Fuller et al.* 1999]. Once soluble matter condense on BC and the particle volume and hygroscopicity increase, the efficiency of BC to become a cloud condensation nucleus and form clouds increases, while its atmospheric lifetime decreases. It is crucial to include the information about the non-BC material, when modelling the radiative impact of BC [*Stier et al.* 2006].

The aging of BC can influence how far the particles are transported in the atmosphere. In climate models, the different treatments of BC aging may therefore lead to different spatial distributions of BC [*Kinne et al.* 2006, *Textor et al.* 2007]. Most of the BC measured in the Arctic, is transported from lower latitudes [*Law and Stohl* 2007, *Quinn et al.* 2007]. In a model comparison study, Koch et al. [2009b] found large differences in the vertical distribution of BC in the Arctic between the different models (Figure 5). In general, the models underestimate the BC concentrations near the surface and free troposphere, but tend to overestimate the concentrations in the upper troposphere. The

previous model version of NorESM, UiO GCM, is given in dashed dark blue. Compared with long-term measurements from surface stations in the Arctic, most models underestimate BC concentrations in winter and spring and do not capture the strong seasonal cycle of BC concentrations [*Shindell et al.* 2008, *Huang et al.* 2010]. The underestimation of the Arctic surface concentrations of BC during winter and early spring by current models is linked to uncertainties in emissions, transport and removal [*Textor et al.* 2007, *Wang et al.* 2013]. Transport and removal can depend on each other, since aerosols that are transported to higher altitudes is more likely to have a longer lifetime and can then be transported farther away. The dominant process is considered to be wet removal, which is also one of the most uncertain processes in aerosol climate models [*Textor et al.* 2006].

During wintertime, sources from Eurasia can more easily be transported into the high-Arctic, since the Arctic front usually shifts to lower latitudes, in particular, in the Russian sector [*Stohl* 2006]. Stohl et al. [2013] used the FLEXPART model and included a new emission data set (ECLIPSE), which contains emissions from flaring and implemented a seasonal variation in the domestic sector that depended on the outside temperature. Even though flaring only makes up 3 % of the global emissions of BC, it is one of the largest BC emission sources north of 66 ° N, mostly in Oil and gas regions northwest in Russia. These sources of BC have a higher probability of getting deposited on the snow and sea-ice, since the aerosols are emitted directly into the Arctic planetary boundary layer. The new implementations resulted in a doubling of the Arctic surface concentrations of BC during winter/early spring, indicating the importance of local sources for BC at surface levels in the Arctic.

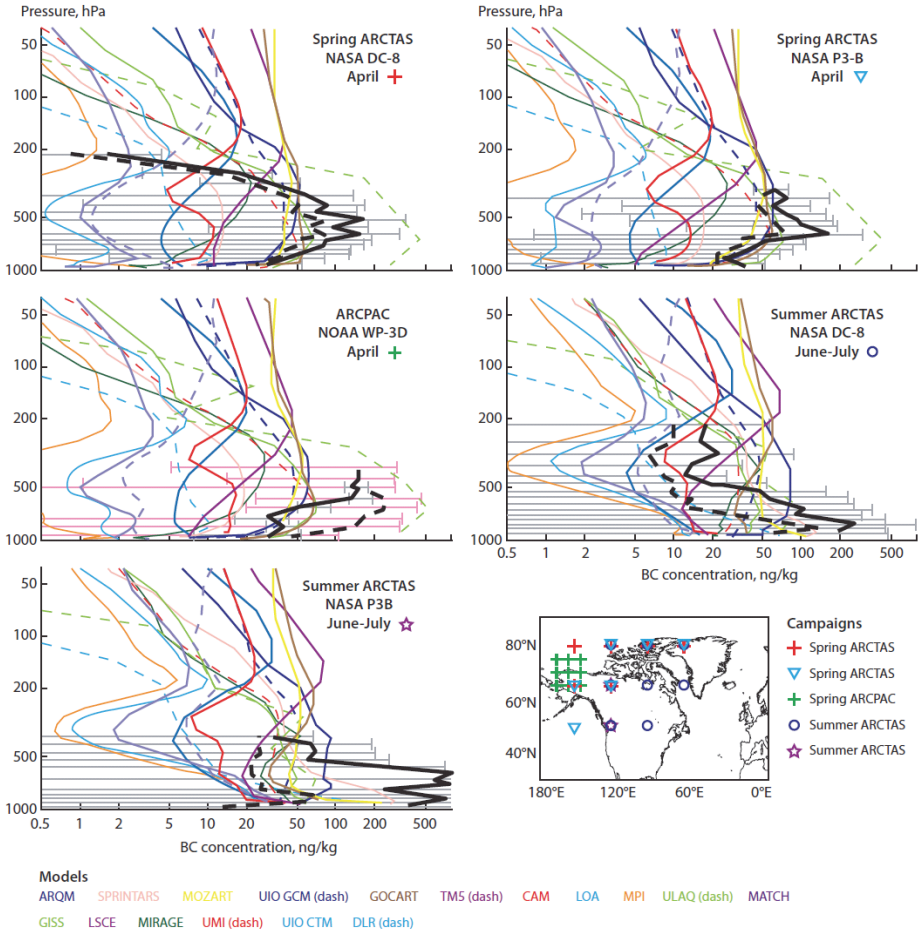

Figure 5: Comparison of the vertical BC profiles in climate models (given in colours) and observations (black) averaged over the points in the map. Dashed line is the mean and solid line is the median in the observations. The observations are from the IPY POLARCAT campaign spring and summer 2008. From Koch et al. [2009b].

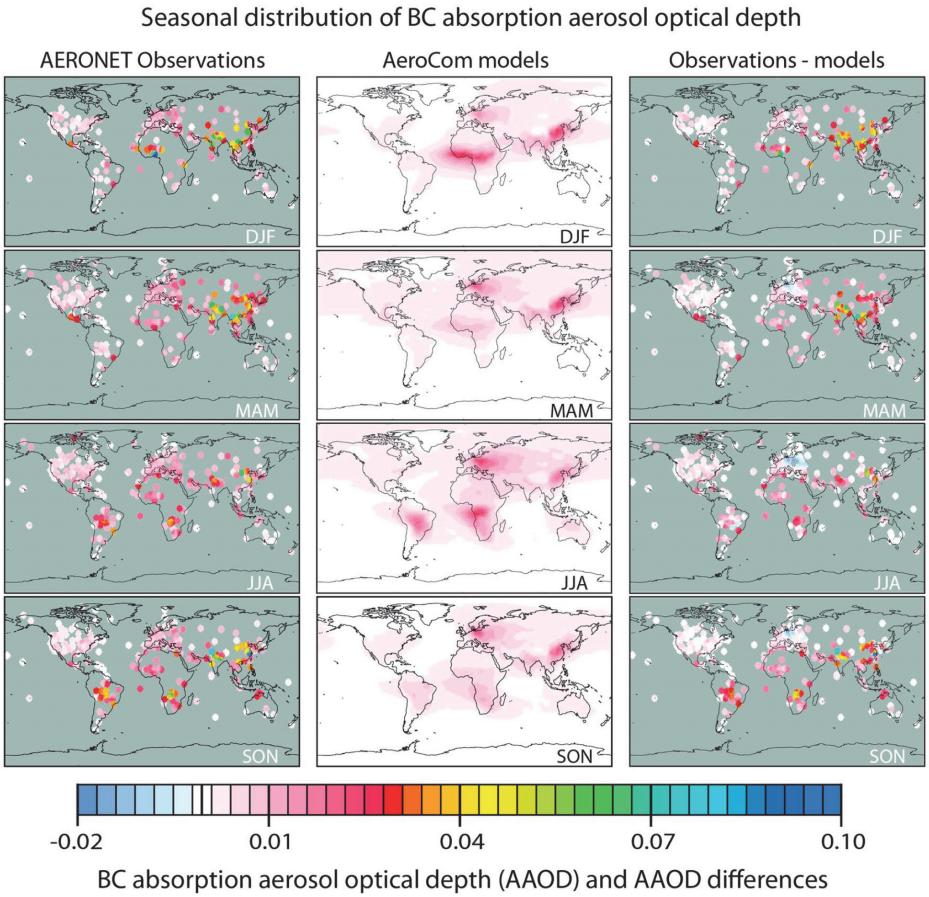

Figure 6: The absorption aerosol optical depth (AAOD) due to BC inferred from observations and models at 550 nm. The AERONET stations are indicated in the right panel, with seasonal mean BC AAOD sampled between 2000-2010. The middle panel shows the median BC AAOD from 15 AeroCom models year 2000. The left panel show the difference between models and observations. Figure from Bond et al. [2013].

Aerosol optical depth is a measure on the vertically integrated extinction of radiation caused by aerosols. The total extinction is the sum of the scattering and absorption. Aerosol absorption optical depth (AAOD) is the extinction of radiation by absorption only. AAOD is more closely linked to the BC column burden compared to AOD, since BC absorption makes up a larger fraction of the total absorption. Compared to observations provided by remote sensing from AERONET, the AAOD is underestimated in climate models in all regions (Figure 6) [*Koch et al.* 2009b, *Bond et al.* 2013]. In order to retrieve the observed BC AAOD, different assumptions must be made to separate AAOD between BC and dust, that also absorb in the visible spectrum. Most models used

in the study did not include internal mixing, underestimating the absorption. The underestimation might also be linked to missing biomass burning inventories and emissions related to energy-use in developing countries [*Bond et al.* 2013].

2.2 BC forcing

BC perturbs the radiative budget directly by absorption and scattering of solar radiation, indirectly by changing the microphysical properties of clouds, and semi-directly by changing the static stability of the atmosphere and the distribution of clouds through atmospheric heating. In addition, when deposited on snow and sea-ice BC lowers the albedo of the surface, referred to as the 'snow/albedo effect'.

The fourth Intergovernmental Panel on Climate Change (IPCC) report gives a direct RF of BC of +0.34 W m^{-2} with an uncertainty estimate of 0.25 W m^{-2} [*Forster et al.* 2007]. The snow/albedo effect was calculated to be 0.1 W m^{-2} (± 0.1 W m^{-2}). A new scientific assessment report provides a much higher number for the industrial era (1750 to 2005) direct RF atmospheric BC of +0.71 W m^{-2} with 90 % uncertainty bounds of (+0.08,+1.27) W m^{-2} [*Bond et al.* 2013]. The large range in the BC direct RF is linked to model differences in emissions (5700-18000 Gg yr^{-1}), lifetime (3.3-10.6 days), mass absorption coefficient (4.3-15 m^2 g^{-1}) and forcing efficiency (91-270 W m^{-2} $AAOD^{-1}$) [*Schulz et al.* 2006, *Bond et al.* 2013]. Including the rapid adjustments from clouds and cryosphere, the industrial era adjusted forcing or climate forcing is +1.1 W m^{-2} (0.17 to 2.1) W m^{-2}. For comparison, the RF including indirect effects from emissions of CO_2 and methane were calculated to +1.56 W m^{-2} and +0.85 W m^{-2} (2005), respectively. The BC forcing in this assessment is higher than the BC forcing provided by the IPCC in 2007, due to both higher absorption per mass and higher BC burdens than was used in the previous IPCC models.

➔ **Can BC RF alone be used to estimate the climate effects of BC?**

The radiative forcing is calculated as the change in the instantaneous radiative imbalance at the TOA with temperatures kept fixed, i.e. before any feedbacks from clouds and snow cover. As BC heats the air and changes the microphysical properties of clouds, it causes rapid adjustments in the climate system. These rapid adjustments, or 'adjusted forcing', change the radiative budget at TOA. It may therefore not be sufficient to only look at the BC radiative forcing, when studying the climate effects of BC [*Hansen et al.* 2005]. In

paper IV we compare the RF of $4\times CO_2$ (7 W m^{-2}) to the corresponding RF of increased emissions of BC. CO_2 is a long-lived greenhouse gas that absorbs radiation in the longwave spectrum and thus has a different climate effect per RF compared to BC. Even though the instantaneous RF is equal for the two components, we find very different adjusted forcings (6.2 W m^{-2} for CO2 vs. 1.7 W m^{-2} for BC), because fast feedbacks radically change the distribution and climate impact of BC.

The altitude of the BC concentrations relative to clouds, affect the forcing efficiency (RF per unit absorption optical depth). Climate models generally overestimate BC concentrations in the upper troposphere in the tropics and mid-latitudes compared to observations [*Koch et al.* 2009b, *Schwarz et al.* 2010]. This might overestimate the BC direct RF, since more BC would be located above clouds and also be subject to a higher solar flux at high altitudes [*Haywood and Ramaswamy* 1998, *Samset and Myhre* 2011]. However, since the RF of BC is not a good measure of the surface temperature response of BC, in some causes the increased solar absorption by BC at higher altitudes may be of secondary importance [*Ban-Weiss et al.* 2012].

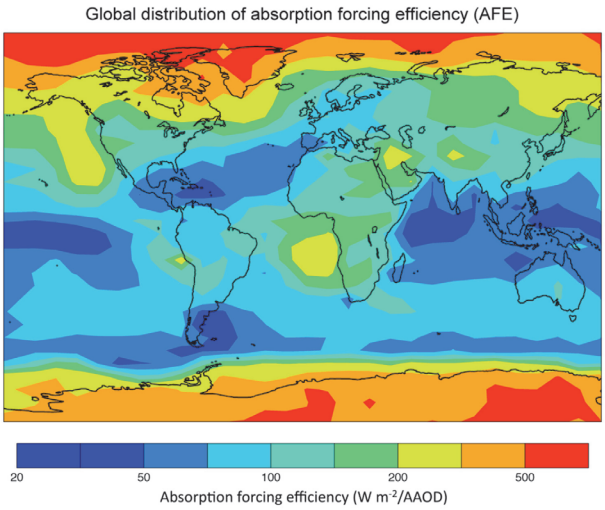

Figure 7: The absorption forcing efficiency (direct RF per AAOD) for the AeroCom median model. Figure from Bond et al. [*2013*].

The direct RF of BC depends on the albedo of the underlying surface. The absorption forcing efficiency (direct RF per AAOD) from the AeroCom median model is shown in

Figure 7. The highest values occur over snow-covered surfaces. There are also higher values over land or when BC is located above stratus clouds.

Influencing the clouds -the indirect and semi-direct effect of BC

One of the largest uncertainties in climate models is clouds and how aerosols interact with clouds. An even higher uncertainty is the role BC may play. BC has an indirect effect on cold and warm clouds, by changing the albedo and lifetime of clouds [*Twomey* 1977, *Albrecht* 1989]. The forcing can be either negative or positive. For example, by adding BC particles in a liquid cloud, the cloud droplet number concentrations could increase, leading to a negative forcing. The indirect effect can be positive with a reduction in cloud droplets, if BC attracts condensing gases that otherwise would form particles [*Bauer et al.* 2010]. The estimated indirect effect is sensitive to BC particle size and internal mixing.

BC can also have a thermodynamical effect on clouds by altering the vertical temperature gradient through local warming, often referred to as semi-direct effects [*Hansen et al.* 1997]. The effects depend on the vertical structure of the BC concentrations relative to the clouds and meteorological conditions [*Johnson et al.* 2004, *Wang* 2004, *Hansen et al.* 2005]. When BC is embedded within or near clouds, the increased warming and reduced relative humidity may lead to evaporation and dissolution of clouds [*Hansen et al.* 1997, *Ackerman et al.* 2000]. Absorbing aerosols located at higher altitudes increase the low-level stability. This effect may strengthen underlying stratocumulus clouds [*Johnson et al.* 2004] with reduced entrainment of dry overlying air. However, the same stabilization effect may suppress convective cloud formation, leading to a net warming effect [*Fan et al.* 2008]. Both the magnitude and sign of the semi-direct of BC is highly uncertain [*Koch and Genio* 2010].

Changing the cryosphere -the snow albedo effect

When BC is deposited on snow it causes a significant reduction in the snow albedo. Even particles with a high ratio of organic aerosol to BC cause positive forcing, due to the high albedo of the snow at visible wavelengths [*Warren and Wiscombe* 1980]. The initial radiative forcing by BC can be significantly amplified by warming-effects in the snow itself (increased snow grain sizes and snow melt rates), which enhance the albedo reductions. BC deposition on snow and associated feedbacks can lead to earlier exposure of the underlying surface. The exposed surface over land and ocean has a much lower albedo than snow (e.g. 0.2 for tundra vs. 0.8 for new snow), leading to increased warming

of the surface and the surrounding air [*Warren and Wiscombe* 1985]. This effect is called the snow/albedo feedback. The effect in the northern hemisphere is largest in spring when both the snow cover and insolation is large [*Flanner et al.* 2009]. Model studies have calculated the radiative forcing and climate response for BC in snow and indicate a climate efficacy 2-4 times larger than that of CO_2 [*Hansen and Nazarenko* 2004, *Jacobson* 2004, *Hansen et al.* 2005, *Flanner et al.* 2007, *Koch et al.* 2009a]. The studies indicate that BC may be playing an important role in the observed rapid retreat of the Arctic sea-ice and the decline in the Eurasian springtime snow cover during the last decades [*Bond et al.* 2013].

Figure 8 shows the total climate forcing (or adjusted forcing) of industrial era BC and the different forcing terms that make up the total forcing from Bond et al., [*2013*]. There is a low to very low scientific understanding on BC cloud indirect effects.

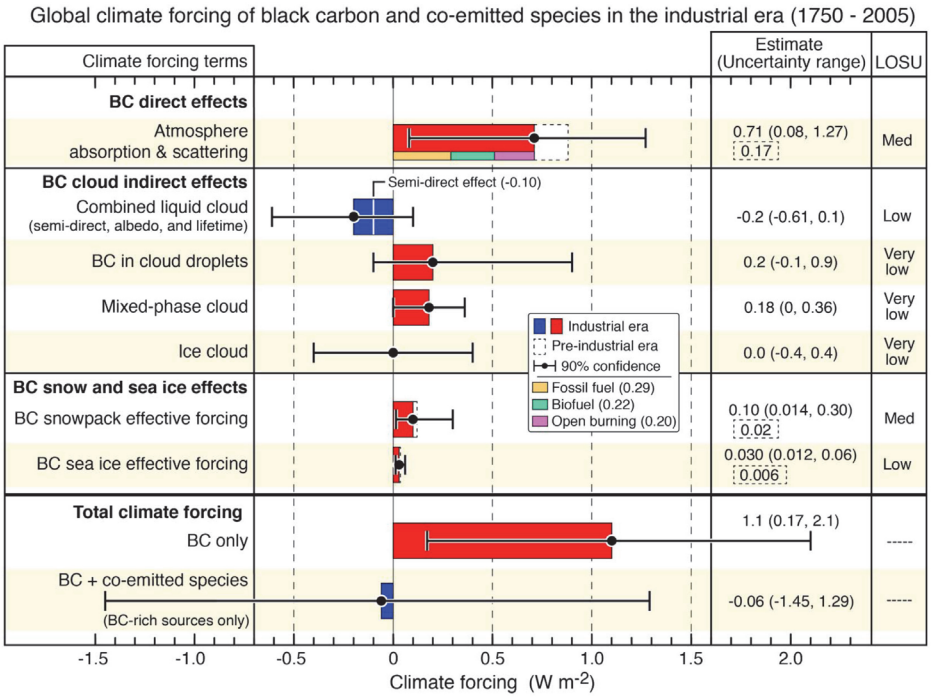

Figure 8: Globally averaged industrial era BC climate forcings (in W m^{-2}). Figure from Bond et al., [*2013*]. Also shown is the level of scientific understanding (LOSU) for each forcing term.

2.3 Climate impact of BC

The climate forcing of BC induces a change in the climate system with associated complex feedback mechanisms. BC forcing warms the troposphere, causing changes in clouds, precipitation, atmospheric circulation and surface temperatures. The climate response can be divided into fast feedbacks, which respond to the forcing in order of days and slow feedbacks on longer timescales associated with the surface temperature response [*Gregory et al.* 2004, *Andrews et al.* 2010]. The slow feedbacks appear less dependent on the forcing component, compared to the rapid feedbacks. The concept of climate sensitivity is often used as a comparative measure of different climate perturbations. The underlying assumption is a linear relationship between the global mean radiative forcing, F, and the global mean surface temperature response, T_s, after the climate system has reach equilibrium:

$$\Delta T_s = \lambda F$$

where λ is the climate sensitivity parameter. Radiative forcing is often used as an *a priori* measure of the ability of a particular climate perturbation to alter surface temperatures. In this way the climate response can be quantified without performing expensive coupled model simulations. The positive radiative forcing of BC at TOA suggested that BC might exert a positive surface temperature change. [*Hansen et al.* 1997] found large differences in λ for BC, mostly linked to clouds.

Several studies have investigated the relationship between the vertical dependence between BC forcing and the climate response [*Cook and Highwood* 2004, *Hansen et al.* 2005, *Ban-Weiss et al.* 2012]. Ban-Weiss et al. [2012] perturbed global BC in 5 different layers in a climate model, and found a decrease in the surface temperature response and precipitation with increasing altitude of the BC layers, despite an increase in the BC forcing. The studies show that for BC radiative forcing is not a sufficient measure for determine the surface temperature response. Flanner [2013] increased the AAOD in the Arctic in different layers in the CESM model, and found a strong surface warming when AAOD was perturbed at the surface and in the snow, and a weak surface warming for forcing at 400-750 hPa and a cooling for forcing at 210-250 hPa.

Changes in the cryosphere

In paper II we investigated how sensitive the Arctic climate is to increased emissions of BC. In this study it was important to include the effect of BC in snow as emissions in the Arctic might lead to higher concentrations in the lower atmospheric layers, and thus, higher probability of deposition events. We find that in the model, more than 2/3 of the Arctic temperature increase following increased BC emissions in the Arctic itself is due to the deposition on snow and sea-ice. In the model, the darkening of the Arctic surface is associated with large responses in the snow cover, the sea-ice, and cloud cover.

The BC snow albedo feedback has a high efficacy and even a small initial forcing can lead to a large surface warming. The reasons for this are partly because the cryosphere has a strong positive snow albedo feedback, which BC exacerbates by warming the snow and sea-ice when it is directly deposited within the cryosphere. Also, due to the stable atmospheric conditions at higher altitudes, surface forcings can drive larger surface temperature changes compared to lower latitudes.

Changes in precipitation

BC can enhance precipitation by warming the surface, but the effect can be counterbalanced or even dominated by stronger shortwave heating of the atmosphere that lead to a decrease in precipitation [*Andrews et al.* 2010, *Ming and Ramaswamy* 2011]. The decrease in precipitation is linked to rapid adjustments, while the enhanced precipitation by surface warming is linked to slow feedbacks. Studies have also shown that BC can cause a northward shift in the Inter Tropical Convergence Zone (ITCZ) by strengthen the Hadley cell in the Northern Hemisphere relative to the Southern Hemisphere. [*Jones et al.* 2007, *Wang* 2007].

Observed climate change due to BC?

It has been difficult to detect any of the observed global warming over the last 50 years to BC, even though there are some evidences for regional climate response. For instance, Menon et al. [2010] finds that anthropogenic BC emissions in India may be responsible for some of the observed patterns and trends in snow/ice cover and precipitation in the region. Flanner et al. [2009] argues that the BC snow/albedo effect is responsible for the decrease in snow cover and increased warming during spring observed in Europe during the last decades. Koch et al. [2011] simulate transient twentieth-century climate and

attribute 20 % of the Arctic warming and snow-cover loss to BC over the century, with a decrease in the effect during the last half of the century.

Figure 9 summarize the current knowledge of the BC effects on climate [*Bond el al*., 2013]. Climate models agree that the warming by BC since preindustrial times is concentrated in the northern hemisphere with an enhanced warming in the high latitudes due to darkening of snow and sea-ice. Models agree that BC may lead to a northward shift in the Intertropical Convergence Zone. BC may also have caused precipitation changes in South Asia.

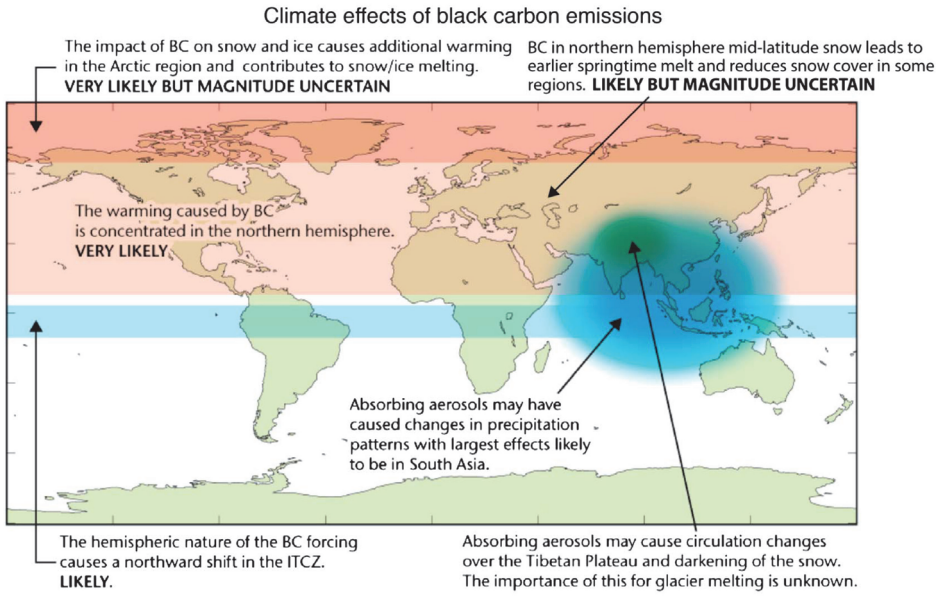

Figure 9: Summary of the current understanding of the climate impacts of BC emissions. Figure from Bond et al. [*2013*].

Chapter 3 Modeling tools: The Norwegian Earth System Model

In this study the global climate model NorESM [*Bentsen et al.* 2013, *Iversen et al.* 2013] has been used to calculate the climate effects of BC. The model is to a large extent based on the CESM4.0 [*Gent et al.* 2011] developed at the National Centre for Atmospheric Research (NCAR). The atmospheric module of NorESM, CAM-Oslo includes a comprehensive treatment of aerosols and their interactions with radiation and clouds [*Kirkevåg et al.* 2013]. Emitted primary particles include sulphate, BC, organic matter, sea salt and mineral dust. Model calculated gas-phase components are DMS and SO_2. Figure 10 illustrates the aerosol processes in CAM-Oslo.

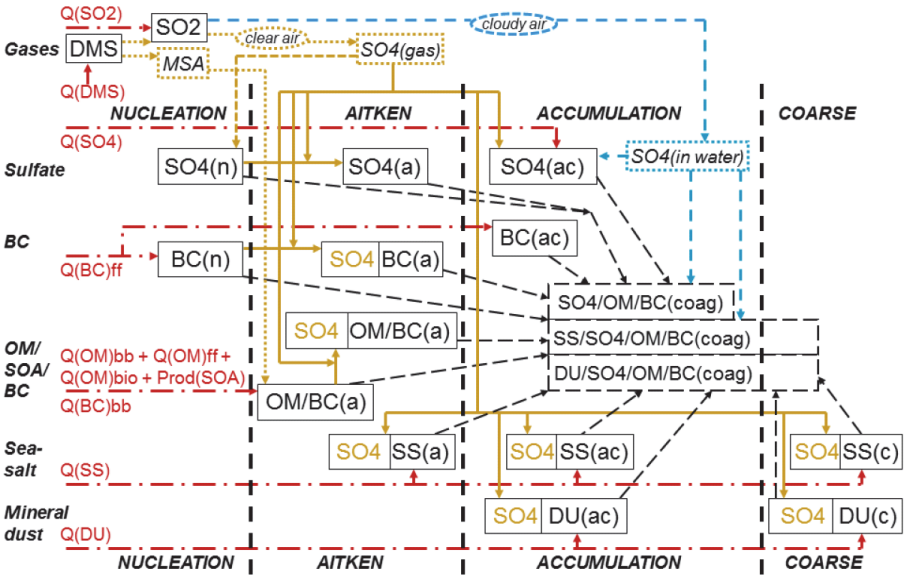

Figure 10: The aerosol-particle processing in CAM4-Oslo [*Kirkevåg et al.* 2013]. The source terms are labeled Q and the source labels bb, ff and bio indicate biomass burning, fossil fuel combustion, and biogenic sources, respectively. The emitted primary particles are indicated in red dashed-dotted arrows. There are four different modes; nucleation (n), aitken (a), accumulation (ac) and course (c). Dotted yellow arrows indicate the transformation from gaseous sulphate (SO_4(gas)) to nucleation-mode sulphate (SO_4(n)). Solid yellow arrows indicate condensation of SO_4. Long-dashed black arrows represent coagulation.

BC from fossil fuel is mostly emitted as nucleation/aitken mode and 10 % is assumed emitted as accumulation mode conglomerates created by self-coagulation in the exhaust.

BC from biomass burning is emitted as internally mixed with organic matter. Once emitted, BC grows in size by condensation of sulphate and/organic matter, or by coagulation. NorESM only take into account coagulation of nucleation and aitken mode particles with accumulation and coarse mode particles. Coagulation of aerosol particles with cloud droplets takes place when there is liquid water present in a grid square. Sulphuric acid gas condenses on all particle surfaces available in a grid volume.

The concentrations of aerosols are tagged according to the size modes and production mechanisms given in Figure 10. There are 11 components for externally mixed particles that are calculated in the life cycle scheme (and transported in the model). In addition there are 9 components that are tagged according to production mechanisms in air or clouds droplets. The transformation from externally mixture to internal mixture for the 11 components is estimated by use of look-up tables. The look-up tables contain values for aerosol optical properties and CCN calculations. The values have been tabulated for a large range of input values for process-tagged concentrations, relative humidity and supersaturation. CCN activation is estimated based on supersaturations calculated from Köhler theory. The main advantage by this method is that the degree of external vs. the internal mixing can be estimated based on physicochemical processes.

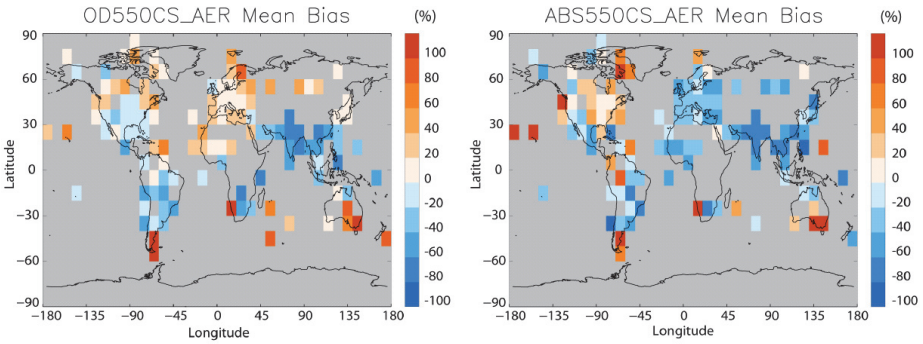

Figure 11: Biases in estimating annual mean aerosol optical depth (AOD) (left) and aerosol absorption optical depth (AAOD) (right) in NorESM compared to AERONET stations 2000-2009. Figure from Kirkevåg et al. [2013].

Figure 11 shows biases in the estimated AOD and AAOD in NorESM (with IPCC emission inventory [*Lamarque et al.* 2010]) compared to observations from the ground-based AERONET stations. The AOD and AAOD are underestimated in large parts of the

tropics and sub-tropics, with the highest underestimation in South Asia. On the other hand, AOD is overestimated in several remote regions at high latitudes.

When using fully-coupled climate models, it is a challenge to separate the climate signal of increased BC from the internal variability. In the climate simulations we performed, it was necessary to scale up the BC concentrations or emissions significantly in order to get a significant signal. We have to assume that the perturbations we have done are linearly scalable. However, there are non-linearities in the climate system that add additional uncertainties in our estimates, but we think nevertheless there are substantial knowledge to be gained from the experiments. The global forcing we achieved by the scaling factors in paper I and II was in order of 1 W m^{-2}. This value is considered acceptable, even though it is not desirable [*Hansen et al.* 2005].

We have used a fully coupled ocean model, which require thousands of model years to reach full equilibrium. Many equilibrium model studies replace the ocean model with a slab-ocean model that has a simple thermodynamic mixed-layer. However, changes in the ocean heat transport, which may influence atmospheric feedbacks and temperatures, are not fully captured in slab-ocean models. A method to calculate the equilibrium climate response in fully-coupled model simulations without running the models to equilibrium, is to use a linear regression method that assumes a linear dependence between the TOA radiative flux and the global-mean surface temperatures [*Gregory et al.* 2004]. In paper IV we apply this method to two experiments with perturbed BC and CO_2, respectively. For BC, this method is insufficient, due to fast responses in the climate system during the first year, as also have been pointed out in other studies [*Hansen et al.* 1997, *Andrews et al.* 2010].

Chapter 7.3 in Iversen et al. [2013] is part of this Ph. D thesis. The paper concerns the climate response and scenario projections of NorESM, and chapter 7.3 focus on the low-frequency variability in the model climate system. To investigate the variability an empirical orthogonal function (EOF) analysis [*Hannachi* 2004] has been applied to the historical runs and the RCP scenarios from NorESM. The EOF analysis can be used to extract coherent variations that are dominant in a time series. It is commonly used to study spatial patterns and how they evolve with time, for instance the North Atlantic Oscillation pattern [*Hurrell and Deser* 2009]. The EOF patterns are found by computing the eigenvalues and the eigenvectors of the anomaly covariance matrix.

Chapter 4 Aim and summary of papers

This thesis consists of four papers. All the papers are devoted to the topic of climate modelling, in which three papers focus particularly on the climate impact on BC aerosols. The first two papers concern the Arctic climate response to BC. The third paper discusses the climate sensitivity and low-frequent natural variability of the climate model used in this study, and the fourth paper discusses how the natural variability in the model influences the climate response of BC.

I. The Arctic climate response to local and remote forcing of black carbon

M. Sand[1], T.K. Berntsen[1], J.E. Kay[2], J.F. Lamarque[2], Ø. Seland[3], A. Kirkevåg[3].

[1]Department of Geosciences, Meteorology and Oceanography Section, University of Oslo, Oslo, Norway

[2]National Center for Atmospheric Research, Boulder, Colorado, USA

[3]Norwegian Meteorological Institute, Oslo, Norway

In his study we have investigated how atmospheric BC in the mid-latitudes remotely influences the Arctic climate, using a coupled climate model. We have compared this with the response to atmospheric BC located in the Arctic itself. The study was motivated by the findings of [*Shindell and Faluvegi* 2009], who looked at the regional climate response to different forcing locations. They found a negative surface temperature response in the Arctic to Arctic BC forcing (direct effect only). As the results were counter-intuitive, we wanted to see if we got a consistent result with a different model, and look more into the processes for the surface cooling.

In this study, idealized climate simulations were carried out with a fully coupled Earth System Model, which included a comprehensive treatment of aerosol microphysics. Present-day atmospheric BC concentrations were scaled up in the mid-latitudes (28N-60N) and in the Arctic (60N-90N), respectively.

Key findings:

- Our calculations show that increased BC forcing in the Arctic atmosphere reduces the surface air temperature in the Arctic with a corresponding increase in the sea-ice fraction, despite the increased planetary absorption of sunlight.

- The analysis indicates that this effect is due to a combination of a weakening of the northward heat transport caused by a reduction in the meridional temperature gradient and a dimming at the surface.
- On the other hand we find that BC forcing at the mid-latitudes warms the Arctic surface significantly and decreases the sea-ice fraction.
- These results suggest that mitigation strategies for the Arctic climate should also address BC sources in locations outside the Arctic even if they do not contribute much to BC in the Arctic.

A key point in this study is that the BC perturbation in the Arctic is mainly in the upper part of the troposphere due to the location of the major BC sources at lower latitudes.

II. The Arctic climate sensitivity to emissions of black carbon in the Arctic or mid-latitudes

M. Sand[1], T.K. Berntsen[1], Ø. Seland[2], J. E. Kristjánsson[1].

[1]Department of Geosciences, Meteorology and Oceanography Section, University of Oslo, Oslo, Norway

[2]Norwegian Meteorological Institute, Oslo, Norway

The results in paper I are less relevant for policies that focus on mitigation of BC emissions at high latitudes, as the study does not look into the impact of emissions of BC in the Arctic. In this paper we have focused on increased emissions in the Arctic, and included the effect of BC deposited on snow. Today there are few within-Arctic sources of BC, but the emissions are expected to grow due to increased human activity in the Arctic. We find that there is a great need to improve cleaner technologies if further development is to take place in the Arctic. In this study we have used a new emission inventory for BC (ECLIPSE), which includes emissions from flaring. In the domestic sector we have implemented a seasonal cycle, to account for increased space heating during the winter season.

Key Findings:

- BC emissions in the Arctic cause BC perturbations much closer to the surface giving a very different climate impact than the forcing perturbation in paper I, including a strong contribution from BC deposited on snow and ice.

- During winter, BC emitted in North-Eurasia is transported into the high Arctic at low altitudes. Using the new emissions data set the BC surface concentrations in the high-Arctic (70-90N) doubles compared to emissions without flaring and seasonal cycle in the domestic sector.
- A large fraction of the surface temperature response from BC in the model is due to increased absorption when BC is deposited on snow and sea-ice with associated feedbacks.
- Because of this, BC emitted within the Arctic has an almost 5-times larger Arctic surface temperature response (per unit of emitted mass) compared to emissions at mid-latitudes.

III. The Norwegian Earth System Model, NorESM1-M – Part 2: Climate response and scenario projections

T. Iversen[1,2,*], M. Bentsen[3,4], I. Bethke[3,4], J. B. Debernard[1], A. Kirkevåg[1], Ø. Seland[1], H. Drange[4,5], J. E. Kristjánsson[2], I. Medhaug[4,5], M. Sand[2], and I. A. Seierstad[1]

[1]Norwegian Meteorological Institute, P.O. Box 43, Blindern, 0313 Oslo, Norway

[2]Department of Geosciences, University of Oslo, P.O. Box 1047 Blindern, 0315 Oslo, Norway

[3]Uni Bjerknes Centre, Uni Research AS, P.O. Box 7810, 5020 Bergen, Norway

[4]Bjerknes Centre for Climate Research, P.O. Box 7810, 5020 Bergen, Norway

[5]Geophysical institute, University of Bergen, P.O. Box 7803, 5020 Bergen, Norway

[*]currently at: ECMWF, Shinfield Park, Reading, RG2 9AX, UK

The NorESM1-M simulation results for CMIP5 (http://cmip-pcmdi.llnl.gov/cmip5/index.html) are described and discussed. NorESM1-M is estimated to have equilibrium climate sensitivity ca. 2.9 K, a transient climate response ca. 1.4 K, and is less sensitive than most other models in the CMIP5 project. Cloud feedbacks damp the response, and a strong AMOC reduces the heat fraction available for increasing near surface temperatures, for evaporation, and for melting ice.

In the paper, section 7.3 ‘NH EOF-analysis’ is part of this Ph.D thesis. In order to describe the low frequency variability in the NorESM1-M, an EOF analysis has been applied to monthly mean 500 hPa geopotential height anomalies during extended winter seasons (DJFM) from 1976 to 2005. The EOFs are compared with reanalysis data from the same period. The model has some differences that can be linked to the systematic

errors in the storminess and the blocking occurrence in NH. For instance, the model variability is dominated by the Pacific North American pattern and the North Atlantic Oscillation pattern is displaced eastward compared to reanalysis data.

IV. **Uniqueness of the climate response to black carbon aerosols**

M. Sand[1], T. Iversen[2], A. Kirkevåg[2], I. Seierstad[2] and Ø. Seland[2].

[1]Department of Geosciences, Meteorology and Oceanography Section, University of Oslo, Oslo, Norway

[2]Norwegian Meteorological Institute, Oslo, Norway

In this paper we discuss how the earth's global climate may respond to changes in the abundance of BC aerosol particles. The discussions emphasize the role of interactions between atmospheric dynamics and regional ground surface feedbacks which can be expected to be more important for light-absorbing aerosols than other climate forcing agents. We conduct several experiments using NorESM and investigate the interplay between the dynamic atmospheric response and local feedbacks during different phases of the natural variations, when changes are driven by BC aerosols. We also compare

Key Findings:

- The global impact on present-day BC is significant when averaging over the last 50 model years.
- However, on shorter timescales, the natural variability dominates regionally, which makes it difficult to extract the climate signal from BC and to translate the global response into a regional response.
- With the unique way BC creates forcing over reflective surfaces, the internal natural variations are more important for BC compared to CO_2, due to regional negative feedbacks and the strong interaction between the surface albedo and BC.
- Thus, BC possesses unique properties compared to most other anthropogenic sources of potential climate impact, and this makes it difficult to apply the standard concepts of climate sensitivity.

Chapter 5 Summary and future perspectives

In this thesis I have investigated the climate response to BC aerosols by conducting different experiments in a global climate model. As a first order approximation to estimate the temperature response it has been common to use radiative forcing. For instance, the AMAP report perturbed different climate forcers and reported only radiative forcing numbers in the Arctic [*AMAP* 2011]. However, for a given region there is no simple relationship between the forcing and the response [*Boer and Yu* 2003], especially for absorbing aerosols in the Arctic [*Shindell and Faluvegi* 2009]. In this case, even the sign of the BC forcing and the surface temperature response was different. In paper I, we confirmed the findings of Shindell and Faluvegi [2009] that showed an Arctic surface cooling from BC forcing in the Arctic, and we further analyzed the mechanisms controlling the Arctic surface temperature change to BC concentrations located in the Arctic and in the mid-latitudes, respectively. The absorption of solar radiation resulted in a large positive radiative forcing at TOA, while the surface received less solar radiation. The maximum heating of air occurred between 350 hPa and 150 hPa where the maximum in the BC concentrations was located. The heated air lead to a decrease in the northward heat transport and increased static stability that suppressed the heat exchange between the free troposphere and the surface. The net result was a cooling of the surface and an increase in the sea-ice cover. In addition, the study shows that BC in the mid-latitudes may remotely warm the Arctic surface by increasing the northward heat transport by local warming. Does this mean that BC emission reductions within the Arctic would lead to an Arctic warming? The study does not show or imply that increased BC emissions in the Arctic will cool the Arctic surface temperatures, or that reduction of BC emissions in general would lead to an Arctic warming. First of all, the study did not include the effect on BC in snow and ice. Second, the forcing was conducted by perturbing present-day atmospheric concentrations of BC from all sources. Since most of the BC in the Arctic is transported there from lower latitudes, a large fraction is located at higher altitudes, in particular in the models. If the BC emissions in the Arctic increased, the BC concentrations would be located closer to the surface, with a higher probability of BC deposition events and air-surface heat exchange. Third, BC located in the mid-latitude remotely warms the Arctic by local warming and increased heat transport, highlighting the importance of BC emission reductions outside the Arctic. The study shows that forcing estimates for the Arctic may not be an adequate way of describing the climate

response. In order to make meaningful analysis of mitigation actions for the Arctic, it might be necessary to use coupled runs with emissions and climate response, and that was one of the main motivations for making the second paper. In paper II it was investigated how regional emissions of BC affect the Arctic, both from the region itself and in the mid-latitudes, where most of BC reaching the Arctic is emitted. In this study it was crucial to include the effect of BC in snow and ice. We found that BC emitted in the Arctic itself, is more likely to stay in the lower atmosphere and get deposited in the snow, while emissions from lower latitudes is more likely to remain at higher altitudes. The warming effect due to the BC snow/albedo effect explained a large fraction of the temperature increase. Because of this, in our model the Arctic surface temperatures are almost five times more sensitive to BC emitted within the Arctic than to emissions from mid-latitudes. We also find that BC emitted in the mid-latitudes warms the Arctic, both in the atmosphere only and when the deposition effect is included. This confirms the findings from paper I that BC in the mid-latitudes remotely warms the Arctic surface. Even though the BC deposition effect dominates the surface temperature response, the Arctic warms three times more when BC is emitted within the Arctic compared to mid-latitudes in the runs where BC deposition is switched off. The reason why the Arctic surface warms by the direct effect of BC in this case, is because BC is located closer to the surface compared to in paper I.

The BC climate response in this thesis is model dependent. The third paper discusses the climate sensitivity and low-frequent natural variability of the climate model used in this study. The fourth paper discusses how the natural variability in the model influences the climate response of BC. In paper IV we investigate the processes and mechanisms regarding BC climate response in more detail and look at which factors that affect the climate response. We conducted experiments comparing BC and CO_2, and found a large difference in the climate efficacies, partly because fast feedbacks regulate the climate forcing of BC. This makes it inadequate to use any linear regression model to estimate the equilibrium climate response to BC, and emphasize that radiative forcing may not be a good way to represent the surface temperature response to BC. We also studied regional and global responses in experiments with and without present-day BC concentrations. The present-day BC-induced climate responses were significant when averaging over the final 50 model years. However, for shorter time-periods, the natural decadal variations complicated the detection of the BC signal on a regional scale.

When studying BC in this thesis we have only perturbed BC concentrations and emissions. However, as BC is never emitted alone, there is a variety of other co-emitted gases and/or particles that may either warm or cool the climate [*Bond et al.*, 2013]. Thus, the net forcing for a given source may be either positive or negative depending on the amount and chemical composition of the co-emitted species. Deposited in snow however, all aerosols with a single-scattering albedo less than that of ice grains (i.e. less than 0.9999), have a positive forcing when deposited in the snow [*Flanner et al.* 2009]. In order to analyze mitigation actions for different emissions activities, it is important to include all the co-emitted species. Future studies regarding mitigation to reduce Arctic warming, would be to investigate the impact of emissions of short lived components from different sectors or smaller geographical areas. This has been performed with CTM models with RF calculations, but the results suggest that similar studies must be conducted with climate models [*Skeie et al.* 2011].

Today BC is an important forcing agent in the Arctic. Will BC still be important in the future if most of the snow and sea-ice in the Arctic have melted during the summer months? While the BC emission are continuing to grow in Asia [*Lei et al.* 2011], observations suggest that BC emissions are decreasing in Europe and North-America [*Legrand et al.* 2007, *Murphy et al.* 2011]. The Alert and Zeppelin stations in the Arctic show that near-surface BC concentrations have been declining in the recent decades compared to the early measurements [*Sharma et al.* 2006, *Eleftheriadis et al.* 2009]. At the Barrow station in Alaska there has been a possible slight increase since 2003[*Sharma et al.* 2006]. Hirdman et al. [2010] links a large fraction of the trends in the Arctic stations to changes in emissions. Even though these emissions have decreased, it may be possible to reduce the emissions even further. Future changes in Artic shipping and oil/gas production may increase the emissions.

During the last decades the climate models have undergone rapid development and are continually implemented with new improvements. For instance, more models have now developed aerosols that interacts with clouds, radiation and the dynamics, and through these, the direct and indirect effects of aerosols are more extensively included. Also, interactive atmosphere chemistry is being implemented in climate models, with the potential of improving BC aging and the role of co-emitted species. We have not used interactive chemistry in this thesis. The current version of NorESM does not treat the

influence of BC on ice nucleation. Ice nucleation scavenging affects a relatively small amount of particles, but there are a range of potentially large indirect effects linked to ice clouds [*Kärcher et al.* 2007, *Penner et al.* 2009]. It is uncertain how important BC is as an ice nucleus. Today there are few models that include activation of ice nuclei and the influence of the ice phase in clouds on the indirect effects of aerosols. Koch et al. [2009b] found that their global model gave an optical agreement with observations, if 12 % of the removal was frozen removal relative to liquid cloud removal. The liquid cloud fraction is important in determining the aerosol removal. Wang et al. [2013] suggested that the overestimation of liquid-containing cloud at mid- and high latitudes simulated by CAM5 (which also is the case for NorESM), is a key contributor to the excessive removal of aerosols during their transport to the Arctic. In their study, improvements in the consistency in the liquid cloud fraction lead to a three-fold increase in the Arctic BC burden during the winter season.

The models are constantly evaluated with available observations from in-situ measurements of BC concentrations and from remote sensing of the column aerosol absorption optical depth from ground-based stations and satellites. Remote sensing from satellites has the largest spatial coverage, but does not measure BC concentrations directly. Uncertainties arise if other light-absorbing particles are present. In situ observations of BC in the atmosphere and in snow can measure BC concentrations directly, but are limited by measurement techniques and the spatial and temporal distribution. The ground-based measurements are most sparse in Africa and most of Asia, areas with some of the highest emissions. There are large uncertainties in the BC emission inventory, and they vary across models by 7.5 to 19 Tg C yr^{-1} [*Textor et al.* 2006]. Bond et al. [2013] suggests that emission estimates might be biased low by a factor of two. Extensive field campaigns provide snap-shots of the aerosols and their advantage is that many observations (air-borne or on land or ships) are taken at the same time. As the field campaigns only takes place at one location in the order of days or weeks, it is not always representative of the average in the area. Measurements of the vertical profiles of BC are sparse, both spatial and temporal. As the vertical distribution of BC determines the climate response to BC, a correct simulation of the vertical distribution of BC is crucial. Since there currently are too few measurements, we are not sure if the models simulate the profile correctly. There are indications that the models overestimate BC concentrations in the upper troposphere [*Koch et al.* 2009b, *Schwarz et al.* 2010].

A number of the questions asked in this thesis have policy-relevance, and we have tried to address them using the best methods that were available at the time. Whatsoever, we have run a model that underestimates surface concentrations of BC in the Arctic on a course grid resolution (~2°), and we had to scale up the BC concentrations substantially to get a statistically significant signal. The NorESM is currently undergoing testing for running on a 1 ° resolution and it might be possible to run on a 0.25 ° horizontal grid in the near future. Increasing the resolution may improve the BC concentrations by a more consistent liquid cloud fraction and removal, but it may also improve the climate response to BC. For example, too course resolution is believed to underestimate the number of blocking events in the northern hemisphere, and this would have a large impact on the response in the northward heat transport. Dawson et al. [2012] showed that a global climate model with horizontal resolution typical of that used in operational numerical weather prediction (T1279) was able to simulate the blocking events in the Atlantic sector, while the same model on a resolution of typical climate models (T159) were not able to simulate these structures. There is a great need for future generations of climate models to run at higher resolutions, and this will require considerable enhancements in computer power.

References

Ackerman, A. S., O. B. Toon, D. E. Stevens, A. J. Heymsfield, V. Ramanathan and E. J. Welton (2000). "Reduction of Tropical Cloudiness by Soot." Science **288**(5468): 1042-1047.

Ackerman, T. P. and O. B. Toon (1981). "Absorption of visible radiation in atmosphere containing mixtures of absorbing and nonabsorbing particles." Appl. Opt. **20**(20): 3661-3667.

Albrecht, B. A. (1989). "Aerosols, cloud microphysics, and fractional cloudiness." Science **245**(4923): 1227-1230.

AMAP (2011). The Impact of Black Carbon on Arctic Climate. AMAP Technical Report No. 4 (2011). Arctic Monitoring and Assessment Programme (AMAP), Oslo, Norway**:** 70.

AMAP (2012). "Snow, water, Ice and Permafrost in the Arctic (SWIPA) 2011 Overview Report." Arctic Monitoring and Assessment Programme (AMAP), Oslo, Norway.

Andrews, T., P. M. Forster, O. Boucher, N. Bellouin and A. Jones (2010). "Precipitation, radiative forcing and global temperature change." Geophys. Res. Lett. **37**(14): L14701.

Andrews, T., P. M. Forster, O. Boucher, N. Bellouin and A. Jones (2010). "Precipitation, radiative forcing and global temperature change." Geophys. Res. Lett. **37**.

Ban-Weiss, G., L. Cao, G. Bala and K. Caldeira (2012). "Dependence of climate forcing and response on the altitude of black carbon aerosols." Clim. Dynam. **38**(5-6): 897-911.

Bauer, S., S. Menon, D. Koch, T. Bond and K. Tsigaridis (2010). "A global modeling study on carbonaceous aerosol microphysical characteristics and radiative effects." Atmos. Chem. Phys **10**: 7439-7456.

Bentsen, M., I. Bethke, J. B. Debernard, T. Iversen, A. Kirkevåg, Ø. Seland, H. Drange, C. Roelandt, I. A. Seierstad, C. Hoose and J. E. Kristjánsson (2013). "The Norwegian Earth System Model, NorESM1-M – Part 1: Description and basic evaluation of the physical climate." Geosci. Model Dev. **6**(3): 687-720.

Blanchet, J.-P. (1989). "Toward estimation of climatic effects due to arctic aerosols." Atmos. Environ. **23**(11): 2609-2625.

Boer, G. and B. Yu (2003). "Climate sensitivity and response." Clim. Dyn. **20**(4): 415-429.

Bond, T. C. and R. W. Bergstrom (2006). "Light Absorption by Carbonaceous Particles: An Investigative Review." Aerosol Science and Technology **40**(1): 27-67.

Bond, T. C., S. J. Doherty, D. W. Fahey, P. M. Forster, T. Berntsen, B. J. DeAngelo, M. G. Flanner, S. Ghan, B. Kärcher, D. Koch, S. Kinne, Y. Kondo, P. K. Quinn, M. C. Sarofim, M. G. Schultz, M. Schulz, C. Venkataraman, H. Zhang, S. Zhang, N. Bellouin, S. K. Guttikunda, P. K. Hopke, M. Z. Jacobson, J. W. Kaiser, Z. Klimont, U. Lohmann, J. P. Schwarz, D. Shindell, T. Storelvmo, S. G. Warren and C. S. Zender (2013). "Bounding the role of black carbon in the climate system: A scientific assessment." J. Geophys. Res.

Clarke, A. D., R. J. Charlson and L. F. Radke (1984). "Airborne observations of Arctic aerosol, IV: Optical properties of Arctic haze." Geophys. Res. Lett. **11**(5): 405-408.

Clarke, A. D. and K. J. Noone (1985). "Soot in the Arctic snowpack: a cause for perturbations in radiative transfer." Atmos. Environ. **19**(12): 2045-2053.

Cook, J. and E. J. Highwood (2004). "Climate response to tropospheric absorbing aerosols in an intermediate general-circulation model." Quart. J. Roy. Meteor. Soc. **130**(596): 175-191.

Dawson, A., T. N. Palmer and S. Corti (2012). "Simulating regime structures in weather and climate prediction models." Geophys. Res. Lett. **39**(21): L21805.

Doherty, S. J., S. G. Warren, T. C. Grenfell, A. D. Clarke and R. E. Brandt (2010). "Light-absorbing impurities in Arctic snow." Atmos. Chem. Phys. **10**(23): 11647-11680.

Eleftheriadis, K., S. Vratolis and S. Nyeki (2009). "Aerosol black carbon in the European Arctic: Measurements at Zeppelin station, Ny-Ålesund, Svalbard from 1998–2007." Geophys. Res. Lett. **36**(2): L02809.

Fan, J., R. Zhang, W.-K. Tao and K. I. Mohr (2008). "Effects of aerosol optical properties on deep convective clouds and radiative forcing." J. Geophys. Res. **113**(D8): D08209.

Flanner, M., C. Zender, J. Randerson and P. Rasch (2007). "Present-day climate forcing and response from black carbon in snow." J. Geophys. Res **112**: D11202.

Flanner, M. G. (2013). "Arctic climate sensitivity to local black carbon." J. Geophys. Res. **118**: 1-12.

Flanner, M. G., C. S. Zender, P. G. Hess, N. M. Mahowald, T. H. Painter, V. Ramanathan and P. J. Rasch (2009). "Springtime warming and reduced snow cover from carbonaceous particles." Atmos. Chem. Phys. **9**(7): 2481-2497.

Forster, P. M., V. Ramaswamy, P. Artaxo, T. K. Berntsen, R. Betts, D. W. Fahey, J. M. Haywood, J. Lean, D. C. Lowe, G. Myhre, J. Nganga, R. Prinn, G. Raga, M. Schultz and R. Van Dorland (2007). Changes in atmospheric constituents and in radiative forcing Climate Change 2007: The Physical Science Basis. Contribution of Working Group I to the Fourth Assessment Report of the Intergovernmental Panel on Climate Change. S. Solomon, D. Qin, M. Manning et al. Cambridge, United Kingdom

Fuller, K. A., W. C. Malm and S. M. Kreidenweis (1999). "Effects of mixing on extinction by carbonaceous particles." J. Geophys Res. **104**(D13): 15941-15954.

Gent, P. R., G. Danabasoglu, L. J. Donner, M. M. Holland, E. C. Hunke, S. R. Jayne, D. M. Lawrence, R. Neale, P. J. Rasch, M. Vertenstein, P. Worley, Z.-L. Yang and M. Zhang (2011). "The Community Climate System Model Version 4." J. Climate **24**(19): 4973-4991.

Gregory, J. M., W. J. Ingram, M. A. Palmer, G. S. Jones, P. A. Stott, R. B. Thorpe, J. A. Lowe, T. C. Johns and K. D. Williams (2004). "A new method for diagnosing radiative forcing and climate sensitivity." Geophys. Res. Lett. **31**(3): L03205.

Hannachi, A. (2004). A primer for EOF analysis of climate data, Department of Meteorology, University of Reading, UK 33p.

Hansen, A. D. A. and H. Rosen (1984). "Vertical distributions of particulate carbon, sulfur, and bromine in the Arctic haze and comparison with ground-level measurements at Barrow, Alaska." Geophys. Res. Lett. **11**(5): 381-384.

Hansen, A. D. A., H. Rosen and T. Novakov (1982). "Real-time measurement of the absorption coefficient of aerosol particles." Appl. Opt. **21**(17): 3060-3062.

Hansen, J. and L. Nazarenko (2004). "Soot climate forcing via snow and ice albedos." P. Natl. Acad. Sci. USA **101**(2): 423-428.

Hansen, J., M. Sato and R. Ruedy (1997). "Radiative forcing and climate response." J. Geophys. Res **102**(D6): 6831–6864.

Hansen, J., M. Sato, R. Ruedy, A. Lacis and V. Oinas (2000). "Global warming in the twenty-first century: An alternative scenario." P. Natl. Acad. Sci. USA **97**(18): 9875-9880.

Hansen, J., M. Sato, R. Ruedy, L. Nazarenko, A. Lacis, G. A. Schmidt, G. Russell, I. Aleinov, M. Bauer, S. Bauer, N. Bell, B. Cairns, V. Canuto, M. Chandler, Y. Cheng, A. Del Genio, G. Faluvegi, E. Fleming, A. Friend, T. Hall, C. Jackman, M. Kelley, N. Kiang, D. Koch, J. Lean, J. Lerner, K. Lo, S. Menon, R. Miller, P. Minnis, T. Novakov, V. Oinas, J. Perlwitz, J. Perlwitz, D. Rind, A. Romanou, D. Shindell, P. Stone, S. Sun, N. Tausnev, D. Thresher, B. Wielicki, T. Wong, M. Yao and S. Zhang (2005). "Efficacy of climate forcings." J. Geophys. Res. **110**: D18104.

Haywood, J. M. and V. Ramaswamy (1998). "Global sensitivity studies of the direct radiative forcing due to anthropogenic sulfate and black carbon aerosols." J. Geophys. Res. **103**(D6): 6043-6058.

Hirdman, D., J. F. Burkhart, H. Sodemann, S. Eckhardt, A. Jefferson, P. K. Quinn, S. Sharma, J. Ström and A. Stohl (2010). "Long-term trends of black carbon and sulphate aerosol in the Arctic: changes in atmospheric transport and source region emissions." Atmos. Chem. Phys. **10**(19): 9351-9368.

Hirdman, D., H. Sodemann, S. Eckhardt, J. F. Burkhart, A. Jefferson, T. Mefford, P. K. Quinn, S. Sharma, J. Ström and A. Stohl (2010). "Source identification of short-lived air pollutants in the Arctic using statistical analysis of measurement data and particle dispersion model output." Atmos. Chem. Phys. **10**(2): 669-693.

Huang, L., S. L. Gong, C. Q. Jia and D. Lavoué (2010). "Importance of deposition processes in simulating the seasonality of the Arctic black carbon aerosol." J. Geophys. Res. **115**(D17): D17207.

Hurrell, J. W. and C. Deser (2009). "North Atlantic climate variability: The role of the North Atlantic Oscillation." J. Marine Syst.**78**(1): 28-41.

IPCC (2007). Climate Change 2007: Synthesis Report. Contribution of Working Groups I, II and III to the Fourth Assessment Report of the Intergovernmental Panel on Climate Change, IPCC.

Iversen, T., M. Bentsen, I. Bethke, J. B. Debernard, A. Kirkevåg, Ø. Seland, H. Drange, J. E. Kristjansson, I. Medhaug, M. Sand and I. A. Seierstad (2013). "The Norwegian Earth System Model, NorESM1-M -Part 2: Climate response and scenario projections." Geosci. Model Dev. **6**(2): 389-415.

Jacobson, M. Z. (2000). "A physically-based treatment of elemental carbon optics: Implications for global direct forcing of aerosols." Geophys. Res. Lett. **27**(2): 217-220.

Jacobson, M. Z. (2002). "Control of fossil-fuel particulate black carbon and organic matter, possibly the most effective method of slowing global warming." J. Geophys. Res **107**(4410): 4.

Jacobson, M. Z. (2004). "Climate response of fossil fuel and biofuel soot, accounting for soot's feedback to snow and sea ice albedo and emissivity." J. Geophys. Res **109**: D21201.

Jacobson, M. Z. (2010). "Short-term effects of controlling fossil-fuel soot, biofuel soot and gases, and methane on climate, Arctic ice, and air pollution health." J. Geophys. Res. **115**: D14209.

Johnson, B. T., K. P. Shine and P. M. Forster (2004). "The semi-direct aerosol effect: Impact of absorbing aerosols on marine stratocumulus." Quart. J. Roy. Meteor. Soc. **130**(599): 1407-1422.

Jones, A., J. M. Haywood and O. Boucher (2007). "Aerosol forcing, climate response and climate sensitivity in the Hadley Centre climate model." J. Geophys. Res. **112**(D20): D20211.

Kinne, S., M. Schulz, C. Textor, S. Guibert, Y. Balkanski, S. E. Bauer, T. Berntsen, T. F. Berglen, O. Boucher, M. Chin, W. Collins, F. Dentener, T. Diehl, R. Easter, J. Feichter, D. Fillmore, S. Ghan, P. Ginoux, S. Gong, A. Grini, J. Hendricks, M. Herzog, L. Horowitz, I. Isaksen, T. Iversen, A. Kirkevåg, S. Kloster, D. Koch, J. E. Kristjansson, M. Krol, A. Lauer, J. F. Lamarque, G. Lesins, X. Liu, U. Lohmann, V. Montanaro, G. Myhre, J. Penner, G. Pitari, S. Reddy, O. Seland, P. Stier, T. Takemura and X. Tie (2006). "An AeroCom initial assessment – optical properties in aerosol component modules of global models." Atmos. Chem. Phys. **6**(7): 1815-1834.

Kirkevåg, A., T. Iversen, Ø. Seland, C. Hoose, J. E. Kristjánsson, H. Struthers, A. M. L. Ekman, S. Ghan, J. Griesfeller, E. D. Nilsson and M. Schulz (2013). "Aerosol–climate interactions in the Norwegian Earth System Model – NorESM1-M." Geosci. Model Dev. **6**(1): 207-244.

Koch, D., S. E. Bauer, A. Del Genio, G. Faluvegi, J. R. McConnell, S. Menon, R. L. Miller, D. Rind, R. Ruedy, G. A. Schmidt and D. Shindell (2011). "Coupled Aerosol-Chemistry–Climate Twentieth-Century Transient Model Investigation: Trends in Short-Lived Species and Climate Responses." J. Climate **24**(11): 2693-2714.

Koch, D. and A. D. D. Genio (2010). "Black carbon semi-direct effects on cloud cover: review and synthesis." Atmos. Chem. Phys. **10**(16): 7685-7696.

Koch, D. and J. Hansen (2005). "Distant origins of Arctic black carbon: A Goddard Institute for Space Studies ModelE experiment." J. Geophys. Res. **110**(D4): D04204.

Koch, D., S. Menon, A. Del Genio, R. Ruedy, I. Alienov and G. A. Schmidt (2009a). "Distinguishing Aerosol Impacts on Climate over the Past Century." J. Climate **22**(10): 2659-2677.

Koch, D., M. Schulz, S. Kinne, C. McNaughton, J. R. Spackman, Y. Balkanski, S. Bauer, T. Berntsen, T. C. Bond, O. Boucher, M. Chin, A. Clarke, N. De Luca, F. Dentener, T. Diehl, O. Dubovik, R. Easter, D. W. Fahey, J. Feichter, D. Fillmore, S. Freitag, S. Ghan, P. Ginoux, S. Gong, L. Horowitz, T. Iversen, Kirkevåg, A. g, Z. Klimont, Y. Kondo, M. Krol, X. Liu, R. Miller, V. Montanaro, N. Moteki, G. Myhre, J. E. Penner, J. Perlwitz, G. Pitari, S. Reddy, L. Sahu, H. Sakamoto, G. Schuster, J. P. Schwarz, Ø. Seland, P. Stier, N. Takegawa, T. Takemura, C. Textor, J. A. van Aardenne and Y. Zhao (2009b). "Evaluation of black carbon estimations in global aerosol models." Atmos. Chem. Phys. **9**(22): 9001-9026.

Kärcher, B., O. Möhler, P. J. DeMott, S. Pechtl and F. Yu (2007). "Insights into the role of soot aerosols in cirrus cloud formation." Atmos. Chem. Phys. **7**(16): 4203-4227.

Lamarque, J., T. Bond, V. Eyring, C. Granier, A. Heil, Z. Klimont, D. Lee, C. Liousse, A. Mieville, B. Owen, M. G. Schultz, D. Shindell, S. J. Smith, E. Stehfest, J. Van Aardenne, O. R. Cooper, M. Kainuma, N. Mahowald, J. R. McConnell, V. Naik, K. Riahi and D. P. van Vuuren (2010). "Historical (1850–2000) gridded anthropogenic and biomass burning emissions of reactive gases and aerosols: methodology and application." Atmos. Chem. Phys. **10**: 7017-7039.

Law, K. S. and A. Stohl (2007). "Arctic air pollution: Origins and impacts." Science **315**(5818): 1537-1540.

Lee, S.-H., D. M. Murphy, D. S. Thomson, and A. M. Middlebrook (2002). "Chemical components of single particles measured with Particle Analysis by Laser Mass Spectrometry (PALMS) during the Atlanta SuperSite Project: Focus on organic/sulfate, lead, soot, and mineral particles" J. Geophys. Res. 107 (D1): 2156-2202

Legrand, M., S. Preunkert, M. Schock, M. Cerqueira, A. Kasper-Giebl, J. Afonso, C. Pio, A. Gelencsér and I. Dombrowski-Etchevers (2007). "Major 20th century changes of carbonaceous aerosol components (EC, WinOC, DOC, HULIS, carboxylic acids, and cellulose) derived from Alpine ice cores." J. Geophys. Res. **112**(D23): D23S11.

Lei, Y., Q. Zhang, K. B. He and D. G. Streets (2011). "Primary anthropogenic aerosol emission trends for China, 1990–2005." Atmos. Chem. Phys. **11**(3): 931-954.

Liousse, C., J. E. Penner, C. Chuang, J. J. Walton, H. Eddleman and H. Cachier (1996). "A global three-dimensional model study of carbonaceous aerosols." J. Geophys. Res. **101**(D14): 19411-19432.

Lu, Z., Q. Zhang and D. G. Streets (2011). "Sulfur dioxide and primary carbonaceous aerosol emissions in China and India, 1996–2010." Atmos. Chem. Phys. **11**(18): 9839-9864.

McConnell, J. R., R. Edwards, G. L. Kok, M. G. Flanner, C. S. Zender, E. S. Saltzman, J. R. Banta, D. R. Pasteris, M. M. Carter and J. D. W. Kahl (2007). "20th-Century Industrial Black Carbon Emissions Altered Arctic Climate Forcing." Science **317**(5843): 1381-1384.

Menon, S., J. Hansen, L. Nazarenko and Y. Luo (2002). "Climate effects of black carbon aerosols in China and India." Science **297**(5590): 2250-2253.

Menon, S., D. Koch, G. Beig, S. Sahu, J. Fasullo and D. Orlikowski (2010). "Black carbon aerosols and the third polar ice cap." Atmos. Chem. Phys. **10**(10): 4559-4571.

Ming, Y. and V. Ramaswamy (2011). "A Model Investigation of Aerosol-Induced Changes in Tropical Circulation." J. Climate **24**(19): 5125-5133.

Murphy, D. M., J. C. Chow, E. M. Leibensperger, W. C. Malm, M. Pitchford, B. A. Schichtel, J. G. Watson and W. H. White (2011). "Decreases in elemental carbon and fine particle mass in the United States." Atmos. Chem. Phys. **11**(10): 4679-4686.

Penner, J. E., Y. Chen, M. Wang and X. Liu (2009). "Possible influence of anthropogenic aerosols on cirrus clouds and anthropogenic forcing." Atmos. Chem. Phys. **9**(3): 879-896.

Pueschel, R. F. and S. A. Kinne (1995). "Physical and radiative properties of Arctic atmospheric aerosols." Sci. Total Environ. **160–161**(0): 811-824.

Quinn, P. K., T. S. Bates, E. Baum, N. Doubleday, A. M. Fiore, M. Flanner, A. Fridlind, T. J. Garrett, D. Koch, S. Menon, D. Shindell, A. Stohl and S. G. Warren (2008). "Short-lived pollutants in the Arctic: their climate impact and possible mitigation strategies." Atmos. Chem. Phys. **8**(6): 1723-1735.

Quinn, P. K., G. Shaw, E. Andrews, E. G. Dutton, T. Ruoho-Airola and S. L. Gong (2007). "Arctic haze: current trends and knowledge gaps." Tellus B **59**(1): 99-114.

Rosen, H. and A. D. A. Hansen (1984). "Role of combustion-generated carbon particles in the absorption of solar radiation in the Arctic haze." Geophys. Res. Lett. **11**(5): 461-464.

Rosen, H., T. Novakov and B. A. Bodhaine (1981). "Soot in the Arctic." Atmos. Environ. **15**(8): 1371-1374.

Samset, B. H. and G. Myhre (2011). "Vertical dependence of black carbon, sulphate and biomass burning aerosol radiative forcing." Geophys. Res. Lett. **38**(24): L24802.

Schultz, M. G., A. Heil, J. J. Hoelzemann, A. Spessa, K. Thonicke, J. G. Goldammer, A. C. Held, J. M. C. Pereira and M. van het Bolscher (2008). "Global wildland fire emissions from 1960 to 2000." Global Biogeochem. Cycles **22**(2): GB2002.

Schulz, M., C. Textor, S. Kinne, Y. Balkanski, S. Bauer, T. Berntsen, T. Berglen, O. Boucher, F. Dentener and S. Guibert (2006). "Radiative forcing by aerosols as derived from the AeroCom present-day and pre-industrial simulations." Atmos. Chem. Phys. **6**(12): 5246.

Schwarz, J. P., J. R. Spackman, R. S. Gao, L. A. Watts, P. Stier, M. Schulz, S. M. Davis, S. C. Wofsy and D. W. Fahey (2010). "Global-scale black carbon profiles observed in the remote atmosphere and compared to models." Geophys. Res. Lett. **37**(18)

Sharma, S., E. Andrews, L. Barrie, J. Ogren and D. Lavoue (2006). "Variations and sources of the equivalent black carbon in the high Arctic revealed by long-term observations at Alert and Barrow: 1989–2003." J. Geophys. Res. **111**(D14): D14208.

Sheridan, P. J. (1989). "Characterization of size segregated particles collected over Alaska and the CAnadian high Arctic, AGASP-II flights 204–206." Atmos. Environ. (1967) **23**(11): 2371-2386.

Shindell, D., M. Chin, F. Dentener, R. Doherty, G. Faluvegi, A. Fiore, P. Hess, D. Koch, I. MacKenzie and M. Sanderson (2008). "A multi-model assessment of pollution transport to the Arctic." Atmos. Chem. Phys. **8**(17): 5353-5372.

Shindell, D. and G. Faluvegi (2009). "Climate response to regional radiative forcing during the twentieth century." Nature Geosci. **2**(4): 294-300.

Shindell, D., J. C. I. Kuylenstierna, E. Vignati, R. van Dingenen, M. Amann, Z. Klimont, S. C. Anenberg, N. Muller, G. Janssens-Maenhout, F. Raes, J. Schwartz, G. Faluvegi, L. Pozzoli, K. Kupiainen, L. Höglund-Isaksson, L. Emberson, D. Streets, V. Ramanathan, K. Hicks, N. T. K. Oanh, G. Milly, M. Williams, V. Demkine and D. Fowler (2012). "Simultaneously Mitigating Near-Term Climate Change and Improving Human Health and Food Security." Science **335**(6065): 183-189.

Skeie, R. B., T. Berntsen, G. Myhre, C. A. Pedersen, J. Ström, S. Gerland and J. A. Ogren (2011). "Black carbon in the atmosphere and snow, from pre-industrial times until present." Atmos. Chem. Phys. **11**(14): 6809-6836.

Stier, P., J. H. Seinfeld, S. Kinne, J. Feichter and O. Boucher (2006). "Impact of nonabsorbing anthropogenic aerosols on clear-sky atmospheric absorption." J. Geophys Res. **111**(D18): D18201.

Stohl, A. (2006). "Characteristics of atmospheric transport into the Arctic troposphere." J. Geophys. Res. **111**: D11306.

Stohl, A., Z. Klimont, S. Eckhardt, K. Kupiainen, V. P. Shevchenko, V. M. Kopeikin, and A. N. Novigatsky (2013). " Black carbon in the Arctic: the underestimated role of gas flaring and residential combustion." Atmos. Chem. Phys. **13**: 8833–8855.

Ström, J., K. Okada and J. Heintzenberg (1992). "On the state of mixing of particles due to Brownian coagulation." J. Aerosol Sci. **23**(5): 467-480.

Textor, C., M. Schulz, S. Guibert, S. Kinne, Y. Balkanski, S. Bauer, T. Berntsen, T. Berglen, O. Boucher, M. Chin, F. Dentener, T. Diehl, R. Easter, H. Feichter, D. Fillmore, S. Ghan, P. Ginoux, S. Gong, A. Grini, J. Hendricks, L. Horowitz, P. Huang, I. Isaksen, I. Iversen, S. Kloster, D. Koch, A. Kirkevåg, J. E. Kristjansson, M. Krol, A. Lauer, J. F. Lamarque, X. Liu, V. Montanaro, G. Myhre, J. Penner, G. Pitari, S. Reddy, Ø. Seland, P. Stier, T. Takemura and X. Tie (2006). "Analysis and quantification of the diversities of aerosol life cycles within AeroCom." Atmos. Chem. Phys. **6**(7): 1777-1813.

Textor, C., M. Schulz, S. Guibert, S. Kinne, Y. Balkanski, S. Bauer, T. Berntsen, T. Berglen, O. Boucher, M. Chin, F. Dentener, T. Diehl, J. Feichter, D. Fillmore, P. Ginoux, S. Gong, A. Grini, J. Hendricks, L. Horowitz, P. Huang, I. S. A. Isaksen, T. Iversen, S. Kloster, D. Koch, A. Kirkevåg, J. E. Kristjansson, M. Krol, A. Lauer, J. F. Lamarque, X. Liu, V. Montanaro, G. Myhre, J. E. Penner, G. Pitari, M. S. Reddy, Ø. Seland, P. Stier, T. Takemura and X. Tie (2007). "The effect of harmonized emissions on aerosol properties in global models – an AeroCom experiment." Atmos. Chem. Phys. **7**(17): 4489-4501.

Twomey, S. (1977). "The influence of pollution on the shortwave albedo of clouds." J. Atmos. Sci. **34**: 1149-1152.

Valero, F. P. J., T. P. Ackerman and W. J. Y. Gore (1984). "The absorption of solar radiation by the Arctic atmosphere during the haze season and its effects on the radiation balance." Geophys. Res. Lett. **11**(5): 465-468.

Wang, C. (2004). "A modeling study on the climate impacts of black carbon aerosols." J. Geophys. Res. **109**(D3): D03106.

Wang, C. (2007). "Impact of direct radiative forcing of black carbon aerosols on tropical convective precipitation." Geophys. Res. Lett. **34**(5): L05709.

Wang, H., R. C. Easter, P. J. Rasch, M. Wang, X. Liu, S. J. Ghan, Y. Qian, J. H. Yoon, P. L. Ma and V. Velu (2013). "Sensitivity of remote aerosol distributions to representation of cloud-aerosol interactions in a global climate model." Geosci. Model Dev. Discuss. **6**(1): 331-378.

Warren, S. G. and W. J. Wiscombe (1980). "A Model for the Spectral Albedo of Snow. II: Snow Containing Atmospheric Aerosols." J. Atmos. Sci. **37**(12): 2734-2745.

Warren, S. G. and W. J. Wiscombe (1985). "Dirty snow after nuclear war." Nature **313**(6002): 467-470.

I

Atmos. Chem. Phys., 13, 211–224, 2013
www.atmos-chem-phys.net/13/211/2013/
doi:10.5194/acp-13-211-2013

Atmospheric Chemistry and Physics

The Arctic response to remote and local forcing of black carbon

M. Sand[1], T. K. Berntsen[1], J. E. Kay[2], J. F. Lamarque[2], Ø. Seland[3], and A. Kirkevåg[3]

[1]Department of Geosciences, Meteorology and Oceanography Section, University of Oslo, Oslo, Norway
[2]National Center for Atmospheric Research, Boulder, Colorado, USA
[3]Norwegian Meteorological Institute, Oslo, Norway

Correspondence to: M. Sand (maria.sand@geo.uio.no)

Received: 15 June 2012 – Published in Atmos. Chem. Phys. Discuss.: 26 July 2012
Revised: 13 December 2012 – Accepted: 18 December 2012 – Published: 9 January 2013

Abstract. Recent studies suggest that the Arctic temperature response to black carbon (BC) forcing depend strongly on the location of the forcing. We investigate how atmospheric BC in the mid-latitudes remotely influence the Arctic climate, and compare this with the response to atmospheric BC located in the Arctic itself. In this study, idealized climate simulations are carried out with a fully coupled Earth System Model, which includes a comprehensive treatment of aerosol microphysics. In order to determine how BC transported to the Arctic and BC sources not reaching the Arctic impact the Arctic climate, atmospheric BC concentrations are scaled up in the mid-latitudes (28–60° N) and in the Arctic (60–90° N), respectively. Estimates of the impact on the Arctic energy budget are represented by analyzing radiation fluxes at the top of the atmosphere and at the surface, surface turbulent fluxes, and meridional heat transport in the atmosphere. Our calculations show that increased BC forcing in the Arctic atmosphere reduces the surface air temperature in the Arctic with a corresponding increase in the sea-ice fraction, despite the increased planetary absorption of sunlight. The analysis indicates that this effect is due to a combination of a weakening of the northward heat transport caused by a reduction in the meridional temperature gradient and a dimming at the surface. On the other hand we find that BC forcing at the mid-latitudes warms the Arctic surface significantly and decreases the sea-ice fraction. Our model calculations indicate that atmospheric BC forcing outside the Arctic may be more important for the Arctic climate change than the forcing in the Arctic itself. These results suggest that mitigation strategies for the Arctic climate should also address BC sources in locations outside the Arctic even if they do not contribute much to BC in the Arctic.

1 Introduction

Arctic temperatures have increased at a rate about twice as fast as the global mean rate during the last decades (AMAP, 2011a). Many inter-related factors arising both from internal climate variability and external climate forcing could have contributed to this greater-than-global Arctic warming. Strong local feedbacks (snow/ice-albedo, clouds) enhance the warming by long-lived greenhouse gases and other forcings. In addition increased poleward heat transport and absorbing aerosols (black carbon) may have contributed to the amplification (IPCC, 2007). Accompanied by the temperature increase, the Arctic has experienced a longer melt season with an earlier spring melt and a decrease in the sea-ice extent (AMAP, 2011a). Black carbon (BC) aerosols absorb solar radiation and heat the surrounding air. This direct effect of BC may be potentially large in the Arctic, as the absorbing aerosols are located over highly reflective snow/ice surfaces (Pueschel and Kinne, 1995; Hansen and Nazarenko, 2004). In general added atmospheric heat will increase the downward fluxes of longwave radiation and sensible heat, and thus warm the underlying surface. However, models and measurements (Koch et al., 2009a) indicate that BC aerosols are located mainly the free troposphere and in may further stabilize the Arctic atmosphere, thereby limiting the downward flux of sensible heat and the potential surface warming.

BC aerosols in the Arctic originate from emissions mainly at mid-latitudes that are transported northwards (Barrie, 1986; Law and Stohl, 2007). Sources of BC include both anthropogenic sources (e.g. energy and industrial production, domestic combustion and transport) and natural sources (forest and grassfires induced from lightening). During winter the northward transport is strongest, and the lifetime of BC

in the atmosphere is longer, causing a maximum BC concentration in the Arctic in late winter and spring (Sharma et al., 2006). The elevated BC concentrations also extend into the melting season, which could make BC particularly important in the Arctic. BC aerosols affect the atmospheric temperature gradients and can therefore change the atmospheric heat transport. In addition, BC aerosols can have an indirect effect on clouds by influencing the cloud properties and cloud lifetime via microphysical interactions. BC can also affect the distribution of clouds by changing the stability of the atmosphere, often referred to as the semi-direct effect (Koch and Genio, 2010).

Absorbing aerosols affect the climate in numerous ways and thus there are large uncertainties in estimating the net BC forcing. While the direct radiative forcing of BC increases with increasing altitude of the BC perturbation (e.g. Samset and Myhre, 2011), models indicate that the climate efficacy (surface temperature response per unit forcing) is decreasing with increasing altitude of the BC (Hansen et al., 2005; Ban-Weiss et al., 2011). Because of the short lifetime of BC compared to well-mixed greenhouse gases, BC has a potential for short-term climate control strategies (Hansen et al., 2000; Levy et al., 2008; Jacobson, 2010; Shindell et al., 2012). In order to identify the best options for emission reductions there is a need for improving the understanding of the role of BC aerosols in the Arctic (AMAP, 2011b) and how the response of the Arctic climate depends on the location of BC forcing. Shindell (2007) demonstrated that the climate response in the Arctic is highly correlated with mid-latitude forcing during non-summer seasons, due to the large-scale dynamics influencing the Arctic climate. In these months the Arctic surface temperature response can show opposite signs to the local forcing. Results from Menon et al. (2002) also indicate that forcing from BC can have a climate impact away from the forcing area, by local atmospheric heating and dynamical transport. Shindell and Faluvegi (2009) perturbed forcings by enhancing the concentrations of BC aerosols in different latitude bands and found that for the Arctic latitude band, the Arctic surface air temperature (SAT) decreased, despite a positive forcing at the top of the atmosphere, i.e. a regional negative climate efficacy. Shindell and Faluvegi attributed this mainly to a reduction in the poleward heat flux following increased absorption of incoming solar radiation by BC and local heating in the free troposphere. For positive direct forcing by BC aerosols in the mid-latitude band the Arctic surface temperature response was positive (warming).

With the increasing focus on the effect of BC aerosols on the Arctic climate, there is a need to test the robustness of the findings by Shindell and Faluvegi by reproducing parts of the experiment with a different climate model; to analyze the Arctic climate response to BC perturbations in the Arctic (60–90° N) and northern mid-latitude (28–60° N) atmosphere respectively. Expanding on the previous study, we want to understand and quantify the contribution from the different processes that are important for forcing by components absorbing short-wave radiation and the response in the Arctic, including an analysis of the perturbation to the energy budget of the Arctic atmosphere. Idealized climate simulations with increased BC concentrations in the two separate latitude bands have been performed with a fully coupled earth system model, the NorESM, to include dynamic responses, feedbacks from sea ice cover and sea surface temperatures (SSTs). The atmospheric model includes a comprehensive treatment of aerosol microphysics, accounting for aerosol nucleation, condensation, coagulation and cloud processing, and calculates the conversion of BC to a hydrophilic state where it can be scavenged by precipitation (Kirkevåg et al., 2008; Seland et al., 2008). The wet deposition is calculated in full integration with the cloud and precipitation schemes. The two experiments are compared with a control run to analyze the response in the Arctic temperatures to the two forcings, including changes in sea-ice, cloud cover and the meridional energy transport into the Arctic.

2 Data and methods

2.1 NorESM

The climate model used in this study is the Norwegian Earth System Model, NorESM (Bentsen et al., 2012; Iversen et al., 2012), to a large extent based on the Community Climate System Model CCSM4.0 (Gent et al., 2011), developed at the National Center for Atmospheric Research (NCAR). The model is run fully coupled with an atmospheric model, an ocean model, a land model and a sea-ice model. The atmospheric part of NorESM, CAM4-Oslo, includes a scheme for calculating the life-cycle of aerosols along with their optical and physical properties and is thoroughly described in Kirkevåg et al. (2008); Seland et al. (2008) and Kirkevåg et al. (2012). The ocean model in NorESM, MICOM, is an updated version from the Bergen Climate Model, BCM (Furevik et al., 2003; Otterå et al., 2009). The sea-ice model (CICE4) and the land model (CLM4) in NorESM are the same as in CCSM4.0, except that the deposition of BC and mineral dust aerosols onto snow and sea-ice are given by CAM4-Oslo instead of using pre-calculated deposition fields as is done in CCSM4.0.

Aerosols in NorESM

The prognostic aerosols and aerosol precursors in CAM4-Oslo include sea-salt, mineral dust, dimethyl sulfide (DMS), sulphur dioxide, sulphate, BC and particulate organic matter (OM) and they interact online with the cloud microphysics, radiation and meteorology in the model. The present-day (2000) emissions are taken from Lamarque et al. (2010). Aerosol optical properties and size distributions (for calculation of cloud droplet number concentrations, CDNC) are calculated by use of look-up tables, where the entries in the tables are calculated by a single air parcel model for a wide

range of atmospheric conditions. Both the direct effect and the first and second indirect effects are calculated. The direct effect of aerosols is caused by the scattering and absorption of radiation, mainly in the shortwave spectrum. The indirect effects of aerosols are due to their interaction with clouds, by acting as cloud condensation nuclei or ice nuclei. The aerosols can change the number and size of cloud droplets (the first indirect effect; Twomey, 1977) and the lifetime of clouds (the second indirect effect; Albrecht, 1989). In the model the only process which causes the second indirect effect is the auto-conversion of cloud droplets to precipitation in warm clouds (Hoose et al., 2009). Absorbing aerosols embedded in or near a cloud layer may also reduce the cloud cover by heating the air and promoting cloud evaporation, leading to a positive semi-direct effect (Hansen et al., 1997). The semi-direct effect of BC can also be negative (e.g. if the BC increase the static stability). In the look-up tables, size distributed aerosol number concentrations and composition, as well as bulk optical properties, have been calculated from basic physico-chemical processes. The concentrations are tagged according to size mode (nucleation, aitken, accumulation, coarse) and production mechanism (nucleation, condensation, coagulation, aqueous chemistry).

BC is emitted from biomass burning, fossil fuel combustion and biofuels. The total annual emissions of BC are $7.7\,\mathrm{Tg\,yr^{-1}}$. When emitted from biomass burning, BC and OM are assumed internally mixed with each other. Primary BC particles are emitted as nucleation and accumulation mode BC and internally mixed aitken mode OM and BC. Externally mixed BC is hydrophobic, and turns gradually into hydrophilic, internally mixed aerosols by condensation of gaseous sulphate, or by coagulation with sulphate, sea-salt or OM. BC is removed from the atmosphere by dry deposition and wet removal, although the latter process dominates the total numbers.

2.2 Experimental setup

The model is set up with a Finite Volume dynamical core with 26 vertical layers and with a $1.9 \times 2.5°$ horizontal grid resolution. For each simulation the model is run 60 yr from a 140 yr spin-up with the same initial conditions and the same present-day emissions. In the two perturbed simulations the model is run with the same emissions as the control run, but in the radiation code the BC concentrations are multiplied by a factor of 10 in the Arctic (60–90° N; "the ARC experiment") and mid-latitudes (28–60° N; "the MID experiment"), respectively. The BC concentrations have been multiplied by 10 in order to get a statistically significant climate signal in the 60 yr simulations. It is worth noting that the scaling is larger than in previous studies (e.g. Shindell and Faluvegi, 2009; Koch et al., 2009b), however, many previous studies have used models with a simpler q-flux slab ocean, while in this study we use a fully coupled ocean. A substantial scaling is necessary to obtain a robust result, however, it should not be too large so that the underlying assumption that the response is close to linear is not valid. Hansen et al. (2005) found that the response was close to linear for scaling giving a global aerosol RF of the order of $1\,\mathrm{W\,m^{-2}}$. The global RF following the scaling applied here is always below $1.5\,\mathrm{W\,m^{-2}}$ (cf. Sect. 3.2). A recent study by Chung et al. (2012) shows that the direct radiative forcing from absorbing carbonaceous aerosols could be a factor 2 higher than previously estimated (e.g. Forster et al., 2007). In order to calculate the radiative forcing at the TOA with identical meteorology for each simulation, the same 3 experiments ($1 \times$ BC, $10 \times$ BC mid latitudes and $10 \times$ BC in the Arctic) is repeated in separate 5 yrs offline simulations. In the offline simulations the meteorology is driven by prescribed NCAR CAM4 aerosols, CDNC and greenhouse gases and is not affected by the perturbation in the BC concentrations. In the online 60 yr simulations on the other hand, the aerosol, cloud and radiation is fully coupled so the aerosols are allowed to affect the meteorology and thus the meteorology in the online simulations is different from the offline simulations. The BC concentrations in the offline and the online simulations are comparable in size (differ 13 % in the Arctic and 6 % in the mid latitudes), so the two simulations set-ups can be used side-by-side. Note that only atmospheric BC has been perturbed in this study and the radiative forcing and climate response from BC deposition on snow and ice (e.g. Flanner et al., 2007) lie outside the scope of this study.

2.3 The Arctic energy budget

To understand the responses in the Arctic climate due to the BC perturbations we analyze the energy budget of the Arctic atmosphere in detail. The forcing and the temperature response in the Arctic influence the meridional temperature gradient, which may dampen or strengthen the atmospheric heat transport into the Arctic. When studying Arctic climate change and local feedbacks, it is important to include the energy transport because of the strong coupling between Arctic feedback mechanisms and the energy transport into the Arctic (Hwang et al., 2011). The northward heat transport (NHT) is defined as the net atmospheric flux of heat from lower latitudes into the Arctic region. Following Porter et al. (2010) and Kay et al. (2012a) the atmospheric NHT can be calculated by looking at the energy budget for an atmospheric column,

$$\mathrm{NHT} = \frac{\mathrm{d}E}{\mathrm{d}t} - F_{\mathrm{TOA}} + F_{\mathrm{SURF}} \quad (1)$$

E is the atmospheric energy, F_{TOA} is the net energy budget at the top of the atmosphere and F_{SURF} is the net energy budget at the surface. F_{TOA} is defined as:

$$F_{\mathrm{TOA}} = \mathrm{SW_{TOA}} + \mathrm{LW_{TOA}} \quad (2)$$

SW_{TOA} is the net incoming shortwave radiation and LW_{TOA} is the net outgoing long wave radiation. F_{SURF} is defined as:

$$F_{SURF} = SW_{SURF} + LW_{SURF} + LHFLX + SHFLX \quad (3)$$

SW_{SURF} is the net surface shortwave radiation, LW_{SURF} is the net surface long wave radiation, LHFLX is the latent heat flux and SHFLX is the sensible heat flux. The model is run with a fully coupled ocean model allowing for changes in the heat transport in the ocean. With the atmospheric perspective adopted here, the impact of this will be represented by a change in the surface fluxes. Since the LHFLX model output ($LHFLX_{output}$) does not include the latent heat released when water droplets freeze and form snow that reach the surface, this has been calculated using

$$LHFLX = -(LHf \cdot \rho \cdot PRECsnow) - LHFLX_{output} \quad (4)$$

LHf is the latent heat of fusion (in J kg^{-1}), ρ is the density of water (in kg m^{-3}) and $PREC_{snow}$ is the snow precipitation rate (water equivalent) (in m s^{-1}).

We use the same sign convention as Kay et al. (2012a), with all terms in F_{TOA} defined positive when the atmosphere gains energy and all term in F_{SURF} defined positive when the surface gains energy; i.e. positive downward both for the F_{TOA} and the F_{SURF}. For annual averages, the energy storage term is small and negligible compared to F_{TOA}, F_{SURF} and NHT. The net atmospheric NHT can then be calculated as a residual of the remaining terms, F_{TOA} and F_{SURF}.

3 Simulated black carbon

3.1 BC concentrations

The simulated annual mean BC column burden, the zonal annual mean BC concentrations and the Arctic monthly mean BC column burden for the reference run are shown in Fig. 1. Because of the short lifetime of BC on the order of days, the concentrations are largest close to the source regions near the surface; over densely populated and industrialized areas in China, Europe and the United States and over areas with biomass burning in Africa and South America. In the Arctic, on the other hand, the concentrations increase with height and the maximum concentrations are found in the middle troposphere (Fig. 1b). The strong static stability in the Arctic suppresses turbulent mixing between the surface and the upper troposphere, in particular during winter and early spring. The global mean BC column burden in the model is 280 µg m^{-2}. This is in good agreement with the multi-model mean value of 250 µg m^{-2} in the AeroCom model intercomparison project (Schulz et al., 2006). Averaged in each latitude band, the BC column burden is 180 µg m^{-2} in the Arctic and 360 µg m^{-2} in the mid-latitudes. In the model, the BC concentrations have a seasonal pattern in the Arctic, with a build up during winter, due to a combination of stronger northward transport and longer lifetime of the aerosols (Bauer et al., 2010; Liu et al., 2011; Lund and Berntsen, 2012). In the model this leads to a maximum in the BC column burden in the Arctic during May.

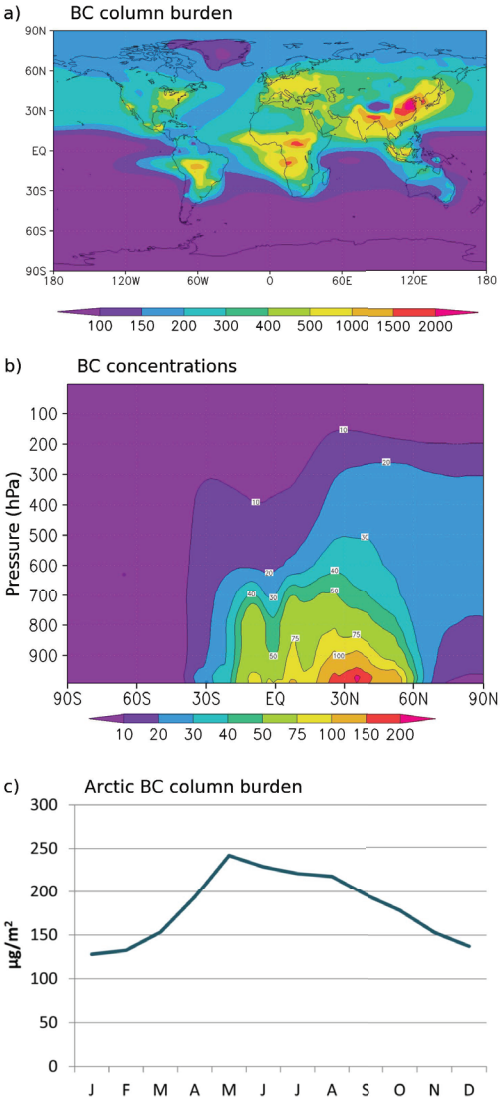

Fig. 1. (a) Annual mean BC column burden (in µg m^{-2}); **(b)** zonal annual mean BC concentration (in ng m^{-3}) and **(c)** Arctic monthly mean BC column burden (in µg m^{-2}) for the CONTROL run with 2000 emissions.

Koch et al. (2009a) compared the vertical distribution of BC in different models to observations from aircraft

campaigns. They showed that the models (including a predecessor of the NorESM model, labeled UiOGCM in Koch et al., 2009a) in general underestimate high latitude BC concentrations in the lower troposphere and tend to overestimate the BC concentrations in the upper troposphere. A comparison of the monthly mean observed and modeled surface BC concentrations of three Arctic stations for the years 2005 and 2006 is included in Fig. 2a). The measurements from Barrow are from the NOAA GMD database (www.esrl.noaa.gov/gmd) and measurements from Zeppelin station are provided by K. Eleftheriadis and S. Vratolis (Eleftheriadis et al., 2009) from the EBAS database (http://ebas.nilu.no). The measurements for the Alert station are provided by S. Sharma at Environment Canada. The concentrations show a wintertime build-up of Arctic haze and a summertime minimum. The variability in the observed concentrations are greater than in the modeled concentrations as should be expected since the observations are point sources from 2 yr only, while the modeled concentrations constitutes a climatology for a larger grid cell box ($\sim 2°$). The May 2006 measurement from the Zeppelin station is an outlier, as this was a week coincident with an extreme weather situation and agricultural fires, causing a direct transport of agricultural fires from Eastern Europe to the Zeppelin station and record-high air pollution levels in the European Arctic (Stohl et al., 2007). The modeled surface concentrations are significantly underestimated during winter and early spring. There are a number of possible causes for the underestimation of BC at ground level, such as too low BC emissions at high latitudes, too rapid aging and/or too stable boundary layer in the model. The anthropogenic emissions, including domestic wood burning, are included as annual averages, and emissions from flaring, a potentially important high latitude source, is not included at all due to lack of emission data. Generally, climate models tend to underestimate the wintertime surface BC concentrations in the Arctic compared to measurements (Shindell et al., 2008). NorESM has a larger aerosol absorption optical depth at higher latitudes compared to most other models in the model comparison study AEROCOM (Myhre et al., 2012; Samset et al., 2012). The model may overestimate BC concentrations in the Arctic free troposphere, but the vertical profile of Arctic BC is not well known due to sparse vertical measurements. In terms of the climate response to direct absorption by BC aerosols which is the focus here, the large underestimation of surface BC at high latitudes during the dark season is of minor importance. During the summer season and early autumn (May–October) the modeled surface concentrations are within the range of the observed concentrations.

Modeled and observed monthly mean BC surface concentrations for 11 stations at mid latitudes are shown in Fig. 2b). The observed concentrations are from the EMEP database (http://www.emep.int) for 2002/2003. The model underestimates the observed concentrations for most stations particularly during the winter season and lacks a pronounced seasonal variation. For a further model validation of BC the reader is referred to Kirkevåg et al. (2012). In Kirkevåg et al. (2012) it is shown that the NorESM model with 2000 emissions underestimates surface BC concentrations globally by 36 %.

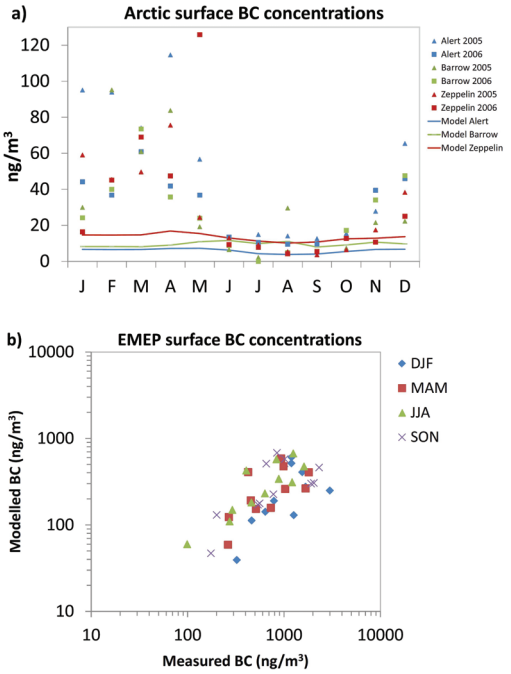

Fig. 2. (a) Monthly mean observed (markers) and modeled (lines) surface BC concentrations from 3 Arctic stations 2005/2006; **(b)** seasonal mean observed and modeled surface BC concentrations in Europe (from the EMEP 2002/2003 campaign). The modeled surface concentrations are from the control run. All units in ng m^{-3}.

3.2 BC forcing in the Arctic and the mid-latitudes

The direct and indirect radiative forcing of BC is calculated as the difference in incoming and outgoing solar radiation at the TOA between the offline perturbed runs and the control run. The annual 28–60° N mean direct radiative forcing at the TOA for the MID experiment is estimated to 7.3 W m^{-2} (1.5 W m^{-2} global average) and the indirect forcing is estimated to 0.2 W m^{-2} (0.03 W m^{-2}). For ARC experiment the estimated annual 60–90° N mean direct radiative forcing at the TOA is 6.0 W m^{-2} (0.4 W m^{-2}) and the indirect local forcing at the TOA is 0.1 W m^{-2} (0.01 W m^{-2}). The geographical distribution of the BC annual mean direct radiative forcing from ARC and MID is shown in Fig. 3. The distribution depends on the column burden of BC, but also on the albedo of the underlying surface, vertical distribution

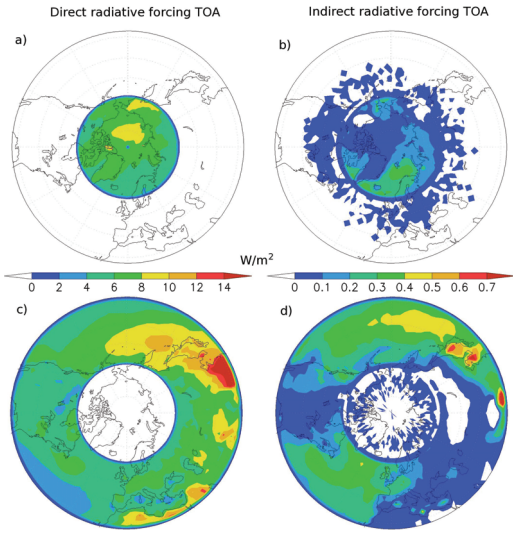

Fig. 3. Annual mean direct radiative forcing (left) and indirect radiative forcing (right) at the TOA for the ARC-CONTROL (top) and the MID-CONTROL (bottom). All units in W m^{-2}.

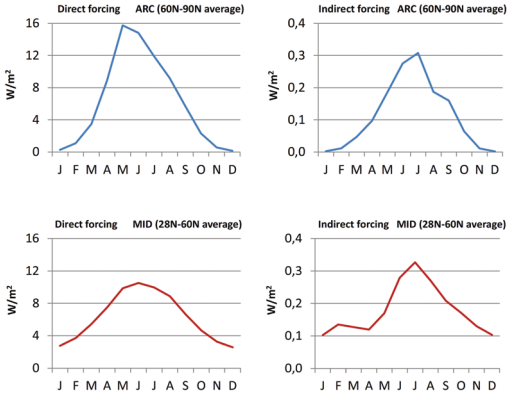

Fig. 4. Monthly mean direct forcing (left) and indirect forcing (right) at the TOA for the ARC-CONTROL 60–90° N average (top) and the MID-CONTROL 28–60° N average (bottom). All units in W m^{-2}.

of the aerosols relative to the clouds and the amount of incoming solar radiation. The high surface albedo in the Arctic regions causes the BC radiative forcing to be large in this area, despite the smaller BC burden (see Fig. 1). The forcing effiency (RF normalized to burden change) is thus significantly higher in the Arctic (3600 W g^{-1}) than at mid-latitudes (and 2300 W g^{-1}). In the fully coupled simulations there can be a small radiative forcing outside the region where the BC concentrations are scaled up (i.e. the ARC or the MID region), because of the changes in surface and cloud albedo and redistribution of BC due to changes in circulation and scavenging rates. The indirect effect of BC aerosols is largest over the oceans, and is much smaller than the direct radiative effects of BC.

Figure 4 shows the monthly mean BC direct radiative forcing at TOA for the ARC experiment (60–90° N average) and the MID experiment (28–60° N average). The forcing peaks in May in the Arctic (15 W m^{-2}) for several reasons; the solar insolation and the BC concentrations are both close to their maxima, and it is early in the melt season, with still a great amount of snow and ice-covered surface with a high surface albedo. May is one of the months when the modeled BC concentrations are underestimated compared to observations (see Fig. 2). During the polar night, the Arctic forcing approaches zero. The mid latitude forcing peaks in the summer, but is still fairly high during the winter months, due to a combination of higher solar radiation in the mid-latitudes compared to the Arctic, as well as higher BC emissions and surface albedo in the mid-latitudes during winter compared to the summer season.

4 Climate response

The next section show figures from the fully coupled runs, in which the BC aerosols are allowed to affect the meteorology. The change in the vertical temperature profile for the ARC and the MID experiment is shown in Fig. 5. In both experiments the temperature increases above 800 hPa in the Arctic. The maximum temperature increase is found around 200 hPa, in the latitude band where the BC profile has been scaled up. The temperature increase is larger over a much larger volume of the atmosphere for the MID experiment than for the ARC experiment. In both our experiments the warming in the Arctic is most pronounced in the upper troposphere, but for very different reasons. In the ARC case warming is caused by the direct absorption of solar radiation by BC in the free troposphere, and further enhanced by semi-direct and surface albedo effects. In the MID experiment the heat is generated by absorption and heating at all altitudes at mid-latitudes, but since the transport to the Arctic mainly follows isentropic surfaces (Hoskins, 1991), the maximum heating in the Arctic is also in this case in the upper troposphere. While there is a warming throughout the troposphere in the MID experiment, the ARC forcing causes a cooling at the surface north of 60° N, in agreement with the response found by Shindell and Faluvegi (2009).

Figure 6 shows the seasonal cycle for the Arctic temperature response, averaged north of 60° N for both the ARC and the MID forcing. The cooling at the surface for the ARC forcing is prominent all year except in the summer

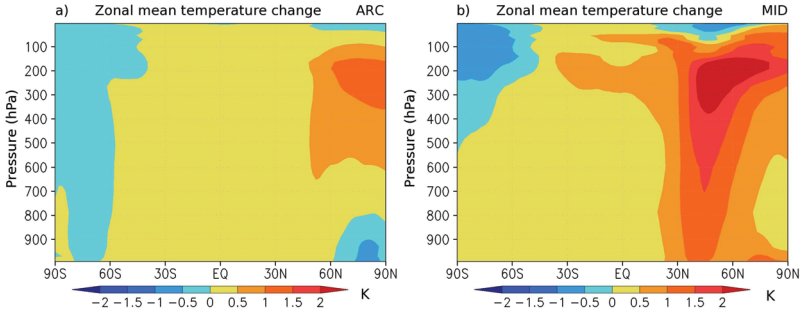

Fig. 5. Zonal annual mean temperature change (in K) for **(a)** the ARC-CONTROL and **(b)** the MID-CONTROL.

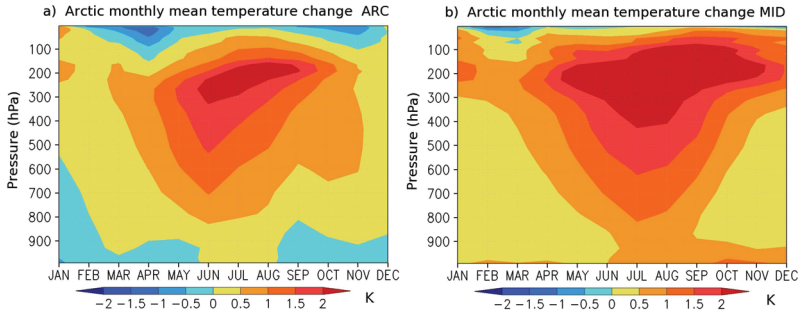

Fig. 6. Monthly Arctic mean (60–90° N) temperature change (in K) for **(a)** the ARC-CONTROL and **(b)** the MID-CONTROL.

months. The warming of the Arctic surface in the summer is likely due to a combined effect of lower static stability during summer/autumn and increased downward longwave radiation and heat fluxes. In both experiments the warming increases rapidly with height, in particular during summer. The period of surface warming is not centered round mid summer in June when the incoming solar radiation is at its maximum, but is slightly shifted towards the autumn when the snow/sea-ice cover in the Arctic is at its minimum. For the MID forcing the surface warming is strongest during summer and autumn. The warming in the upper troposphere has a maximum during summer and early autumn. It is worth noting that even in the MID case where there is no local forcing in the free troposphere due to enhanced absorption by BC, there is a comparable vertical gradient in the warming as in the ARC case and thus an increase in the static stability.

The geographical distribution of the annual mean SAT response from the ARC and the MID forcing is shown in Fig. 7. The Arctic annual mean SAT response is −0.4 K for the ARC forcing with a cooling over most of the Arctic Ocean and a warming over Greenland. There is a maximum cooling 2 K over the Barents Sea. For the MID forcing the Arctic annual mean SAT response is 1.1 K with a warming across the entire Arctic Ocean and with a maximum warming of 2 K over the Barents Sea. This area along the sea-ice edge is the area with particularly large climate variability and large local feedbacks. Our results in general agree with the response in SAT from BC forcing in Shindell and Faluvegi (2009). Shindell and Faluvegi estimated an Arctic SAT response per unit global forcing of $-1.2\,\mathrm{K\,W^{-1}\,m^2}$ from BC aerosols in the Arctic and $0.8\,\mathrm{K\,W^{-1}\,m^2}$ Arctic SAT response from BC aerosols in the mid latitudes. Our estimated Arctic SAT response per unit global forcing is $-1.1\,\mathrm{K\,W^{-1}\,m^2}$ from BC aerosols in the Arctic and $0.7\,\mathrm{K\,W^{-1}\,m^2}$ from BC aerosols in the mid latitudes, respectively. The global SAT response per unit global forcing is $0.2\,\mathrm{K\,W^{-1}\,m^2}$ for both experiments, in accordance with Shindell and Faluvegi.

Shindell and Faluvegi explained the negative surface temperature response mainly as a result of a reduction in the pole-ward heat flux following local heating by absorbing BC aerosols. However, there are also significant changes in the surface energy fluxes due to direct and semi-direct effects of the BC aerosols as well as local feedbacks.

Through a number of factors BC aerosols may affect the cloud cover in the Arctic, including different semi-direct effects like changes in the static stability or "burn-off" effects, or changes related to a general climate impulse, including changes in surface fluxes, surface albedo and heat transport.

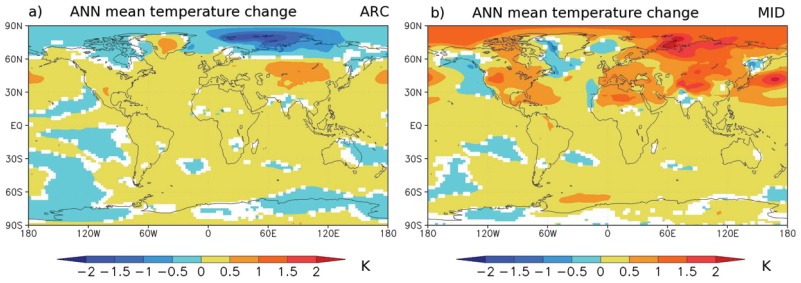

Fig. 7. Annual mean surface air temperature change (in K) for **(a)** the ARC-CONTROL and **(b)** the MID-CONTROL. White areas are not significant on a 95 % level.

The Arctic monthly mean total cloud cover is shown in Fig. 8. Both experiments show an increase in the Arctic total cloud cover during summer when the cloud fraction is peaking. The increase is related to low clouds. For the ARC experiment there is a reduction in the high clouds from April to October. The decrease in the high cloud cover in Arctic for the ARC experiment during the seasons with solar radiation available may indicate a burn-off effect, while the increase in low clouds may be due to changes in the surface temperatures, as both experiments show an increase in the low cloud cover during summer when the surface temperature change is positive. In addition a stabilizing effect by the BC aloft in the ARC experiment may have contributed in this experiment. Kay and Gettelman (2009) found, using observations and atmospheric reanalysis, that near-surface static stability and surface cover can exert significant control on low Arctic cloud presence. It is worth noting that the Arctic clouds in the model are too optically thick because they have excessive liquid water paths when compared to observations (de Boer et al., 2011; Kay et al., 2012b). Too high amounts of cloud water in the model may suppress the aerosol indirect effect.

The geographical distribution of the annual mean cloud cover fraction for low and high clouds is shown in Fig. 9. Both experiments show a decrease in the high cloud cover in the latitude band where BC is scaled up. The cloud cover decreases over the Barents Sea in the ARC experiment, associated with the increase in sea ice and cooling of the surface in this area. The cloud cover increases in most parts in the Arctic for the MID experiment both for low and high clouds. At mid latitudes there is a reduction in the low clouds over land areas. The low cloud cover increases over the oceans. Over the oceans, the BC aerosols are located higher up in the atmosphere and may enhance the underlying stratocumulus clouds, by stabilizing the atmosphere beneath, and reduce mixing with dry air above (Johnson et al., 2004).

The geographical distribution of the changes in the sea-ice cover is shown in Fig. 10. For the ARC forcing there is an increase in the sea-ice cover, increasing the surface albedo. The geographical pattern closely resembles the geographical

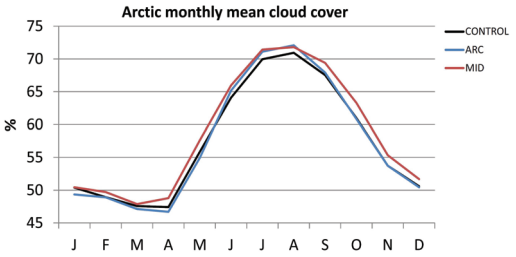

Fig. 8. Monthly Arctic mean cloud cover (in %) for the CONTROL run (black), the ARC experiment (blue) and the MID experiment (red).

patterns of the surface temperature response. For the MID forcing there is a corresponding decrease in the sea-ice cover.

5 Heat budget analysis

A perturbation to the atmospheric concentrations of absorbing aerosols leads to a radiative forcing and a climate response as described above. The full climate response can be analyzed in terms of forcing specific fast responses and general climate feedbacks. The fast response or rapid adjustment refers to the adjustment of the stratosphere, troposphere and the land surface before any change in annual-mean surface temperature (ΔT_S) occurs. The response that depends on ΔT_S is called the slow response or feedback and is usually represented as change in the specific variable per unit ΔT_S (Hansen et al., 2005; Bala et al., 2010). In the case of absorbing aerosols the fast response include semi-direct and indirect cloud effects. At high latitudes even parts of the response in the sea-ice cover could be due to a fast response as the energy balance of the ice is not only determined by heat conduction from the atmosphere and sea water, but also by the surface radiation budget. Hansen et al. (2005) suggested quantifying the fast responses by looking at the difference between an atmospheric only simulation (approximated by

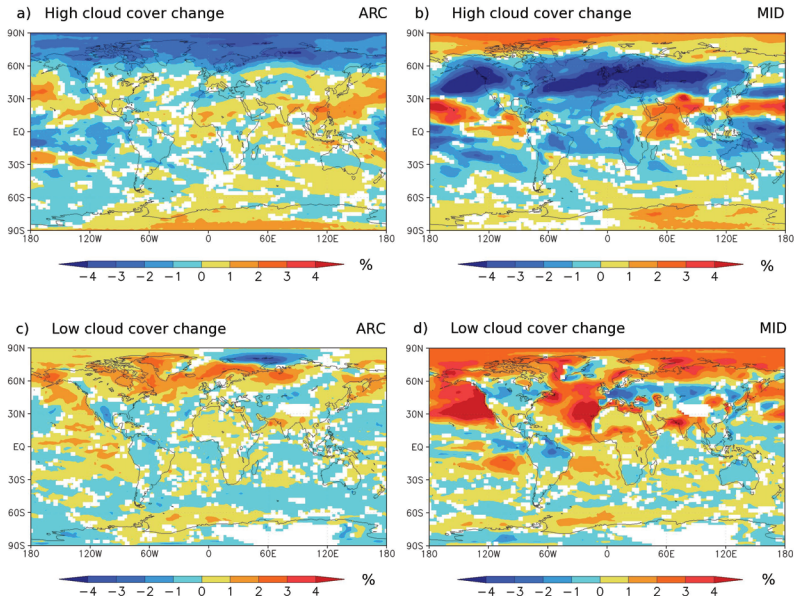

Fig. 9. Annual mean cloud cover change (in %) for high clouds (top) and low clouds (bottom) for ARC-CONTROL (left) and the MID-CONTROL (right). White areas are not significant on a 95 % level.

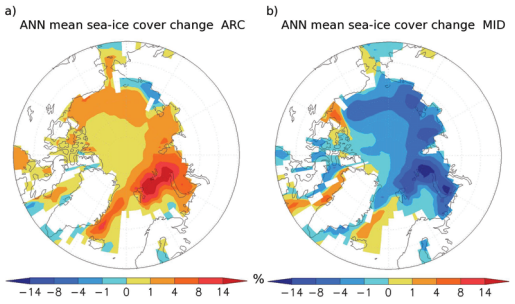

Fig. 10. Annual mean sea-ice cover change (in %) for **(a)** the ARC-CONTROL and **(b)** the MID-CONTROL. White areas are not significant on a 95 % level.

a simulation with fixed SSTs) and the response in the fully coupled system.

In the study presented here we have not performed an atmospheric only simulation and it is therefore not possible to identify to what extent the responses are pure feedbacks in the system. The Arctic is a region with potentially strong feedbacks through snow/ice-albedo relation. This feedback mechanism is certainly operative in the model. However, we can not rule out the possibility that in the regions where surface cooling occur and sea ice extent increase this can be caused by reduction in net radiation to the surface through direct forcing and fast responses followed by increased sea ice extent and then reduced ΔT_S through decreased fluxes of sensible and latent heat. In the cause-effect chain described above, the increase in sea ice will through the feedback loop further decrease ΔT_S, but it may not be initialized by a change in ΔT_S.

Despite the positive BC forcing at TOA and the heating of the air in the free troposphere, the surface temperature response in the Arctic is negative for the ARC forcing, and positive for the MID forcing. To analyze how BC aerosols affect the Arctic climate, we have calculated the energy budget for the Arctic atmosphere. A summary of the change in the annual mean energy budget terms for the two experiments is given Fig. 11. The terms are positive at TOA when the atmosphere gains energy and positive at the surface when the surface gains energy. Note that all changes in the budget terms are the response to a combination of forcing, fast responses and feedbacks in the Arctic region. For the ARC experiment, the primary forcing through the absorption of solar radiation by the BC aerosols is the main cause for the increase in the net downward SW flux of 5.4 W m^{-2} at the TOA. The associated warming of the air in the free troposphere and changes in clouds and surface properties lead to an increase in the outgoing LW flux at TOA of 1.2 W m^{-2} (thus the negative change in Fig. 11). The net radiative effect, including clouds and aerosol feedbacks (SW-LW) is thus 4.2 W m^{-2} (Arctic

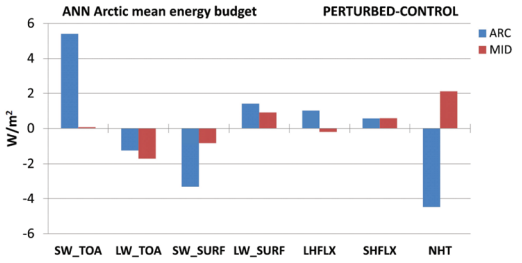

Fig. 11. Difference in the annual mean Arctic atmospheric energy budget terms for the ARC-CONTROL (blue) and MID-CONTROL (red). All units in W m^{-2}. SW_TOA and LW_TOA are the net SW and LW radiation fluxes at TOA; SW_SURF and LW_SURF are the net SW and LW radiation fluxes at the surface; LHFLX and SHFLX are the latent and sensible heat fluxes and NHT is the net atmospheric heat transport. All units in W m^{-2}.

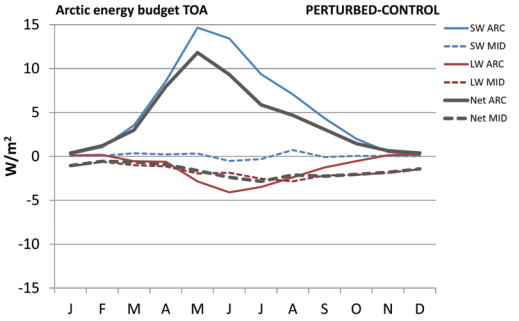

Fig. 12. Changes in the Arctic monthly mean radiative fluxes TOA; incoming SW (blue), outgoing LW (red) and net (black) for the ARC-CONTROL (solid) and MID-CONTROL (dashed). All units in W m^{-2}.

average) which, due to the small heat capacity of the air, must be closely balanced by corresponding negative changes in the heat flux at the boundaries (lateral or to the ocean). However, at the surface the net energy budget is -0.3 W m^{-2}, meaning that in the ARC case the NHT in the atmosphere must be reduced. At the surface, there is a significant reduction in the downward SW flux of 3.3 W m^{-2} due to the dimming effect of the absorption by the BC aerosols in the ARC case. Increased cloudiness and surface albedo may also contribute to the reduction in the net downward SW flux at the surface. The decrease in the NHT for the ARC case is likely to be a result of the increase in the temperatures in the upper Arctic troposphere, decreasing the meridional temperature gradient.

For the MID experiment the primary forcing is located outside the Arctic region, and the change in the net SW flux at the TOA is small, even if there is a consistent increase in the cloud fraction over the Arctic (Fig. 8). However, the heating of the free troposphere by increased NHT and the increase in surface temperatures lead to an increase in the outgoing LW radiation at TOA which is larger than in the ARC case (1.7 W m^{-2} vs. 1.2 W m^{-2}). For the MID forcing the change in the NHT is positive, consistent with the positive temperature response in the mid-latitudes, increasing the meridional temperature gradient between the mid-latitudes and the Arctic, and increasing the heat transport into the Arctic.

Figure 12 shows the seasonal cycle of the changes in the Arctic mean SW and LW radiative fluxes at the TOA for the two perturbed experiments. The seasonal cycle in the TOA radiative imbalance (SW+LW, grey curves) is very different in the two experiments. In the ARC case it is positive and follows the seasonal cycle in the primary forcing (SW) with a sharp peak in late spring (May), while in the MID case it is negative mainly through the changes in the LW fluxes and with a much broader maximum during late summer and fall. The change in the Arctic mean SW flux is close to zero for the MID experiment. This is due to a balance between the increase in albedo due to increased cloud cover (Fig. 8) and the decrease in albedo due to less sea ice (Fig. 10) and snow cover (not shown). The outgoing LW radiation increases for both runs, consistent with the higher temperatures in the free troposphere. The increase in the outgoing LW radiation is largest during the summer season for both runs, when the temperatures are peaking. For the MID forcing the increase in outgoing LW radiation is prominent all year.

Figure 13 shows the seasonal cycle of the Arctic mean energy fluxes at the surface for the control run (top) and for the change in the fluxes between the control run and the two experiments (bottom). The net SW flux decreases for both experiments, with the largest decrease in the ARC experiment during summer (-9 W m^{-2}). The decrease in the net SW flux means that less radiation is reaching the surface, consistent with increased SW absorption by BC higher up in the atmosphere and increased cloudiness, and/or an increase in the amount of reflected radiation from the surface, due to the higher surface albedo. The decrease in annual downwelling solar radiation is twice as large for the ARC experiment as for the MID experiment (5 W m^{-2} vs. 2.6 W m^{-2}). Even though the surface albedo increases in the ARC experiment, the net change in the reflected SW flux is negative because the total amount of radiation reaching the surface is smaller. The MID run shows an increase in the net SW flux in the areas with decreased sea-ice, consistent with increased absorption of SW by the exposed darker ocean in a warmer climate, and a decrease in areas with increased cloudiness. Thus, averaged over the Arctic domain the change in SW flux in the MID experiment is negative.

The net longwave flux at the surface increase for both experiments, which means that more longwave radiation is transferred to the surface from the atmosphere. The factors causing this change are changes in the air temperature and cloudiness as well as the surface temperatures and sea-ice

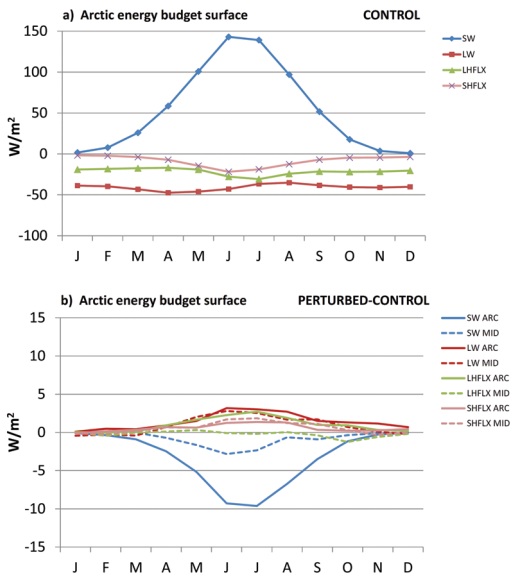

Fig. 13. Seasonal cycle of the Arctic mean energy fluxes at the surface for **(a)** the CONTROL run and **(b)** the changes in the radiative fluxes ARC-CONTROL (solid) and MID-CONTROL (dashed); net SW radiation (blue); net LW radiation (red); latent heat flux (green) and sensible heat flux (pink). All units in W m^{-2}.

cover. For the MID experiment there is decreased net longwave flux at the sea-ice-edge where more long wave radiation is emitted to the atmosphere when the sea-ice melts.

In the reference run, the sensible heat flux is positive downward over the Arctic Ocean, associated with the temperature inversion caused by the net radiative energy loss from the surface. Averaged over 60–90° N however, the sensitive heat flux is negative downward (more energy from the surface to the atmosphere). The change in the Arctic mean sensible heat flux is slightly positive downward for both experiments, which means that more energy is transported from the atmosphere to the surface. The latent heat flux increases downward for the ARC experiment, consistent with the colder surface temperatures, while the latent heat flux is slightly reduced downward during autumn for the MID experiment. During the summer months, the longwave radiative flux and the heat fluxes for the ARC experiment have a maximum (more flux to the surface).

6 Summary and discussion

There is no straightforward one-to-one relationship between the radiative forcing and the temperature response at a given location, as have been shown in previous studies (Boer and Yu, 2003; Shindell and Faluvegi, 2009). BC aerosols heat the surrounding air and alter the local static stability in the atmosphere. Regional changes in the BC concentration also change the temperature gradients affecting the meridional heat transport. Using the NorESM model we find that when BC concentrations are scaled up in the Arctic according to its current vertical profile, the regional surface temperature response is negative despite a positive radiative forcing at TOA. The Arctic surface temperature response is similar to the results found in Shindell and Faluvegi (2009). We find that the BC climate response has a regional nature and this regionality is likely linked to sea ice loss. The surface cooling can be explained by a combination of changes in the vertical fluxes of heat and radiation, cloud cover and a reduction in the meridional heat transport from lower latitudes. There is an upper troposphere heating by absorption of SW radiation, a surface dimming effect that reduces the downwelling solar radiation, a decrease in the high cloud cover and an increase in the low cloud cover. The reduction in the meridional heat transport is likely caused by a reduction in the meridional temperature gradient. Even though BC aerosols are mainly emitted in the mid-latitudes and only a small fraction enter the Arctic, they may impact the Arctic climate. We estimate that BC aerosols at mid-latitudes lead to increased transport of heat into the Arctic, causing a warming, both at the surface and in the atmospheric. The largest increase in the temperatures is found in the upper troposphere during summer due to transport of heat along isentropic surfaces. In this case the temperature response is enhanced through snow/ice albedo feedback. In a recent study, Allen et al. (2012) argued that BC and tropospheric ozone are the main drivers of the Northern Hemisphere Hadley cell expansion, by heating primarily in the mid latitudes, causing a poleward shift in the storms tracks. In our study we also find a poleward shift of the jet stream for the MID experiment with local warming at mid latitudes (not shown).

It should be noted that the NorESM model has a relatively low climate sensitivity compared to most other climate models (Andrews et al., 2012). Iversen et al. (2012) calculate the forcing from $4 \times CO_2$ to 6.3 W m^{-2} and the global temperature response to 5.7 K in NorESM using the Gregory linear regression method (Gregory et al., 2004). The equilibrium climate sensitivity is calculated to be slightly smaller than 2.9 K, and the transient climate response is below 1.4 K. Possible explanations for the low sensitivity are relatively large cloud feedbacks and a strong Atlantic meridional overturning circulation in the model (Iversen et al., 2012).

Compared to observations, the model clearly underestimates BC concentrations at the surface, but there are also indications that the model overestimates the BC concentrations in the upper troposphere in the Arctic. This bias may enhance the vertical response pattern we see in the Arctic for the ARC run. The temperature response to the BC forcing depends on the vertical distribution of the BC aerosols. In idealized climate simulations Ban-Weiss et al. (2011) showed

that as the altitude of the BC increases, the surface temperature response decreases. In this study we have scaled up the background vertical profile of the BC aerosols in the model, where most of the Arctic BC aerosols are located in the free troposphere. If the emissions of BC aerosols in the Arctic are increased in the future, e.g. by increased shipping or oil production, the BC aerosols would be emitted directly into the Arctic planetary boundary layer and a different temperature response might be evident. The BC aerosols in the planetary boundary layer would have a stronger interaction with the surface, both by deposition of BC on snow and ice and by radiative and sensible heat fluxes down to the surface. In such a model study it would be important to include the effect of the deposition of BC on snow and sea-ice covered surfaces.

Our idealized model calculations indicate that atmospheric BC forcing outside the Arctic may be more important for the Arctic climate change compared to the forcing in the Arctic itself (with the linear assumption that the $10 \times$ BC response is scalable down to $1 \times$ BC). Although the albedo effect of BC on snow does show a more regional response to an Arctic forcing, these results suggest that mitigation strategies for the Arctic climate should also address BC sources in locations outside the Arctic even if they do not contribute much to BC in the Arctic.

Acknowledgements. We thank two anonymous reviewers for useful comments and to help increase the quality of the paper. We thank the Aerosol groups at the National Oceanic and Atmospheric Administration (NOAA), Global Monitoring Division for providing measurement data from Barrow, Konstantinos Eleftheriadis and Sterios Vratolis at the Institute of Nuclear Technology and Radiation Protection for providing measurement data from Zeppelin and Sangeeta Sharma at Environmental Canada for providing measurement data from Alert. We acknowledge the EBAS (http://ebas.nilu.no/Default.aspx), the NOAA ESRL (http://www.esrl.noaa.gov/gmd) and the EMEP (http://www.emep.int) databases. This study was partly funded by the Research Council in Norway through the Earthclim project, the Norwegian research Council's Programme for supercomputing (NOTUR) through a grant for computing time, and the ACCESS project supported by the European Commission 7th Framework Programme. The CESM project is supported by the National Science Foundation and the Office of Science (BER) of the US Department of Energy. The National Center for Atmospheric Research is operated by the University Corporation for Atmospheric Research under sponsorship of the National Science Foundation.

Edited by: R. Krejci

References

Albrecht, B. A.: Aerosols, cloud microphysics, and fractional cloudiness, Science, 245, 1227–1230, 1989.

Allen, R. J., Sherwood, S. C., Norris, J. R., and Zender, C. S.: Recent Northern Hemisphere tropical expansion primarily driven by black carbon and tropospheric ozone, Nature, 485, 350–354, 2012.

AMAP: Snow, Water, Ice and Permafrost in the Arctic (SWIPA): Climate Change and the Cryosphere. Arctic Monitoring and Assessment Programme (AMAP), Oslo, xii + 538 pp., 2011a.

AMAP: The Impact of Black Carbon on Arctic Climate, by: Quinn, P. K., Stohl, A., Arneth, A., Berntsen, T., Burkhart, J. F., Christensen, J., Flanner, M., Kupiainen, K., Lihavainen, H., Shepherd, M., Shevchenko, V., Skov, H., and Vestreng, V.: Arctic Monitoring and Assessment Programme (AMAP), Oslo, 72 pp., 2011b.

Andrews, T., Gregory, J. M., Webb, M. J., and Taylor, K. E.: Forcing, feedbacks and climate sensitivity in CMIP5 coupled atmosphere-ocean climate models, Geophys. Res. Lett., 39, L09712, doi:10.1029/2012gl051607, 2012.

Bala, G., Caldeira, K., and Nemani, R.: Fast versus slow response in climate change: implications for the global hydrological cycle, Clim. Dynam., 35, 423–434, 2010.

Ban-Weiss, G. A., Cao, L., Bala, G., and Caldeira, K.: Dependence of climate forcing and response on the altitude of black carbon aerosols, Clim. Dynam., 38, 1–15, 2011.

Barrie, L. A.: Arctic air pollution: an overview of current knowledge, Atmos. Environ., 20, 643–663, 1986.

Bauer, S. E., Menon, S., Koch, D., Bond, T. C., and Tsigaridis, K.: A global modeling study on carbonaceous aerosol microphysical characteristics and radiative effects, Atmos. Chem. Phys., 10, 7439–7456, doi:10.5194/acp-10-7439-2010, 2010.

Bentsen, M., Bethke, I., Debernard, J. B., Iversen, T., Kirkevåg, A., Seland, Ø., Drange, H., Roelandt, C., Seierstad, I. A., Hoose, C., and Kristjánsson, J. E.: The Norwegian Earth System Model, NorESM1-M – Part 1: Description and basic evaluation, Geosci. Model Dev. Discuss., 5, 2843–2931, doi:10.5194/gmdd-5-2843-2012, 2012.

Boer, G. J. and Yu, B.: Climate sensitivity and response, Clim. Dynam., 20, 415–429, doi:10.1007/s00382-002-0283-3, 2003.

Chung, C. E., Ramanathan, V., and Decremer, D.: Observationally constrained estimates of carbonaceous aerosol radiative forcing, P. Natl. Acad. Sci. USA, 109, 11624–11629, doi:10.1073/pnas.1203707109, 2012.

de Boer, G., Chapman, W., Kay, J., Medeiros, B., Shupe, M. D., Vavrus, S. and Walsh, J.: A characterization of the present-day Arctic atmosphere in CCSM4, J. Climate, 25, 2676–2695, 2011.

Eleftheriadis, K., Vratolis, S., and Nyeki, S.: Aerosol black carbon in the European Arctic: measurements at Zeppelin station, Ny-Ålesund, Svalbard from 1998–2007, Geophys. Res. Lett., 36, L02809, doi:10.1029/2008GL035741, 2009.

Flanner, M., Zender, C., Randerson, J. and Rasch, P.: Present-day climate forcing and response from black carbon in snow, J. Geophys. Res., 112, D11202, doi:10.1029/2006JD008003, 2007.

Forster, P., Ramaswamy, V., Artaxo, P., Berntsen, T., Betts, R., Fahey, D. W., Haywood, J., Lean, J., Lowe, D. C., Myhre, G., Nganga, J., Prinn, R., Raga, G., Schulz M., and Van Dorland, R.: Changes in Atmospheric Constituents and in Radiative Forcing, in: Climate Change 2007: The Physical Science Basis. Contribution of Working Group I to the Fourth Assessment Report

of the Intergovernmental Panel on Climate Change, edited by: Solomon, S., Qin, D., Manning, M., Chen, Z., Marquis, M., Averyt, K. B., Tignor, M., and Miller, H. L., Cambridge University Press, Cambridge, United Kingdom and New York, NY, USA, 2007.

Furevik, T., Bentsen, M., Drange, H., Kindem, I., Kvamstø, N. G., and Sorteberg, A.: Description and evaluation of the Bergen climate model: ARPEGE coupled with MICOM, Clim. Dynam., 21, 27–51, 2003.

Gent, P. R., Danabasoglu, G., Donner, L. J., Holland, M. M., Hunke, E. C., Jayne, S. R., Lawrence, D. M., Neale, R. B., Rasch, P. J., Vertenstein, M., Worley P. H., Yang, Z.-L., and Zhang, M.: The community climate system model version 4, J. Climate, 24, 4973–4991, 2011.

Gregory, J. M., Ingram, W. J., Palmer, M. A., Jones, G. S., Stott, P. A., Thorpe, R. B., Lowe, J. A., Johns, T. C., and Williams, K. D.: A new method for diagnosing radiative forcing and climate sensitivity, Geophys. Res. Lett., 31, L03205, doi:10.1029/2003GL018747, 2004.

Hansen, J. and Nazarenko, L.: Soot climate forcing via snow and ice albedos, P. Natl. Acad. Sci. USA, 101, 423–428, 2004.

Hansen, J., Sato, M., and Ruedy, R.: Radiative forcing and climate response, J. Geophys. Res., 102, 6831–6864, 1997.

Hansen, J., Sato, M., Ruedy, R., Lacis, A., and Oinas, V.: Global warming in the twenty-first century: An alternative scenario, P. Natl. Acad. Sci. USA, 97, 9875–9880, 2000.

Hansen, J., Sato, M., Ruedy, R., Nazarenko, L., Lacis, A., Schmidt, G. A., Russell, G., Aleinov, I., Bauer, M., Bauer, S., Bell, N., Cairns, B., Canuto, V., Chandler, M., Cheng, Y., Del Genio, A., Faluvegi, G., Fleming, E., Friend, A., Hall, T., Jackman, C., Kelley, M., Kiang, N., Koch, D., Lean, J., Lerner, J., Lo, K., Menon, S., Miller, R., Minnis, P., Novakov, T., Oinas, V., Perlwitz, J., Perlwitz, J., Rind, D., Romanou, A., Shindell, D., Stone, P., Sun, S., Tausnev, N., Thresher, D., Wielicki, B., Wong, T., Yao, M., and Zhang, S.: Efficacy of climate forcings, J. Geophys. Res., 110, D18104, doi:10.1029/2005JD005776, 2005.

Hoose, C., Kristjànsson, J. E., Iversen, T., Kirkevåg, A., Seland, Ø., and Gettelman, A.: Constraining cloud droplet number concentration in GCMs suppresses the aerosol indirect effect, 20, Geophys. Res. Lett., 36, L12807, doi:10.1029/2009GL038568, 2009.

Hoskins, B. J.: Towards a PV-θ view of the general circulation, Tellus A, 43, 27–35, 1991.

Hwang, Y. T., Frierson, D. M. W., and Kay, J. E.: Coupling between Arctic feedbacks and changes in poleward energy transport, Geophys. Res. Lett., 38, L17704, doi:10.1029/2011GL048546, 2011.

IPCC: Climate change 2007: the physical science basis: contribution of Working Group I to the Fourth Assessment Report of the Intergovernmental Panel on Climate Change, Cambridge Univ Pr, Cambridge, United Kingdom and New York, NY, USA, 2007.

Iversen, T., Bentsen, M., Bethke, I., Debernard, J. B., Kirkevåg, A., Seland, Ø., Drange, H., Kristjánsson, J. E., Medhaug, I., Sand, M., and Seierstad, I. A.: The Norwegian Earth System Model, NorESM1-M – Part 2: Climate response and scenario projections, Geosci. Model Dev. Discuss., 5, 2933–2998, doi:10.5194/gmdd-5-2933-2012, 2012.

Jacobson, M. Z.: Short-term effects of controlling fossil-fuel soot, biofuel soot and gases, and methane on climate, Arctic ice, and air pollution health, J. Geophys. Res., 115, D14209, doi:10.1029/2009JD013795, 2010.

Johnson, B. T., Shine, K. P., and Forster, P. M.: The semi-direct aerosol effect: Impact of absorbing aerosols on marine stratocumulus, Q. J. Roy. Meteor. Soc., 130, 1407–1422, 2004.

Kay, J. E. and Gettelman, A.: Cloud influence on and response to seasonal Arctic sea ice loss, J. Geophys. Res, 114, D18204, doi:10.1029/2009JD011773, 2009.

Kay, J. E., Holland, M. M., Bitz, C. M., Blanchard-Wrigglesworth, E., Gettelman, A., Conley, A., and Bailey, D.: The influence of local feedbacks and northward heat transport on the equilibrium Arctic climate response to increased greenhouse gas forcing, J. Climate, 25, 5433–5450, doi:10.1175/JCLI-D-11-00622.1, 2012a.

Kay, J. E., Hillman, B. R., Klein, S. A., Zhang, Y., Medeiros, B., Pincus, R., Gettelman, A., Eaton, B., Boyle, J., Marchand, R., and Ackerman, T. P.: Exposing global cloud biases in the Community Atmosphere Model (CAM) using satellite observations and their corresponding instrument simulators, J. Climate, 25, 5190–5207, doi:10.1175/JCLI-D-11-00469.1, 2012b.

Kirkevåg, A., Iversen, T., Seland, Ø., Debernard, J., Storelvmo, T. and Kristjánsson, J.: Aerosol-cloud-climate interactions in the climate model CAM-Oslo, Tellus, 60, 492–512, 2008.

Kirkevåg, A., Iversen, T., Seland, Ø., Hoose, C., Kristjánsson, J. E., Struthers, H., Ekman, A. M. L., Ghan, S., Griesfeller, J., Nilsson, E. D., and Schulz, M.: Aerosol-climate interactions in the Norwegian Earth System Model – NorESM, Geosci. Model Dev. Discuss., 5, 2599–2685, doi:10.5194/gmdd-5-2599-2012, 2012.

Koch, D. and Del Genio, A. D.: Black carbon semi-direct effects on cloud cover: review and synthesis, Atmos. Chem. Phys., 10, 7685–7696, doi:10.5194/acp-10-7685-2010, 2010.

Koch, D., Schulz, M., Kinne, S., McNaughton, C., Spackman, J. R., Balkanski, Y., Bauer, S., Berntsen, T., Bond, T. C., Boucher, O., Chin, M., Clarke, A., De Luca, N., Dentener, F., Diehl, T., Dubovik, O., Easter, R., Fahey, D. W., Feichter, J., Fillmore, D., Freitag, S., Ghan, S., Ginoux, P., Gong, S., Horowitz, L., Iversen, T., Kirkevåg, A., Klimont, Z., Kondo, Y., Krol, M., Liu, X., Miller, R., Montanaro, V., Moteki, N., Myhre, G., Penner, J. E., Perlwitz, J., Pitari, G., Reddy, S., Sahu, L., Sakamoto, H., Schuster, G., Schwarz, J. P., Seland, Ø., Stier, P., Takegawa, N., Takemura, T., Textor, C., van Aardenne, J. A., and Zhao, Y.: Evaluation of black carbon estimations in global aerosol models, Atmos. Chem. Phys., 9, 9001–9026, doi:10.5194/acp-9-9001-2009, 2009a.

Koch, D., Menon, S., Del Genio, A., Ruedy, R., Alienov, I., and Schmidt, G. A.: Distinguishing aerosol impacts on climate over the past century, J. Climate, 22, 2659–2677, 2009b.

Lamarque, J.-F., Bond, T. C., Eyring, V., Granier, C., Heil, A., Klimont, Z., Lee, D., Liousse, C., Mieville, A., Owen, B., Schultz, M. G., Shindell, D., Smith, S. J., Stehfest, E., Van Aardenne, J., Cooper, O. R., Kainuma, M., Mahowald, N., McConnell, J. R., Naik, V., Riahi, K., and van Vuuren, D. P.: Historical (1850–2000) gridded anthropogenic and biomass burning emissions of reactive gases and aerosols: methodology and application, Atmos. Chem. Phys., 10, 7017–7039, doi:10.5194/acp-10-7017-2010, 2010.

Law, K. S. and Stohl, A.: Arctic air pollution: Origins and impacts, Science, 315, 1537–1540, 2007.

Levy, H. I., Schwarzkopf, M. D., Horowitz, L., Ramaswamy, V., and Findell, K.: Strong sensitivity of late 21st century climate to projected changes in short-lived air pollutants, J. Geophys. Res.,

113, D06102, doi:10.1029/2007JD009176, 2008.

Liu, J., Fan, S., Horowitz, L. W., and Levy II, H.: Evaluation of factors controlling long-range transport of black carbon to the Arctic, J. Geophys. Res., 116, D04307, doi:10.1029/2010JD015145, 2011.

Lund, M. T. and Berntsen, T.: Parameterization of black carbon aging in the OsloCTM2 and implications for regional transport to the Arctic, Atmos. Chem. Phys., 12, 6999–7014, doi:10.5194/acp-12-6999-2012, 2012.

Menon, S., Hansen, J., Nazarenko, L. and Luo, Y.: Climate effects of black carbon aerosols in China and India, Science, 297, 2250–2253, 2002.

Myhre, G., Samset, B. H., Schulz, M., Balkanski, Y., Bauer, S., Berntsen, T. K., Bian, H., Bellouin, N., Chin, M., Diehl, T., Easter, R. C., Feichter, J., Ghan, S. J., Hauglustaine, D., Iversen, T., Kinne, S., Kirkevåg, A., Lamarque, J.-F., Lin, G., Liu, X., Luo, G., Ma, X., Penner, J. E., Rasch, P. J., Seland, Ø., Skeie, R. B., Stier, P., Takemura, T., Tsigaridis, K., Wang, Z., Xu, L., Yu, H., Yu, F., Yoon, J.-H., Zhang, K., Zhang, H., and Zhou, C.: Radiative forcing of the direct aerosol effect from AeroCom Phase II simulations, Atmos. Chem. Phys. Discuss., 12, 22355–22413, doi:10.5194/acpd-12-22355-2012, 2012.

Otterå, O. H., Bentsen, M., Bethke, I., and Kvamstø, N. G.: Simulated pre-industrial climate in Bergen Climate Model (version 2): model description and large-scale circulation features, Geosci. Model Dev., 2, 197–212, doi:10.5194/gmd-2-197-2009, 2009.

Porter, D. F., Cassano, J. J., Serreze, M. C., and Kindig, D. N.: New estimates of the large-scale Arctic atmospheric energy budget, J. Geophys. Res., 115, D08108, doi:10.1029/2009JD012653, 2010.

Pueschel, R. F. and Kinne, S. A.: Physical and radiative properties of Arctic atmospheric aerosols, Sci. Total Environ., 160, 811–824, 1995.

Samset, B. H. and Myhre, G.: Vertical dependence of black carbon, sulphate and biomass burning aerosol radiative forcing, Geophys. Res. Lett., 38, L24802, doi:10.1029/2011gl049697, 2011.

Samset, B. H., Myhre, G., Schulz, M., Balkanski, Y., Bauer, S., Berntsen, T. K., Bian, H., Bellouin, N., Diehl, T., Easter, R. C., Ghan, S. J., Iversen, T., Kinne, S., Kirkevåg, A., Lamarque, J.-F., Lin, G., Liu, X., Penner, J., Seland, Ø., Skeie, R. B., Stier, P., Takemura, T., Tsigaridis, K., and Zhang, K.: Black carbon vertical profiles strongly affect its radiative forcing uncertainty, Atmos. Chem. Phys. Discuss., 12, 28929–28953, doi:10.5194/acpd-12-28929-2012, 2012.

Schulz, M., Textor, C., Kinne, S., Balkanski, Y., Bauer, S., Berntsen, T., Berglen, T., Boucher, O., Dentener, F., Guibert, S., Isaksen, I. S. A., Iversen, T., Koch, D., Kirkevåg, A., Liu, X., Montanaro, V., Myhre, G., Penner, J. E., Pitari, G., Reddy, S., Seland, Ø., Stier, P., and Takemura, T.: Radiative forcing by aerosols as derived from the AeroCom present-day and pre-industrial simulations, Atmos. Chem. Phys., 6, 5225–5246, doi:10.5194/acp-6-5225-2006, 2006.

Seland, Ø., Iversen, T., Kirkevåg, A., and Storelvmo, T.: Aerosol-climate interactions in the CAM-Oslo atmospheric GCM and investigation of associated basic shortcomings, Tellus A, 60, 459–491, 2008.

Sharma, S., Andrews, E., Barrie, L., Ogren, J., and Lavoue, D.: Variations and sources of the equivalent black carbon in the high Arctic revealed by long-term observations at Alert and Barrow: 1989–2003, J. Geophys. Res., 111, D14208, doi:10.1029/2005JD006581, 2006.

Shindell, D.: Local and remote contributions to Arctic warming, Geophys. Res. Lett., 34, L14704, doi:10.1029/2007GL030221, 2007.

Shindell, D. and Faluvegi, G.: Climate response to regional radiative forcing during the twentieth century, Nat. Geosci., 2, 294–300, 2009.

Shindell, D. T., Chin, M., Dentener, F., Doherty, R. M., Faluvegi, G., Fiore, A. M., Hess, P., Koch, D. M., MacKenzie, I. A., Sanderson, M. G., Schultz, M. G., Schulz, M., Stevenson, D. S., Teich, H., Textor, C., Wild, O., Bergmann, D. J., Bey, I., Bian, H., Cuvelier, C., Duncan, B. N., Folberth, G., Horowitz, L. W., Jonson, J., Kaminski, J. W., Marmer, E., Park, R., Pringle, K. J., Schroeder, S., Szopa, S., Takemura, T., Zeng, G., Keating, T. J., and Zuber, A.: A multi-model assessment of pollution transport to the Arctic, Atmos. Chem. Phys., 8, 5353–5372, doi:10.5194/acp-8-5353-2008, 2008.

Shindell, D., Kuylenstierna, J. C. I., Vignati, E., van Dingenen, R., Amann, M., Klimont, Z., Anenberg, S. C., Muller, N., Janssens-Maenhout, G., and Raes, F.: Simultaneously mitigating near-term climate change and improving human health and food security, Science, 335, 183–189, 2012.

Stohl, A., Berg, T., Burkhart, J. F., Fjæraa, A. M., Forster, C., Herber, A., Hov, Ø., Lunder, C., McMillan, W. W., Oltmans, S., Shiobara, M., Simpson, D., Solberg, S., Stebel, K., Ström, J., Tørseth, K., Treffeisen, R., Virkkunen, K., and Yttri, K. E.: Arctic smoke – record high air pollution levels in the European Arctic due to agricultural fires in Eastern Europe in spring 2006, Atmos. Chem. Phys., 7, 511–534, doi:10.5194/acp-7-511-2007, 2007.

Twomey, S.: The in?uence of pollution on the shortwave albedo of clouds, J. Atmos. Sci, 34, 1149–1152, 1977.

II

JOURNAL OF GEOPHYSICAL RESEARCH: ATMOSPHERES, VOL. 118, 7788–7798, doi:10.1002/jgrd.50613, 2013

Arctic surface temperature change to emissions of black carbon within Arctic or midlatitudes

Maria Sand,[1] Terje Koren Berntsen,[1] Øyvind Seland,[2] and Jón Egill Kristjánsson [1]

Received 4 April 2013; revised 28 June 2013; accepted 28 June 2013; published 30 July 2013.

[1] In this study, we address the question of how sensitive the Arctic climate is to black carbon (BC) emitted within the Arctic compared to BC emitted at midlatitudes. We consider the emission-climate response spectrum and present a set of experiments using a global climate model. A new emission data set including BC emissions from flaring and a seasonal variation in the domestic sector has been used. The climate model includes a snow model to simulate the climate effect of BC deposited on snow. We find that BC emitted within the Arctic has an almost five times larger Arctic surface temperature response (per unit of emitted mass) compared to emissions at midlatitudes. Especially during winter, BC emitted in North-Eurasia is transported into the high Arctic at low altitudes. A large fraction of the surface temperature response from BC is due to increased absorption when BC is deposited on snow and sea ice with associated feedbacks. Today there are few within-Arctic sources of BC, but the emissions are expected to grow due to increased human activity in the Arctic. There is a great need to improve cleaner technologies if further development is to take place in the Arctic, especially since the Arctic has a significantly higher sensitivity to BC emitted within the Arctic compared to BC emitted at midlatitudes.

Citation: Sand, M., T. K. Berntsen, Ø. Seland, and J. E. Kristjánsson (2013), Arctic surface temperature change to emissions of black carbon within Arctic or midlatitudes, *J. Geophys. Res. Atmos.*, *118*, 7788–7798, doi:10.1002/jgrd.50613.

1. Introduction

[2] The Arctic has warmed rapidly over the last century with a rate almost twice as fast as the global mean rate [*Intergovernmental Panel on Climate Change*, 2007]. The temperature increase is accompanied by an earlier spring melt and a lengthening of the melting season, a decrease in the sea-ice extent, and a thinning of the Greenland ice sheet [*AMAP*, 2011, 2012]. Studies show an Arctic amplification to global emissions of black carbon (BC), which absorbs solar radiation in the atmosphere and when deposited on snow [e.g., *Hansen and Nazarenko*, 2004; *Jacobson*, 2004; *Flanner et al*., 2007; *Koch et al*., 2009a]. Reduction of BC emissions has been suggested as a short-term climate control strategy [*Hansen et al*., 2000; *Quinn et al*., 2008; *Jacobson*, 2010; *Shindell et al*., 2012]. Several studies have identified the different sources of BC reaching the Arctic and the impact of BC in the Arctic in terms of radiative forcing (per unit emission) [*Koch and Hansen*, 2005; *Stohl*, 2006]. Other studies have calculated the Arctic climate response to local and remote BC forcing [*Shindell*, 2007; *Koch et al*., 2011a]. For absorbing aerosols, such as BC, there is no simple relationship between the forcing and the response in the Arctic [*Hansen et al*., 2005]. In order to establish meaningful mitigation actions for BC, it is necessary to consider the entire emission-climate response spectrum to estimate which emissions contribute to Arctic warming.

[3] Unlike scattering aerosols that exert a weak (negative) forcing over snow, BC aerosols absorb solar radiation and exert a positive forcing over white surfaces, both in the atmosphere and when deposited on snow. This makes the forcing and the potential impact of BC particularly high in the Arctic during spring, when there are large amounts of sunlight available, most of the surfaces are still covered with snow and sea ice, and the BC concentrations are at a maximum [*Hansen and Nazarenko*, 2004; *Flanner et al*., 2009]. Arctic BC originates mostly from source areas outside the Arctic and is a result of a long-range transport from lower latitudes [*Law and Stohl*, 2007]. In the Arctic boundary layer, surfaces of low potential temperatures form a dome over the Arctic [*Klonecki et al*., 2003]. The high static stability associated with strong surface inversions in the Arctic boundary layer suppresses the mixing of pollution and heat from the free troposphere to the boundary layer, and BC reaching the Arctic from lower latitudes is not easily deposited on the Arctic surface. Several model studies highlight the importance of the vertical distribution of BC in regards to the climate response [*Hansen et al*., 2005; *Ban-Weiss et al*., 2012; *Flanner*, 2013; *Samset et al*., 2013]. *Flanner* [2013] perturbed BC mass in different altitudes in the Arctic and found a strong surface warming for BC located

[1]Department of Geosciences, University of Oslo, Oslo, Norway.
[2]Norwegian Meteorological Institute, Oslo, Norway.

Corresponding author: M. Sand, Department of Geosciences, P.O. Box 1022, 0315 Oslo, Norway. (maria.sand@geo.uio.no)

2169-897X/13/10.1002/jgrd.50613

near the surface, a weak surface warming for BC at 400−750 hPa, and a surface cooling for BC at 210–250 hPa. An earlier study showed similar trends in the sign of temperature change for BC perturbations at the global scale [*Ban-Weiss et al*., 2012]. Previous studies have shown that atmospheric absorption by present-day BC in the Arctic atmosphere (i.e., neglecting the impact of surface deposition) may have a small or even negative impact on the surface temperatures, as most of the BC aerosols are located above the Arctic dome [*Shindell and Faluvegi*, 2009; *Sand et al*., 2013]. The studies indicate the mitigation strategies for present-day BC should target emissions outside the Arctic. However, potential BC sources within the Arctic dome are more likely to warm the surface due to the near surface solar heating and the greater likelihood of surface deposition. The boundaries of the Arctic dome are highly variable in time and space, with a maximum extension over Eurasia during winter. Here the snow-covered surfaces make the air sufficiently cold, so that pollution can be transported directly into the high-Arctic boundary layer [*Stohl*, 2006]. Emissions during winter in Eurasia will therefore have a greater impact on the Arctic climate, highlighting the importance of seasonal differences in emissions.

[4] Current inventory estimates show that the dominant BC emissions within the Arctic today are caused by flaring related to the oil and gas fields in North Western Russia [*Stohl et al*., 2013]. Compared to midlatitudes, within-Arctic BC emissions are low, but the emissions are expected to grow due to new developments in the Arctic, the opening of the Northern sea routes to shipping, and enhanced oil and gas exploration [*Corbett et al*., 2010; *Peters et al*., 2011; *Ødemark et al*., 2012]. The use of wood stoves in the Nordic countries, Russia, Canada and Alaska during winter is one example of emissions in the domestic sector that have a large impact per unit emission in the Arctic. These emissions are expected to increase [*AMAP*, 2011, 2012].

[5] As the model studies of *Shindell and Faluvegi* [2009], *Sand et al*. [2013] and *Flanner* [2013] focused on the local climate response to local BC forcing, the studies are less relevant for policies that focus on mitigation of BC emissions at high latitudes. In this study, we want to study the climate effect of emitting BC in different regions. We investigate how anthropogenic BC emissions within-Arctic or from midlatitudes influence the Arctic climate, both through absorption in the atmosphere and through changes in surface albedo when BC is deposited on snow and sea ice. The scientific questions we want to address are: (1) How different will the Arctic climate response to BC emissions be if BC is emitted within the Arctic, compared to if BC is transported from lower latitudes and (2) how much of the BC forcing and response in the Arctic can be attributed to BC deposited on snow and sea ice? Since BC perturbs the climate system in many ways, both directly and indirectly, we have performed climate experiments with a global climate model, together with a snow model to include the effects of BC deposition on snow. A new emission data set has been used for BC that includes BC emissions from flaring, and a seasonal variation in the domestic sector, to account for amplified use of wood stoves during the cold season [*Klimont et al*., 2013].

2. Methods

[6] The experiments in this study have been performed with the Norwegian Earth System Model (NorESM) [*Bentsen et al*., 2013; *Iversen et al*., 2013], largely based on the NCAR CCSM4.0 [*Gent et al*., 2011]. The atmospheric model CAM4 [*Neale et al*., 2010] has been modified to include an aerosol module with separate representation of aerosols, aerosol-radiation, and aerosol-cloud interactions with prognostic cloud droplet number concentration [*Kirkevåg et al*., 2013]. The ocean model is replaced by the MICOM model. A snow model, SNICAR [*Flanner and Zender*, 2005], is applied to calculate the snow/albedo TOA RF from BC in snow on land. The sea-ice and the land models are the same as CCSM4.0 and NCAR CESM1.0, respectively, except that the albedo effects of BC and mineral dust aerosols deposited on snow and sea ice are based on the aerosol calculations in CAM4-Oslo. The sea-ice component is based on version 4 of the Los Alamos National Laboratory sea-ice model (CICE4) as described by *Hunke and Lipscomb* [2008]. The sea ice is deformed and transported in response to the ocean currents and wind field. NorESM has been validated against observations in *Bentsen et al*. [2013].

[7] The aerosol module calculates concentrations of aerosols that are tagged according to production mechanisms and size modes. For each of the mass concentrations, there are up to four size modes (nucleation, aitken, accumulation, and coarse). The production mechanisms are gaseous and aqueous chemical production, gas-to-particle nucleation, condensation on aerosol surfaces, and coagulation of smaller particles onto Aiken, accumulation, and coarse mode particles. The tagged information is transported along with the species. The aerosol life-cycle scheme includes sulphate, BC, organic matter (OM), sea-salt, and mineral dust, in addition to the precursors, SO_2 and DMS. There are 11 components for externally mixed particles that are calculated in the life-cycle scheme (and transported in the model). In addition, there are nine components that are tagged according to production mechanisms in air or clouds droplets. The size-resolved transformations into internal mixture with the 11 components can then be estimated a posteriori by use of look-up tables. Aerosol optical properties and CCN calculations are tabulated for a large number of entry values of the process-tagged concentrations, relative humidity, and supersaturation. Hygroscopic swelling is treated by use of the Köhler equation, and optical properties are estimated from Mie theory. CCN activation is estimated based on supersaturations calculated from Köhler theory. The direct effect of aerosols and both the first and second indirect effects are calculated based on a double-moment liquid microphysical scheme [*Storelvmo et al*., 2006]. The only second indirect effect calculated in the model is the autoconversion of liquid cloud water to rain in warm clouds [*Kristjánsson*, 2002]. The indirect effects associated with ice- and mixed-phase clouds are not calculated. The aerosol module, including the parameterization of optical properties and CCN activation, is described in more detail in *Kirkevåg et al*. [2013].

[8] Globally averaged, almost 40% of BC in the model is emitted from fossil fuel combustion. Most of fossil fuel BC is emitted in the nucleation mode, and 10% is assumed

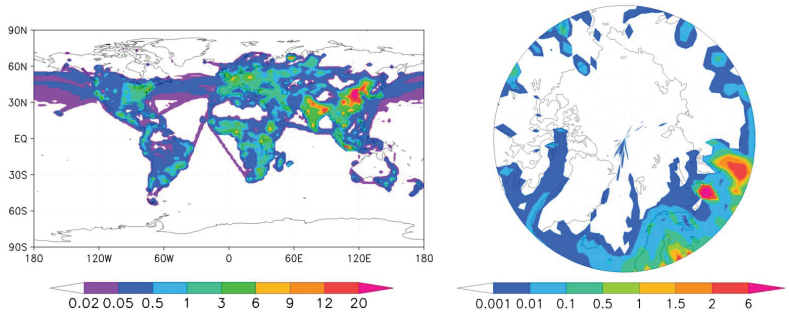

Figure 1. The combined annual mean fossil fuel and biofuel BC emissions for the year 2008 from the reference run. The right figure shows the same quantity within-Arctic only (60–90°N). All units in ng m^{-2} s^{-1}.

emitted as agglomerated BC in the accumulation mode. Emitted fossil fuel BC and OM are assumed externally mixed, while emitted biomass BC and OM are assumed internally mixed. Externally mixed BC is fully hydrophobic. Once emitted, BC gradually turns into hydrophilic, internally mixed aerosols when gaseous sulphate condenses on the particles or by coagulation with sulphate or sea salt. BC is removed from the atmosphere both by dry and wet deposition, although wet deposition dominates the total numbers. The dry deposition velocity depends on particle size, and the relative humidity influences this dependence for hygroscopic particles. Wet deposition is parameterized with an in-cloud scavenging coefficient defined as the mass fraction of the aerosol mode within the cloud droplet. The rainout is then determined by the local precipitation production rate for liquid water.

[9] The 2008 emission inventory that is used for BC fossil fuel and biofuel is from the ECLIPSE project [*Kupiainen and Klimont*, 2007; *Klimont et al*., 2009; *Shindell et al*., 2012; *Klimont et al*., 2013] available through the project website (http://eclipse.nilu.no). All other emissions inventories are from IPCC [*Lamarque et al*., 2010]. In the ECLIPSE inventory, the BC domestic sector has a seasonal variation with a wintertime maximum, and the emissions from flaring are included. The BC emissions from shipping are from the IPCC, as they were not available in ECLIPSE. Emissions from aircrafts are not included as we wanted to focus on ground-based emissions. As the current version of NorESM does not treat the influence of BC on ice nucleation, the impact of aircraft emissions in the Arctic would likely be underestimated [*Jacobson et al*., 2012]. Figure 1 shows the annual mean fossil fuel and biofuel BC emissions for year 2008 used in this study. The global annual mean (fossil fuel and biofuel) BC emissions are 5.5 Tg yr^{-1}. Averaged over the Arctic (60–90°N) and mid-latitudes (28–60°N) only, the emissions are 0.07 Tg yr^{-1} and 2.6 Tg yr^{-1}, respectively.

[10] The model is run on a 1.9° × 2.5° horizontal grid with 26 vertical layers in the atmosphere. The climate simulations have been run for 60 years from a 140 year spin-up with the same 2008 emissions and greenhouse gas levels. The last 30 years have been used for analyses. The climate simulations include one control run, four perturbed runs, and one sensitivity run; six in total. The perturbed runs are: "ARCem" — with BC emissions scaled up north of 60°N, and "MIDem": — with BC emissions scaled up in the midlatitudes (28–60°N). Table 1 shows the annual mean emitted BC mass and column burden for each experiment. The scaling factors were chosen to give regional RF within the Arctic of similar magnitude and to ensure that the results from the climate model were statistically significant. The RF for each experiment is given in Table 2. There is a balance between achieving a statistically significant signal and at the same time limiting nonlinear effects. *Hansen et al*. [2005] found an approximate limit for linearity for scaling giving a global aerosol RF on the order of 1 W m^{-2}. To distinguish the climate impact of BC deposited on snow and sea ice, the two perturbed runs have been repeated without any impact of BC deposited on snow and ice. To further test the Arctic sensitivity to within-Arctic emissions, a highly idealized simulation with identical BC emissions in every Arctic grid cell has been performed (the sensitivity run "gridARC"). The Arctic is defined here as north of 60°N. The instantaneous RF of BC at TOA is estimated in separate five year offline runs with the same experimental setup as the online runs. In the offline runs, the aerosols do not affect the meteorology in the model, so that each simulation has the same meteorology. The snow/albedo RF from BC deposited on snow on land has been calculated with the SNICAR model at each radiative transfer time step as the difference in absorption with and without BC. In the model, BC is deposited both on snow on land and on the sea ice, and change the surface albedo. We lack, however, the instantaneous RF diagnose output for the RF of BC deposited in the sea-ice model. Therefore, the snow/albedo RF reported in this study is for BC deposited on snow on land only. The full climate response in the coupled runs includes the snow/albedo effect of BC deposited on both snow on land and on the sea ice.

Table 1. Emitted BC Mass and BC Column Burden Averaged in Two Latitude Bands (60–90°N and 28–60°N)

	EMITTED BC MASS[a]		BC COLUMN BURDEN[b]	
	Tg BC $year^{-1}$		mg/m^{-2}	
	60–90°N	28–60°N	60–90°N	28–60°N
ARCem	8.8	0	2.4	0.5
MIDem	0	20.8	1.3	2.5
gridARC	9.2	0	1.8	0.3

[a]Annual mean emitted fossil fuel and biofuel BC mass (perturbed control).
[b]Annual mean increase in BC column burden (perturbed control).

Table 2. Radiative Forcing, Surface Temperature Response, and Climate Sensitivity[a]

	RF TOA[b]			Snow/Alb. RF.[c]			Norm. RF[d]		ΔTs		ΔTs nodep[e]		Sensitivity[f]	
	W m^{-2}			W m^{-2}			W m^{-2} (Tg yr^{-1})$^{-1}$		K		K		K (Tg yr^{-1})$^{-1}$	
	60–90°N	28–60°N	global	60–90°N	28–60°N	global	60–90°N	global	60–90°N	global	60–90°N	global	60–90°N	global
ARCem	2.58	0.58	0.31	1.18	0.08	0.09	0.38	0.04	2.32	0.32	0.74	0.24	0.24	0.03
MIDem	3.11	3.44	1.28	0.48	0.19	0.07	0.17	0.07	0.99	0.30	0.20	0.26	0.05	0.01
gridARC	2.59	0.32	0.25	2.22	0.08	0.16	0.47	0.04	3.91	0.42	-	-	0.38	0.04

[a]The quantities are annual means in the Arctic (60–90°N), in the midlatitudes (28–60°N), and global.
[b]Direct and indirect radiative forcing TOA.
[c]TOA RF from BC deposited on snow on land (not sea ice).
[d]Total RF (direct, indirect and snow/albedo effect from BC on snow on land) per global emission increase.
[e]Surface temperature response without deposition of BC (for the ARCem and MIDem experiments only).
[f]Surface temperature change per global emission increase.

3. Results

3.1. BC Concentrations in the Atmosphere and Snow

[11] Figure 2 shows the annual zonal mean BC concentrations for the reference run. While the maxima in BC concentrations at midlatitudes are near the source areas at the surface, in the Arctic, the maximum BC concentrations are found at around 500 hPa. The annual mean concentration of BC deposited in snow on land for the reference run is shown in Figure 3. The maximum is located near the emission hot spot in China with concentrations above 1200 ng per gram of snow. In Figure 4, the modeled concentrations of BC in snow are compared to observations in the Arctic taken from *Doherty et al*. [2010] and from northwestern China from *Ye et al*. [2012]. Each observation is compared to BC concentration in the top snow layer in the nearest model grid box in the actual month in the reference run. The filled circles represent the average of the observations in the different locations, and the lines represent the maximum and minimum observation. Despite the fact that the observations represent point observations at limited time intervals, the monthly mean modeled concentrations agree reasonably well with the observations. NorESM (with IPCC BC emissions) has been validated against BC observations in *Sand et al*. [2013] and *Kirkevåg et al*. [2013]. Here it was shown that NorESM underestimates global BC surface concentrations by 36% and is unable to reproduce the observed Arctic haze during winter and early spring (while during summer and autumn the concentrations are within the same size order). Using the Eclipse emission inventory, the wintertime surface BC concentrations in the high-Arctic are doubled compared to the emission inventory from the IPCC (which did not include flaring or a seasonal variation in the domestic sector), suggesting that a part of the underestimation in the model is linked to emission data.

[12] Figure 5 shows the increase in the zonal mean BC concentrations during the winter and summer seasons for the two experiments, ARCem and MIDem. In MIDem, the highest perturbation of the BC concentrations is during the winter at 30–40°N. In the winter, some of the BC is transported into the Arctic at low altitudes, but most of the BC is lifted above the boundary layer. During summer, the concentrations in midlatitudes and the Arctic are convectively lifted, leading to an increase in the BC concentrations at high altitudes and a

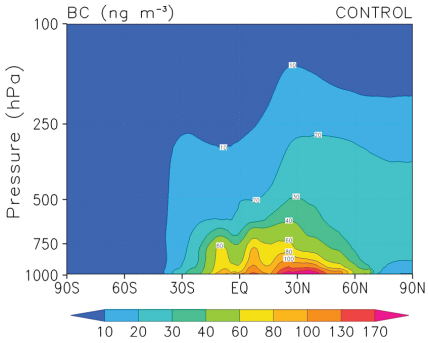

Figure 2. Annual zonal mean BC concentrations (in ng m^{-3}) for the reference run with 2008 emissions.

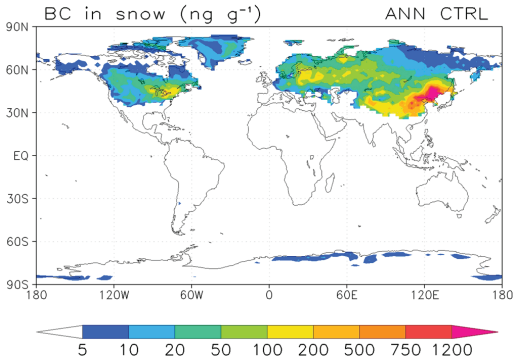

Figure 3. Annual mean BC concentrations in snow on land (in ng BC per g snow) averaged when there is snow present from the reference run with 2008 emissions.

decrease in the concentrations at lower altitudes. For ARCem, there is a larger seasonal difference between the perturbations in the Arctic surface BC concentrations, with a maximum during winter when BC is transported at low altitudes along the cold surface in North-Eurasia into the high-Arctic boundary layer. During summertime, BC perturbations reach the high-Arctic at higher altitudes (900–500 hPa) with a lower enhancement of surface concentrations.

3.2. BC Forcing

[13] The direct and indirect RF of BC in the atmosphere have been calculated as the change in the incoming and outgoing radiation at TOA in the offline runs with and without perturbed BC. Table 2 summarizes the annual mean RF for BC in the atmosphere and RF of the snow/albedo effect on snow on land for the experiments. Following previous studies [*Shindell and Faluvegi*, 2009; *Sand et al*., 2013], we calculate the RF in latitude bands as well as the global mean. For MIDem, the TOA RF at midlatitudes is 3.4 $W m^{-2}$. The Arctic TOA RF for MIDem (3.1 $W m^{-2}$) is higher than for ARCem (2.6 $W m^{-2}$).

[14] Figure 6 shows the Arctic mean seasonal cycle for the direct and indirect RF of atmospheric BC and the snow/albedo effect for ARCem and MIDem. The direct RF for ARCem and MIDem peaks in the summer season when there is maximum insolation while the snow/albedo effect peaks earlier in the melt season when the snow cover is still extensive. As expected, the Arctic annual mean indirect RF is much smaller than the direct RF: 0.17 $W m^{-2}$ for ARCem and 0.08 $W m^{-2}$ for MIDem [*Koch et al*., 2011b]. Note that the indirect forcing in NorESM is calculated for liquid clouds only. While the direct RF for the MIDem case is slightly larger than ARCem, the snow/albedo effect for BC in MIDem is smaller (1.2 $W m^{-2}$ for ARCem and 0.48 $W m^{-2}$ for MIDem). Normalizing each case to the increase in emissions the total forcing (direct and indirect RF of atmospheric BC and the snow/albedo effect) per unit emission is twice as large for ARCem as for MIDem (0.38 $W m^{-2}$ per Tg yr^{-1} vs. 0.17 $W m^{-2}$ per Tg yr^{-1}).

3.3. Arctic Climate Response

[15] The changes in the Arctic annual mean atmospheric energy budget for ARCem and MIDem (from the coupled multidecadal climate simulations) are shown in Figure 7. The direct effect of shortwave radiation at TOA due to increased BC absorption is the main driver for both ARCem and MIDem. For ARCem, the snow/albedo effect is also important. The net surface shortwave radiation, which includes increased absorption at the surface and a reduction due to dimming, is about half of that at TOA. The net shortwave flux at the surface increases both due to absorption of BC at the surface and the lowering of the surface albedo when a darker surface is exposed after melting of snow and sea ice. *Shindell and Faluvegi* [2009] and *Sand et al*. [2013] showed that atmospheric BC forcing (with a vertical profile as in their reference simulations) at midlatitudes had a warming effect on the Arctic surface, while BC forcing in the Arctic had a cooling effect. The MIDem experiment in this study can be considered a combination of both forcings (Arctic + midlatitudes), as BC emitted at midlatitudes is transported into Arctic. *Shindell and Faluvegi* [2009] and *Sand et al*. [2013] found that the atmospheric heating at midlatitudes caused an increase in the northward heat transport, while in their Arctic experiment it decreased. We have calculated the northward heat transport as a residual between the energy budget at TOA and at the surface. The change in the northward heat transport for MIDem in this case is negative by $-2 W m^{-2}$. This indicates that when regional emissions are considered, the effect of BC transported to the Arctic and causing absorption there dominates in the MIDem experiment. Thus, the direction of the northward heat transport perturbation is opposite compared to the response to the concentration perturbations (in latitude bands) studied by *Shindell and Faluvegi* [2009] and *Sand et al*. [2013].

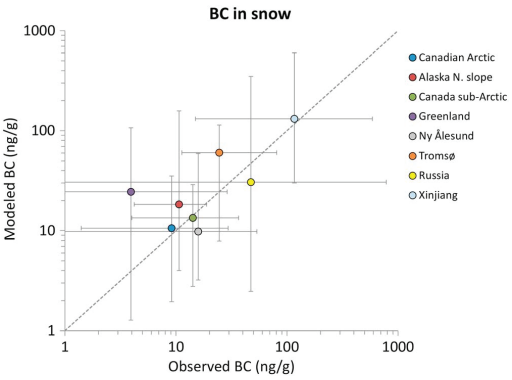

Figure 4. Observed and modeled BC concentrations in snow (in ng BC per g snow). The observations from the seven Arctic sites are taken from *Doherty et al*. [2010], and the observations from China (Xinjiang) are taken from *Ye et al*. [2012]. The dots show the average in the concentrations, and the bars represent the minimum and maximum concentrations. For modeled BC, the average and minimum and maximum are from the 60 year reference run with 2008 emissions with monthly mean concentrations.

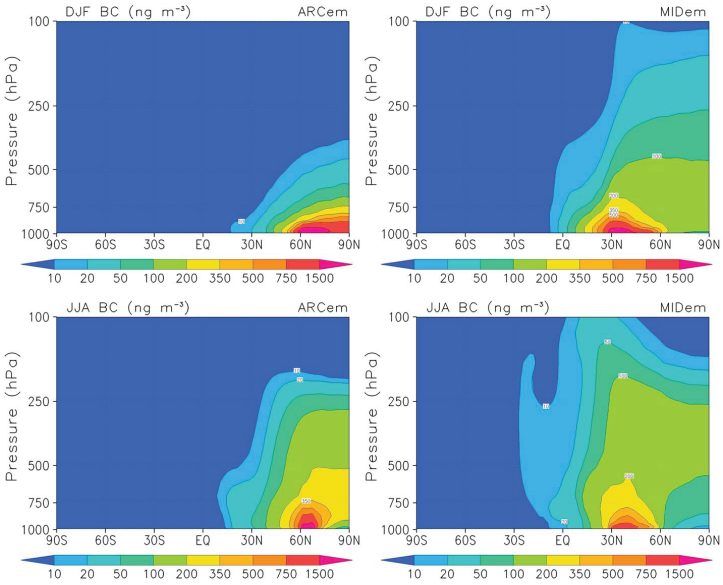

Figure 5. Difference in zonal mean BC concentrations (in ng m^{-3}) for ARCem-CTRL (left) and MIDem-CTRL (right) for the winter season Dec–Feb (top) and the summer season Jun–Aug (bottom).

[16] The zonal mean temperature responses for the two experiments for the winter, spring, and summer seasons are shown in Figure 8. In the summer season, there is a maximum warming in the free troposphere, reflecting the increased vertical mixing of BC due to convection during summer. In MIDem, the largest temperature increase is at altitudes between 500 and 200 hPa. For ARCem, the largest increase is from the surface and up to 400 hPa. For ARCem, there is also an Arctic surface warming during winter and spring. Figure 9 shows the seasonal cycle in the Arctic mean surface temperature change for the two experiments. ARCem has a larger surface temperature response in all months, with a maximum during late autumn/winter. The increase in surface temperatures during winter, when the radiative forcing of BC is very small, may be linked to a dynamical response in the sea ice and/or changes in cloudiness. Figure 10 shows the monthly mean response in the sea ice and snow cover. During the winter season, the sea ice reaches full recovery, and then additional BC leads to enhanced melting in spring and summer. For ARCem, the reduction in the sea ice is 20–50% during summer, reaching a maximum in September when the sea ice has its minimum extension. Model studies and observations show that reductions in sea-ice cover in autumn coincide with an increase in low clouds with enhanced evaporation from the open water [*Palm et al.*, 2010; *Vavrus et al.*, 2011]. Enhancement of low clouds during autumn and

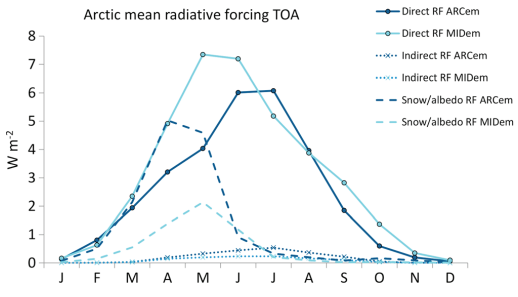

Figure 6. Arctic monthly mean (60–90°N) direct, indirect and snow/albedo (from BC on snow on land) TOA RF for ARCem-CTRL and MIDem-CTRL. Units in W m^{-2}.

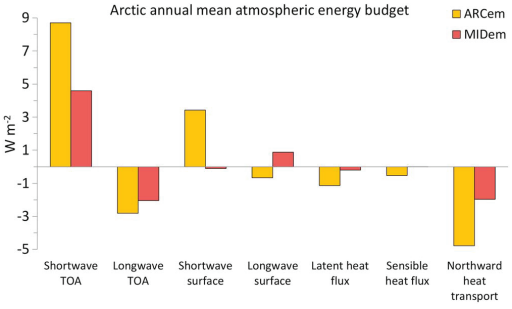

Figure 7. Change in Arctic annual mean (60–90°N) atmospheric energy budget for ARCem-CTRL (yellow) and MIDem-CTRL (red). The northward heat transport is calculated as a residual of the TOA and surface energy budget. All TOA (surface) energy budget terms are defined positive when the atmosphere (surface) gains energy. Units in W m^{-2}.

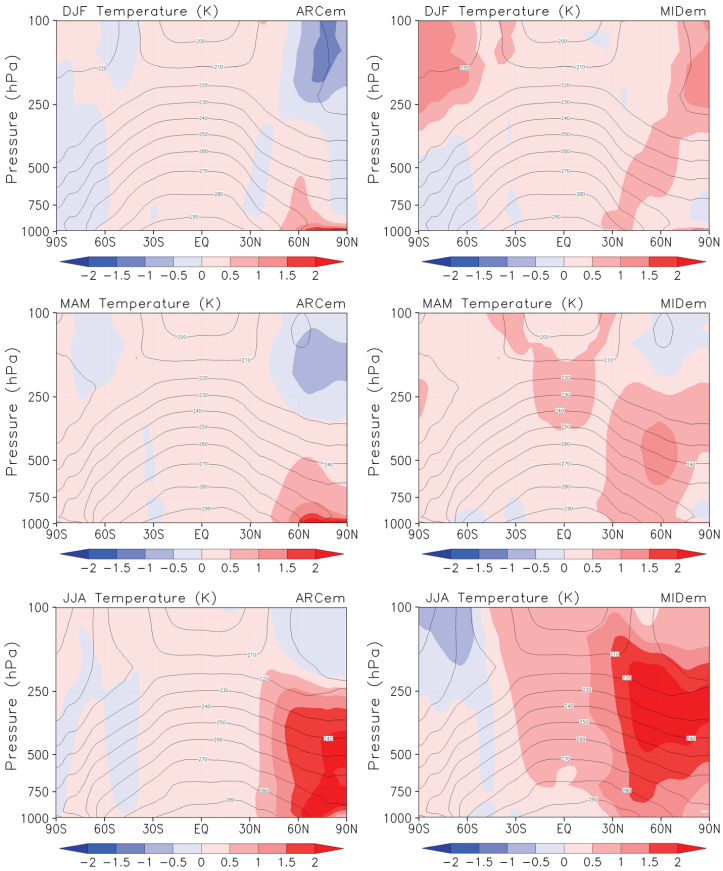

Figure 8. Change in the zonal mean temperature (in K) for ARCem-CTRL (left) and MIDem-CTRL (right) for the winter season Dec–Feb (top), spring Mar–May (middle), and the summer season Jun–Aug (bottom). The contour lines show the zonal mean temperature in the reference run (CTRL).

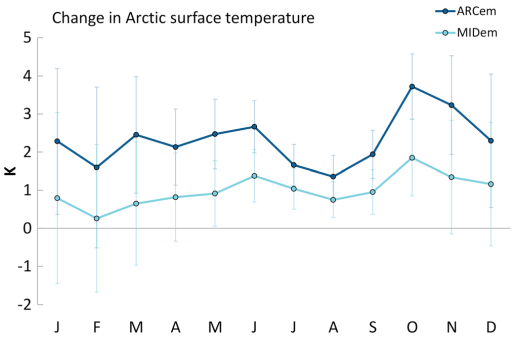

Figure 9. Change in Arctic monthly mean (60–90°N) surface temperature (in K) for ARCem-CTRL and MIDem-CTRL. Bars represent one standard deviation.

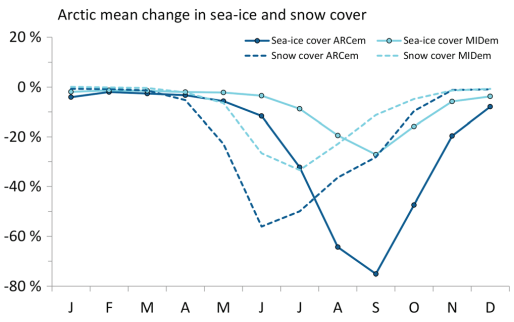

Figure 10. Change in Arctic monthly mean (60–90°N) snow cover and sea-ice cover (in % change) between ARCem-CTRL (solid line) and MIDem-CTRL (stippled line).

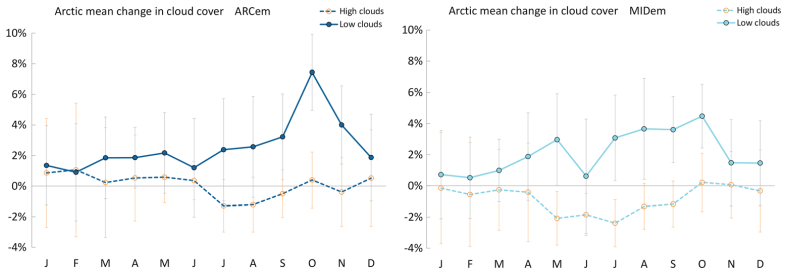

Figure 11. Change in the Arctic monthly mean (60–90°N) high and low cloud cover (in absolute change) for ARCem-CTRL (left) and MIDem-CTRL (right). The lines represent one standard deviation.

winter in the Arctic has a positive feedback on the surface temperatures (and sea-ice loss) as the clouds trap outgoing longwave radiation and reemit some of it back to the surface.

[17] Figure 11 shows the change in cloud cover for high and low clouds. In MIDem, where most of the Arctic BC is located at higher altitudes, there is a decrease in high clouds during summer and an increase in the low clouds. The increase in low clouds is followed by an increase in the downwelling longwave radiation. The increase in low clouds and downwelling longwave radiation is also apparent in ARCem, especially during the late autumn/winter season. The only significant change in clouds within 2 standard

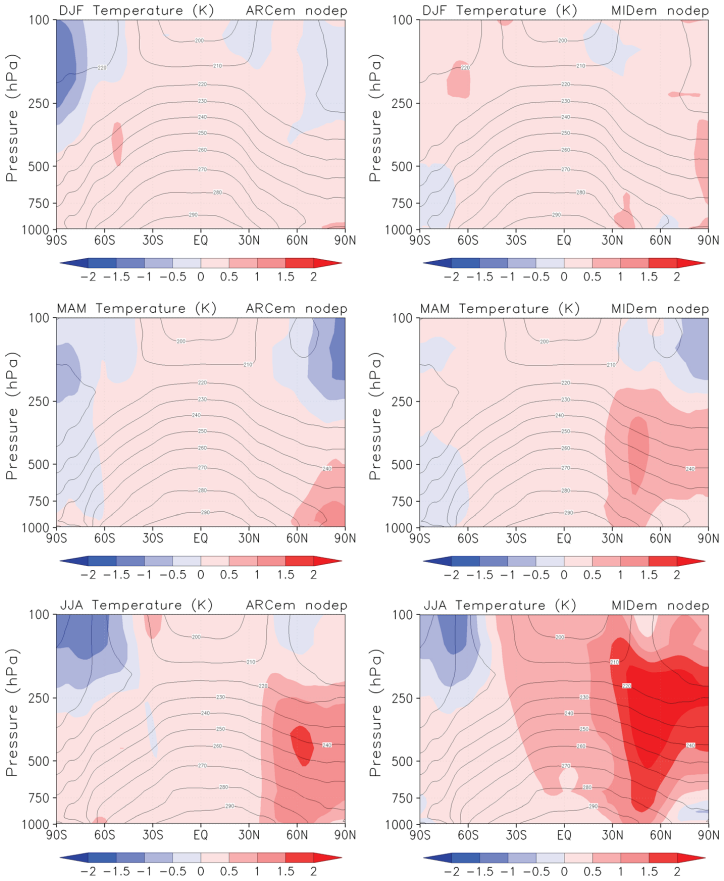

Figure 12. As in Figure 8, but for the experiments without deposition of BC.

deviations is the increase in low clouds during October. The decrease in the high clouds during summer in MIDem, where most of the BC is located in the free troposphere, may be due to a semidirect effect of BC, where the enhanced temperatures evaporate the clouds. However, since we are not applying a feedback analysis in this study, we cannot distinguish whether the changes in cloudiness are caused by a semidirect effect of BC, or to increased temperatures and/or decreased sea-ice cover. In fact, by looking at the first few months of the model run, there is no significant signal in the cloud response, indicating that the slower sea-ice feedback dominates over the fast cloud response. Similar to many other climate models, NorESM overestimates the liquid water content in Arctic clouds during winter, making the clouds too optically thick [*de Boer et al*., 2011; *Kay et al*., 2012]. This may underestimate the indirect effect of BC.

[18] The Arctic annual mean surface temperature response for ARCem is 2.3 K and 0.99 K for MIDem. When the ARCem experiment is run without the climate effect of BC deposition on snow and sea ice, the temperature increase reduces to 0.74 K. Thus, emissions within the Arctic over two thirds of the surface temperature response can be attributed to the darkening of snow and sea ice and associated feedbacks. The reduction in sea-ice cover is significantly less for the ARCem without deposition of BC. The zonal mean temperature response for the experiments without BC deposition is shown in Figure 12. The difference in the temperature response when BC deposition is included, and when it is not, is confined to the surface layer.

[19] The main goal of this study is to estimate the Arctic surface temperature increase in response to increased emissions of BC. Comparing the Arctic RF per unit (global mean) emitted mass for the two different emission regions, we find that ARCem has over a factor two higher forcing per unit emission than MIDem (0.38 vs. 0.17 Wm^{-2} per Tg BC yr^{-1}). The Arctic temperature response per unit emission, however, is almost five times as large for ARCem as for MIDem (0.24 vs. 0.05 K per Tg BC yr^{-1}). According to the results from these simulations, emitting BC north of 60°N will therefore almost give a factor five increase of the surface temperature response in the Arctic compared to emitting the same amount of BC at midlatitudes.

[20] The ARCem experiment is based on present-day emissions in the Arctic associated with large uncertainties [*Stohl et al*., 2013], and the results could be sensitive to the geographical distribution of the emissions (dominated by flaring in Russia). Thus, we have performed an additional coupled experiment emitting a fixed amount of BC in every grid cell north of 60°N ("gridARC"). The experiment has the same forcing per unit emission as ARCem: 0.37 Wm^{-2} per Tg BC yr^{-1}. The Arctic surface temperature change per unit emission in this experiment is 0.38 K per Tg BC yr^{-1} compared to 0.24 K per Tg yr^{-1} for ARCem. The response is slightly higher, but comparable to ARCem, even if the distribution of the emissions is different. This suggests that to first order the response we get in the Arctic can be generalized for future emissions within Arctic.

4. Discussion

[21] In this study, we focus on impacts on Arctic climate from BC emissions in midlatitudes or within the Arctic. Previous studies of Arctic climate response to BC have a somewhat different perspective in that emission are driving the perturbations, but rather perturbation of regional concentration profiles [*Shindell and Faluvegi*, 2009; *Flanner*, 2013; *Sand et al*., 2013]. When the BC aerosols are emitted in the lowest model layer within the Arctic, they tend to remain at lower altitudes and are more easily deposited at the surface. This causes an enhanced Arctic surface warming compared to emissions at lower latitudes. *Flanner* [2013] found similar results for prescribed Arctic BC in the lowest atmospheric layer, while BC perturbations at higher altitudes gave surface cooling. Note that an earlier study showed the same behavior exists for BC perturbations at the global scale [*Ban-Weiss et al*., 2012]. *Shindell and Faluvegi* [2009] and *Sand et al*., [2013] perturbed the distribution of present-day BC from all global sources, keeping the relative vertical profile unchanged. Both studies found a surface cooling for BC in the Arctic atmosphere (neglecting the snow/albedo effect) due to a reduction in both the meridional heat transport and the downward solar radiation at the surface. For present-day Arctic BC, most of the climate models seem to overestimate the concentrations in the free troposphere and underestimate the concentrations near the surface, our model included [*Koch et al*., 2009b]. Such a vertical distribution might underestimate the climate efficacy and the surface warming by BC in the Arctic.

[22] For ARCem, the RF of the snow/albedo reduction is about half of the TOA atmospheric direct effect, while the surface temperature response is to a large extent attributed to increased absorption by BC on snow and sea ice and decreased surface albedo. Even though the model is in good agreement with the observed BC concentrations in snow (Figure 4), one should, however, be careful to conclude, since the relative distribution of BC in the atmosphere and surface is governed by highly uncertain model boundary layer processes. For example, there are indications that NorESM may have a too stable or thin Arctic boundary layer and/or too high convective transport globally which influence the vertical distribution of BC. While NorESM underestimates surface BC concentrations, it is among the models with the highest BC concentrations in the free troposphere [*Samset et al*., 2013]. This indicates that the convective transport in NorESM may be too strong. In the midlatitudes, the convective transport can redistribute the aerosols away from the source areas. Episodes of large-scale blocking events in the Northern hemisphere during winter are a frequent transport source of pollutants from northern Eurasia into the Arctic [*Iversen and Joranger*, 1985; *Stohl*, 2006]. The lack of blocking events, possibly related to the relative coarse resolution of the model, may underestimate the meridional transport toward the Arctic [*Iversen et al*., 2013]. To what extent this influence the perturbations that are analysed here is difficult to quantify.

[23] In order to get a significant signal in the highly variable Arctic climate, we had to scale up the present-day emissions quite substantially. In particular for ARCem, this gave a strong response in the sea-ice cover. We assume that the climate signal we get is linear, so the response is scalable down to 1 × emissions, but we cannot rule out the possibility of nonlinear effects in the climate system.

[24] We have run a coupled earth system model for 60 model years which is not sufficient to reach an equilibrium

state in the ocean model. The final climate response will therefore likely be even larger than reported in this study.

[25] Sources that emit BC also emit a variety of other gases and/or particles that may either warm or cool the climate [*Bond et al*., 2013]. Thus, the net forcing may be either positive or negative depending on the amount and chemical composition of the co-emitted species. The main emitted species that can change the sign of the net forcing are particulate OM and sulfur dioxide. In the Arctic, reflective species like sulfur dioxide may not have a large impact on the albedo effect. Some emission sources, e.g., diesel engines or flaring, have a higher amount of BC relative to the co-emitted species, while emissions from open burning and shipping have a higher amount of co-emitted species. In order to make mitigation actions for different emissions activities, the actual climate change will depend on the effect of all the co-emitted species. This issue is not treated in this study. A step further on this study would be to investigate different sectors emitting BC, and to include the effect of the co-emitted species in the different sectors.

5. Concluding Remarks

[26] Using a coupled climate model we find that the Arctic climate has a significantly larger sensitivity (per unit emitted mass) to BC emitted within the Arctic compared to BC emitted at midlatitudes. Emitting BC in the Arctic will almost give a fivefold increase in the Arctic surface temperature response compared to emitting the same amount of BC at midlatitudes. A large fraction of the emitted BC within the Arctic stays in the lowermost layers in the atmosphere and gets deposited at the surface. The increased absorption of BC deposited on snow and the associated feedbacks in snow cover, sea ice, and clouds in the Arctic explain two thirds of the surface temperature increase.

[27] Since most of the present-day BC is emitted at midlatitudes, in total the emissions from midlatitudes has the largest impact on the Arctic climate, despite the fact that the BC transported into the Arctic has a small or negative impact on the surface temperatures (neglecting the impact of surface deposition) [*Shindell and Faluvegi*, 2009; *Sand et al*., 2013]. Today, emissions of BC in the Arctic are low. However, since the surface temperature response per unit emission is almost five times larger for BC emitted in the Arctic compared to midlatitudes, even a small increase in the emissions would have a large climate impact. Changes in the Arctic climate influence the global climate, and there is a great need for improving cleaner technologies if further development is to take place within the Arctic.

[28] **Acknowledgments.** We would like to thank three anonymous reviewers for useful comments. This study was funded by the Norwegian Research Council through the Earthclim project and the Programme for supercomputing (NOTUR) through a grant for computing time. We acknowledge the CRAICC project. We would also like to thank NCAR and NCAR staff for early access to model code for CCSM/CESM.

References

AMAP (2011). The impact of black carbon on Arctic climate. *AMAP Technical Report No. 4* (2011), Arctic Monitoring and Assessment Programme (AMAP), Oslo, Norway.

AMAP (2012), Snow, Water, Ice and Permafrost in the Arctic (SWIPA) 2011, Arctic Monitoring and Assessment Programme (AMAP), Oslo, Norway.

Ban-Weiss, G., L. Cao, G. Bala, and K. Caldeira (2012), Dependence of climate forcing and response on the altitude of black carbon aerosols, *Clim. Dynam.*, *38*(5-6), 897–911, doi:10.1007/s00382-011-1052-y.

Bentsen, M., et al. (2013), The Norwegian Earth System Model, NorESM1-M – Part 1: Description and basic evaluation of the physical climate, *Geosci. Model Dev.*, *6*(3), 687–720, doi:10.5194/gmd-6-687-2013.

de Boer, G., W. Chapman, J. E. Kay, B. Medeiros, M. D. Shupe, S. Vavrus, and J. Walsh (2011), A characterization of the present-day Arctic atmosphere in CCSM4, *J. Climate*, *25*(8), 2,676–2,695, doi:10.1175/JCLI-D-11-00228.1.

Bond, T. C., et al. (2013), Bounding the role of black carbon in the climate system: A scientific assessment, *J. Geophys. Res. Atmos.*, *118*, 1–173, doi:10.1002/jgrd.50171.

Corbett, J. J., D. A. Lack, J. J. Winebrake, S. Harder, J. A. Silberman, and M. Gold (2010), Arctic shipping emissions inventories and future scenarios, *Atmos. Chem. Phys.*, *10*(19), 9,689–9,704, doi:10.5194/acp-10-9689-2010.

Doherty, S. J., S. G. Warren, T. C. Grenfell, A. D. Clarke, and R. E. Brandt (2010), Light-absorbing impurities in Arctic snow, *Atmos. Chem. Phys.*, *10*(23), 11,647–11,680, doi:10.5194/acp-10-11647-2010.

Flanner, M. G. (2013), Arctic climate sensitivity to local black carbon, *J. Geophys. Res. Atmos.*, *118*, 1–12, doi:10.1002/jgrd.50176.

Flanner, M. G., and C. S. Zender (2005), Snowpack radiative heating: Influence on Tibetan Plateau climate, *Geophys. Res. Lett.*, *32*, L06501, doi:10.1029/2004GL022076.

Flanner, M. G., C. S. Zender, J. T. Randerson, and P. J. Rasch (2007), Present day climate forcing and response from black carbon in snow, *J. Geophys. Res.*, *112*, D11202, doi:10.1029/2006JD008003.

Flanner, M. G., C. S. Zender, P. G. Hess, N. M. Mahowald, T. H. Painter, V. Ramanathan, and P. J. Rasch (2009), Springtime warming and reduced snow cover from carbonaceous particles, *Atmos. Chem. Phys.*, *9*(7), 2,481–2,497, doi:10.5194/acp-9-2481-2009.

Gent, P. R., et al. (2011), The Community Climate System Model Version 4, *J. Climate*, *24*(19), 4,973–4,991, doi:10.1175/2011JCLI4083.1.

Hansen, J., and L. Nazarenko (2004), Soot climate forcing via snow and ice albedos, *P. Natl. Acad. Sci. USA*, *101*(2), 423–428, doi:10.1073/pnas.2237157100.

Hansen, J., M. Sato, R. Ruedy, A. Lacis, and V. Oinas (2000), Global warming in the twenty-first century: An alternative scenario, *P. Natl. Acad. Sci. USA*, *97*(18), 9,875–9,880, doi:10.1073/pnas.170278997.

Hansen, J., et al. (2005), Efficacy of climate forcings, *J. Geophys. Res.*, *110*, D18104, doi:10.1029/2005JD005776.

Hunke, E. C., and W. H. Lipscomb (2008), CICE: The Los Alamos Sea Ice Model, documentation and software, version 4.0, Tech. Rep. LACC-06-012, Los Alamos National Laboratory, Los Alamos, New Mexico, USA.

Intergovernmental Panel on Climate Change (2007), *Climate Change 2007: The Physical Science Basis. Contribution of Working Group I to the Fourth Assessment Report of the Intergovernmental Panel on Climate Change*, Cambridge Univ. Press, Cambridge, U. K.

Iversen, T., and E. Joranger (1985), Arctic air pollution and large scale atmospheric flows, *Atmos. Environ.*, *19*(12), 2,099–2,108, doi:10.1016/0004-6981(85)90117-9.

Iversen, T., et al. (2013), The Norwegian Earth System Model, NorESM1-M -Part 2: Climate response and scenario projections, *Geosci. Model Dev.*, *6*(2), 389–415, doi:10.5194/gmd-6-389-2013.

Jacobson, M. Z. (2004), Climate response of fossil fuel and biofuel soot, accounting for soot's feedback to snow and sea ice albedo and emissivity, *J. Geophys. Res.*, *109*, D21201, doi:10.1029/2004JD004945.

Jacobson, M. Z. (2010), Short-term effects of controlling fossil-fuel soot, biofuel soot and gases, and methane on climate, Arctic ice, and air pollution health, *J. Geophys. Res.*, *115*, D14209, doi:10.1029/2009JD013795.

Jacobson, M. Z., J. Wilkerson, S. Balasubramanian, W. Jr.Cooper, and N. Mohleji (2012), The effects of rerouting aircraft around the arctic circle on arctic and global climate, *Clim. Change*, *115*(3-4), 709–724, doi:10.1007/s10584-012-0462-0.

Kay, J. E., et al. (2012), Exposing global cloud biases in the Community Atmosphere Model (CAM) Using satellite observations and their corresponding instrument simulators, *J. Climate*, *25*(15), 5,190–5,207, doi:10.1175/JCLI-D-11-00469.1.

Kirkevåg, A., et al. (2013), Aerosol–climate interactions in the Norwegian Earth System Model – NorESM1-M, *Geosci. Model Dev.*, *6*(1), 207–244, doi:10.5194/gmd-6-207-2013.

Klimont, Z., et al. (2009), Projections of SO2, NOx and carbonaceous aerosols emissions in Asia, *Tellus B*, *61*(4), 602–617, doi:10.1111/j.1600-0889.2009.00428.x.

Klimont, Z., K. Kupiainen, C. Heyes, P. Purohit, J. Cofala, P. Rafaj, and W. Schoepp (2013), Global anthropogenic emissions of particulate matter, paper in preparation.

Klonecki, A., P. Hess, L. Emmons, L. Smith, J. Orlando, and D. Blake (2003), Seasonal changes in the transport of pollutants into the Arctic troposphere-model study, *J. Geophys. Res.*, *108*(D4), 8367, doi:10.1029/2002JD002199.

Koch, D., and J. Hansen (2005), Distant origins of Arctic black carbon: A Goddard Institute for Space Studies ModelE experiment, *J. Geophys. Res.*, *110*, D04204, doi:10.1029/2004JD005296.

Koch, D., S. Menon, A. Del Genio, R. Ruedy, I. Alienov, and G. A. Schmidt (2009a), Distinguishing aerosol impacts on climate over the past century, *J. Climate*, *22*(10), 2,659–2,677, doi:10.1175/2008JCLI2573.1.

Koch, D., et al. (2009b), Evaluation of black carbon estimations in global aerosol models, *Atmos. Chem. Phys.*, *9*(22), 9,001–9,026, doi:10.5194/acp-9-9001-2009.

Koch, D., et al. (2011a), Coupled aerosol-chemistry–climate twentieth-century transient model investigation: Trends in short-lived species and climate responses, *J. Climate*, *24*(11), 2,693–2,714, doi:10.1175/2011JCLI3582.1.

Koch, D., et al. (2011b), Soot microphysical effects on liquid clouds, a multi-model investigation, *Atmos. Chem. Phys*, *11*, 1,051–1,064, doi:10.5194/acp-11-1051-2011.

Kristjánsson, J. E. (2002), Studies of the aerosol indirect effect from sulfate and black carbon aerosols, *J. Geophys. Res.*, *107*(D15), 4246, doi:10.1029/2001JD000887.

Kupiainen, K., and Z. Klimont (2007), Primary emissions of fine carbonaceous particles in Europe, *Atmos. Environ.*, *41*(10), 2,156–2,170, doi:10.1016/j.atmosenv.2006.10.066.

Lamarque, J., et al. (2010), Historical (1850–2000) gridded anthropogenic and biomass burning emissions of reactive gases and aerosols: Methodology and application, *Atmos. Chem. Phys.*, *10*, 7,017–7,039, doi:10.5194/acp-10-7017-2010.

Law, K. S., and A. Stohl (2007), Arctic air pollution: Origins and impacts, *Science*, *315*(5818), 1,537–1,540, doi:10.1126/science.1137695.

Neale, R. B., et al. (2010), Description of the NCAR Community Atmosphere Model (CAM 4.0), NCAR Technical Note.

Ødemark, K., S. Dalsøren, B. Samset, T. Berntsen, J. Fuglestvedt, and G. Myhre (2012), Short-lived climate forcers from current shipping and petroleum activities in the Arctic, *Atmos. Chem. Phys.*, *12*, 1,979–1,993, doi:10.5194/acp-12-1979-2012.

Palm, S. P., S. T. Strey, J. Spinhirne, and T. Markus (2010), Influence of Arctic sea ice extent on polar cloud fraction and vertical structure and implications for regional climate, *J. Geophys. Res.*, *115*, D21209, doi:10.1029/2010JD013900.

Peters, G. P., T. B. Nilssen, L. Lindholt, M. S. Eide, S. Glomsrød, L. I. Eide, and J. S. Fuglestvedt (2011), Future emissions from shipping and petroleum activities in the Arctic, *Atmos. Chem. Phys.*, *11*(11), 5,305–5,320, doi:10.5194/acp-11-5305-2011.

Quinn, P. K., et al. (2008), Short-lived pollutants in the Arctic: Their climate impact and possible mitigation strategies, *Atmos. Chem. Phys.*, *8*(6), 1,723–1,735, doi:10.5194/acp-8-1723-2008.

Samset, B. H., et al. (2013), Black carbon vertical profiles strongly affect its radiative forcing uncertainty, *Atmos. Chem. Phys.*, *13*(5), 2,423–2,434, doi:10.5194/acp-13-2423-2013.

Sand, M., T. K. Berntsen, J. E. Kay, J. F. Lamarque, Ø. Seland, and A. Kirkevåg (2013), The Arctic response to remote and local forcing of black carbon, *Atmos. Chem. Phys.*, *13*(1), 211–224, doi:10.5194/acp-13-211-2013.

Shindell, D. (2007), Local and remote contributions to Arctic warming, *Geophys. Res. Lett.*, *34*, L14704, doi:10.1029/2007GL030221.

Shindell, D., and G. Faluvegi (2009), Climate response to regional radiative forcing during the twentieth century, *Nat. Geosci.*, *2*(4), 294–300, doi:10.1038/ngeo473.

Shindell, D., et al. (2012), Simultaneously mitigating near-term climate change and improving human health and food security, *Science*, *335*(6065), 183–189, doi:10.1126/science.1210026.

Stohl, A. (2006), Characteristics of atmospheric transport into the Arctic troposphere, *J. Geophys. Res.*, *111*, D11306, doi: 10.1029/2005JD006888.

Stohl, A., Z. Klimont, S. Eckhardt, and K. Kupiainen (2013), Why models struggle to capture Arctic Haze: The underestimated role of gas flaring and domestic combustion emissions, *Atmos. Chem. Phys. Discuss.*, *13*(4), 9,567–9,613, doi:10.5194/acpd-13-9567-2013.

Storelvmo, T., J. E. Kristjánsson, S. J. Ghan, A. Kirkevåg, Ø. Seland, and T. Iversen (2006), Predicting cloud droplet number concentration in Community Atmosphere Model (CAM)-Oslo, *J. Geophys. Res.*, *111*, D24208, doi:10.1029/2005JD006300.

Vavrus, S., M. Holland, and D. Bailey (2011), Changes in Arctic clouds during intervals of rapid sea ice loss, *Clim. Dynam.*, *36*(7-8), 1,475–1,489, doi:10.1007/s00382-010-0816-0.

Ye, H., R. Zhang, J. Shi, J. Huang, S. G. Warren, and Q. Fu (2012), Black carbon in seasonal snow across northern Xinjiang in northwestern China, *Environ. Res. Lett.*, *7*(4), 044002, doi:10.1088/1748-9326/7/4/044002.

III

Geosci. Model Dev., 6, 389–415, 2013
www.geosci-model-dev.net/6/389/2013/
doi:10.5194/gmd-6-389-2013

Geoscientific Model Development
Open Access

The Norwegian Earth System Model, NorESM1-M – Part 2: Climate response and scenario projections

T. Iversen[1,2,*], M. Bentsen[3,4], I. Bethke[3,4], J. B. Debernard[1], A. Kirkevåg[1], Ø. Seland[1], H. Drange[5,4], J. E. Kristjansson[2], I. Medhaug[5,4], M. Sand[2], and I. A. Seierstad[1]

[1]Norwegian Meteorological Institute, P.O. Box 43, Blindern, 0313 Oslo, Norway
[2]Department of Geosciences, University of Oslo, P.O. Box 1047, Blindern, 0315 Oslo, Norway
[3]Uni Bjerknes Centre, Uni Research AS, P.O. Box 7810, 5020 Bergen, Norway
[4]Bjerknes Centre for Climate Research, P.O. Box 7810, 5020 Bergen Norway
[5]Geophysical Institute, University of Bergen, P.O. Box 7803, 5020 Bergen, Norway
[*]currently at: ECMWF, Shinfield Park, Reading, RG2 9AX, UK

Correspondence to: T. Iversen (trond.iversen@met.no)

Received: 26 July 2012 – Published in Geosci. Model Dev. Discuss.: 14 September 2012
Revised: 11 January 2013 – Accepted: 4 February 2013 – Published: 22 March 2013

Abstract. NorESM is a generic name of the Norwegian earth system model. The first version is named NorESM1, and has been applied with medium spatial resolution to provide results for CMIP5 (http://cmip-pcmdi.llnl.gov/cmip5/index.html) without (NorESM1-M) and with (NorESM1-ME) interactive carbon-cycling. Together with the accompanying paper by Bentsen et al. (2012), this paper documents that the core version NorESM1-M is a valuable global climate model for research and for providing complementary results to the evaluation of possible anthropogenic climate change. NorESM1-M is based on the model CCSM4 operated at NCAR, but the ocean model is replaced by a modified version of MICOM and the atmospheric model is extended with online calculations of aerosols, their direct effect and their indirect effect on warm clouds. Model validation is presented in the companion paper (Bentsen et al., 2012). NorESM1-M is estimated to have equilibrium climate sensitivity of ca. 2.9 K and a transient climate response of ca. 1.4 K. This sensitivity is in the lower range amongst the models contributing to CMIP5. Cloud feedbacks dampen the response, and a strong AMOC reduces the heat fraction available for increasing near-surface temperatures, for evaporation and for melting ice. The future projections based on RCP scenarios yield a global surface air temperature increase of almost one standard deviation lower than a 15-model average. Summer sea-ice is projected to decrease considerably by 2100 and disappear completely for RCP8.5. The AMOC is projected to decrease by 12 %, 15–17 %, and 32 % for the RCP2.6, 4.5, 6.0, and 8.5, respectively. Precipitation is projected to increase in the tropics, decrease in the subtropics and in southern parts of the northern extra-tropics during summer, and otherwise increase in most of the extra-tropics. Changes in the atmospheric water cycle indicate that precipitation events over continents will become more intense and dry spells more frequent. Extra-tropical storminess in the Northern Hemisphere is projected to shift northwards. There are indications of more frequent occurrence of spring and summer blocking in the Euro-Atlantic sector, while the amplitude of ENSO events weakens although they tend to appear more frequently. These indications are uncertain because of biases in the model's representation of present-day conditions. Positive phase PNA and negative phase NAO both appear less frequently under the RCP8.5 scenario, but also this result is considered uncertain. Single-forcing experiments indicate that aerosols and greenhouse gases produce similar geographical patterns of response for near-surface temperature and precipitation. These patterns tend to have opposite signs, although with important exceptions for precipitation at low latitudes. The asymmetric aerosol effects between the two hemispheres lead to a southward displacement of ITCZ. Both forcing agents, thus, tend to reduce Northern Hemispheric subtropical precipitation.

Published by Copernicus Publications on behalf of the European Geosciences Union.

1 Introduction

Simulations of the Earth's climate are presented using a version of the Norwegian Earth System Model (NorESM1-M) with online calculations of aerosols and their direct effect and the first and second indirect effects of warm clouds. In the companion paper by Bentsen et al. (2012) the NorESM1-M model system is described in technical detail and validated through the evaluation of its conservative properties and by comparing simulation results with observationally based data for the historical period since 1850. The present paper focuses on the simulated response of NorESM1-M to a selection of experiments, including projections of the future global climate based on scenarios defined in the fifth phase of the Coupled Model Intercomparison Project (CMIP5) (Taylor et al., 2012). Although carbon cycling is included in the ocean and land models of NorESM1-M, another version of NorESM1, called NorESM1-ME, is used to simulate the Earth's climate with an interactive carbon cycle as described by Tjiputra et al. (2013).

A range of climate models and climate model versions participate in CMIP5, thereby providing input to the fifth Assessment Report (AR5) of the Intergovernmental Panel on Climate Change (IPCC) scheduled for publication in 2013. All data produced by the participating models, including NorESM1-M, can be downloaded from the CMIP5 multi-model data archive (http://cmip-pcmdi.llnl.gov/cmip5/index.html).

The main purpose of this paper is to establish that results from the CMIP5 experiments with NorESM1-M are valuable for the climate system science and the evaluation of possible anthropogenic influences on the global climate. The model and the model simulations are briefly summarised in Sect. 2. After discussing climate sensitivity, response and gross feedbacks in Sect. 3, the present paper addresses aspects of the historical simulations and the RCP scenarios produced with NorESM1-M. Section 4 discusses model simulated time-developments of global variables from 1850 to 2005 ("Historic") and onwards for future RCP projections. In Sect. 5, the single forcing experiments for 1850–2005 are addressed, whilst further discussions of the RCP scenario projections are done in Sect. 6. After an analysis of various regional climate patterns are done in Sect. 7, conclusions are drawn in Sect. 8.

2 The model and model simulations

As elaborated by Bentsen et al. (2012), except for the ocean model NorESM1-M is to a large extent based on the fourth version of the Community Climate System Model (CCSM4) developed in the Community Earth System Model (CESM) project centred at the US National Center for Atmospheric Research (NCAR) in collaboration with many partners (Gent et al., 2011; Meehl et al., 2012). The ocean model in both versions of NorESM1 is a considerably elaborated version of the Miami Isopycnic Community Ocean Model (MICOM) adapted for multi-century simulations in coupled mode by Assmann et al. (2010) and Otterå et al. (2010). Further extensions are described by Bentsen et al. (2012) together with a summary of all extensions since the original MICOM. The NorESM1 ocean model is predominantly developed at the Bjerknes Centre in Bergen, Norway, and an earlier version was also used in the Bergen Climate Model (BCM), which was used to provide data for CMIP3 (Meehl et al., 2005) and the AR4 of the IPCC (Furevik et al., 2003; Otterå et al., 2009). Important extensions since the BCM version include improved parameterisation of diapycnal mixing, isopycnal eddy diffusion, thickness eddy diffusion and the mixed layer depth.

The atmospheric model in NorESM1 (which denote both M and ME) is based on the version of the original CAM4 that was publicly released in April 2010 (Neale et al., 2010, 2012). Over the last 15 yr, research and modelling groups at the University of Oslo and the Norwegian Meteorological Institute (also in Oslo) have used a range of earlier NCAR model versions to develop representations of aerosols and their interactions with radiation and warm cloud microphysics. The purpose was to quantify the direct and indirect aerosol forcing (Iversen and Seland, 2002, 2003; Kirkevåg and Iversen, 2002; Kristjànsson, 2002; Storelvmo et al., 2006; Seland et al., 2008; Hoose et al., 2009; Struthers, et al., 2011) and to study aerosol interactions with climate (Kristjánsson et al., 2005; Kirkevåg et al., 2008a, b; Struthers et al., 2013). In these earlier studies of the climate response to aerosol processes, however, the atmospheric model was run coupled to a slab ocean model only. In NorESM1 the climate response of the aerosol processes is estimated in a fully coupled climate/earth system model. The latest version of the aerosol module, which is used in NorESM1, is thoroughly presented and discussed by Kirkevåg et al. (2013), and the CAM4-version with this aerosol module is denoted CAM4-Oslo.

We use the finite volume dynamical core for transport calculations (Rasch et al., 2006) with horizontal resolution 1.9° latitude by 2.5° longitude (in short: 2°) and 26 levels with a hybrid sigma-pressure co-ordinate in the vertical. The horizontal grid mesh size is double of the standard version used in CCSM4, although Gent et al. (2011) also discuss a 2° version. The stratiform cloud parameterisation is based on Rasch and Kristjansson (1998), and the parameterisation of deep convective clouds follows Zhang and McFarlane (1995) extended with the plume dilution and convective momentum transport which is also used in CCSM4 (Richter and Rasch, 2007; Neale et al., 2008). Plume dilution influences the vertical distribution of aerosols (Kirkevåg et al., 2013) and water vapour (Gent et al., 2011), and improves the modelling of tropical deep convection in a way which turns out favourably for reproducing characteristic features of the Madden-Julian Oscillation (MJO) (Subramanian et al.,

2011). The favourable MJO properties are also diagnosed for NorESM1-M by Bentsen et al. (2012). NorESM1-M accounts for the radiative effects of deposited light-absorbing mineral dust and black carbon on snow (Flanner and Zender, 2006) and sea-ice.

A schematic of the CMIP5-experiments with NorESM1-M is shown by Bentsen et al. (2012) in their Fig. 1. Throughout this paper, we use "piControl" to identify the 500 yr control simulation with constant external forcing prescribed at 1850 conditions. This simulation starts in year 700 after a spin-up with the same forcing. As discussed by Bentsen et al. (2012), the spin-up is carried out in order to reduce trends in the piControl after tuning of parameters. Three ensemble members were branched off from the piControl in years 700, 730 and 760 for simulations "Historic1, "Historic2" and "Historic3". From 1850 to 2005, the natural variations of solar radiation (Lean et al., 2005; Wang et al., 2005), the stratospheric sulphate aerosol concentrations from explosive volcanoes (Ammann et al., 2003), and the anthropogenic changes in GHG concentrations, aerosol emissions (Lamarque et al., 2010) and land-cover, were prescribed using the data from http://cmip-pcmdi.llnl.gov/cmip5/forcing.html.

The historical forcing experiments branch off from piControl in year 700 as for Historic1. They are denoted "GHG only", "Aerosol only", and "Natural forcing only", where the forcing is kept constant as in piControl except for the single forcing contribution which is identified by the name. From 2005 onwards, the representative concentration pathway (RCP) scenarios (van Vuuren et al., 2011) were the basis for climate projections until 2100: RCP2.6, RCP4.5, RCP6.0 and RCP8.5, where the numbers are the expected TOA forcing in Wm^{-2} by 2100. The RCP4.5 was extended to run until 2300 keeping external conditions as in 2100. The historical simulations have been extended to 2012 using RCP8.5 for the years 2006–2012.

Bentsen et al. (2012) present a thorough validation analysis of trends in piControl along with comparisons of the historical runs with data that are observationally based or from global re-analyses. In summary, the average radiative heat flux at the top of the atmosphere (TOA) in piControl is positive, but smaller than $0.1\,\mathrm{Wm}^{-2}$. More than 99 % of this excess heat is transferred to the oceans, which experience a statistically significant temperature increase. There are also small negative trends in the ocean salinity, the winter maximum sea-ice area in both hemispheres and the Atlantic meridional overturning circulation (AMOC). Other climatologically important parameters have insignificant global trends during the 500 yr of the piControl, including surface air temperature, cloudiness, precipitation and evaporation. The difference between global evapotranspiration and precipitation (E-P) averaged over a few decades or longer, is not significantly different from zero in any of the experiments, including piControl, implying that the global water cycle budget in NorESM1-M is closed.

In summary from Bentsen et al. (2012), by the end of the 20th century the surface air temperature is simulated to be too low by about 0.8–0.9 K globally and 1.0–1.1 K over land. The global precipitation is estimated to be up to about $0.15\,\mathrm{mm\,day}^{-1}$ too high, the evaporation from oceans is over-estimated with ca. 4 %, and the net flux between oceans and continents are ca. 8 % over-estimated. The intensity of the water-cycle is, therefore, slightly overestimated, while the atmospheric lifetime of water vapour is close to correct (compared to Trenberth et al., 2011). These properties can be linked to the fact that the model underestimates the global cloud fraction considerably (by 15–25 %), while the tropospheric liquid water is over-estimated (Jiang et al., 2012). The double ITCZ is less pronounced in NorESM1-M than in CCSM4 with the same resolution.

The model simulates characteristic flow patterns that can be associated with features diagnosed from observational data. This includes the Madden-Julian Oscillation (MJO), which was simulated with skill already in CCSM4 (Subramanian et al., 2011), ENSO, and the northern and southern annular modes. The AMOC strength is in the upper range found in models contributing to CMIP3 and above the range estimated from synthesized observational data (Medhaug and Furevik, 2011). Whilst the sea-ice extent is overestimated in both hemispheres in summer and in the southern winter, it is underestimated during northern winter. Kirkevåg et al. (2013) used NorESM's atmospheric model CAM4-Oslo to estimate the direct and indirect forcing of aerosol changes between the years 1850 and 2000 (2006) to be $-0.10(-0.08)$ and $-0.91\,\mathrm{Wm}^{-2}$ ($-1.2\,\mathrm{Wm}^{-2}$), respectively. The estimated indirect forcing in warm clouds is modest compared to many other models, and this is achieved without assuming artificial lower thresholds in the number of aerosols or cloud droplets (Hoose et al., 2009). However, the modelled aerosol loadings are at the high end in the free troposphere (Myhre et al., 2013; Samset et al., 2013).

3 Equilibrium climate sensitivity and transient response

Global climate models are useful for diagnosing a range of characteristics for how the global climate may respond to a standard specified forcing. This facilitates the comparison of climate change properties across different climate models. This section discusses results of two such experiments under the CMIP5 protocol using NorESM1-M integrated over 150 and 140 yr, respectively. The simulations were both initiated in year 700, i.e., from the start of piControl after spin-up, and are referred to as "abrupt $4\times\mathrm{CO_2}$" (quadrupling of atmospheric $\mathrm{CO_2}$ concentrations at $t = 0$) and "gradual $4\times\mathrm{CO_2}$" (1 % increase per year until quadrupling). Results are presented in Tables 1, 2, 3 and 4, as well as in Fig. 1. Since we have not applied any proper method for estimating changes in single climate elements (e.g., cloud cover) in response

Table 1. Different estimates of climate sensitivity of the NorESM1-M with 2° resolution. Data for the CCSM4 with 1° resolution included for comparison are provided by Bitz et al. (2012). Symbols are explained in the main text; see also Fig. 1.

	ΔT_{eq} K	ΔT_{eff} K	ΔT_{reg} K	$R_{f_{reg}}$ Wm^{-2}	λ_{reg} $Wm^{-2}\,K^{-1}$	ΔT_{TCR} K	$\Delta T_{TCR,eff}$ K
NorESM1-M, 2°	not calc.	2.86	2.87	3.16	1.101	1.39	2.32
CCSM4, 1°	3.20	2.78	2.80	2.95	1.053	1.72	2.64

Table 2. Global gross feedback response (λ_X) in TOA radiation parameters (X) as determined by linear regression of model simulated annual change (ΔX) with respect to the corresponding annual surface air temperature change (ΔT) after abrupt $4 \times CO_2$. The quantity $\lambda_X = d(\Delta X)/d(\Delta T)$, and X is long-wave (LW) and short-wave (SW) all-sky and clear-sky TOA outgoing radiation, long-wave (LWCF) and short-wave (SWCF) cloud forcing, or net cloud radiative effect (CRE).

	$\lambda_{LWAllsky}$ $Wm^{-2}\,K^{-1}$	$\lambda_{SWAllsky}$ $Wm^{-2}\,K^{-1}$	$\lambda_{LWclearsky}$ $Wm^{-2}\,K^{-1}$	$\lambda_{SWclearsky}$ $Wm^{-2}\,K^{-1}$	λ_{LWCF} $Wm^{-2}\,K^{-1}$	λ_{SWCF} $Wm^{-2}\,K^{-1}$	λ_{CRE} $Wm^{-2}\,K^{-1}$
NorESM1-M, 2°	−1.80	+0.70	−1.86	+0.84	+0.06	−0.15	−0.09

Table 3. Global gross feedback response (λ_X) in parameters (X) characterising the hydro-climate, as determined by linear regression of model simulated annual change (ΔX) with respect to the corresponding annual surface air temperature change (ΔT) after abrupt $4 \times CO_2$. X is annual amounts of evaporation (E), precipitation (P), or the difference (E-P) accumulated globally, from oceans, or from land (10^3 km^3 yr^{-1}).

	$\lambda_{P\text{-GLOB}}$ $10^3\,km^3\,K^{-1}$	$\lambda_{E\text{-OCEAN}}$ $10^3\,km^3\,K^{-1}$	$\lambda_{P\text{-OCEAN}}$ $10^3\,km^3\,K^{-1}$	$\lambda_{(E\text{-}P)\text{-OCEAN}}$ $10^3\,km^3\,K^{-1}$	$\lambda_{E\text{-LAND}}$ $10^3\,km^3\,K^{-1}$	$\lambda_{P\text{-LAND}}$ $10^3\,km^3\,K^{-1}$
NorESM1-M, 2°	14.58	12.42	12.40	+0.02 (−0.29 − +0.32)	2.16	2.18

Table 4. Global gross feedback response (λ_X) in ($X =$) yearly averaged sea-ice area (AREA, 10^6 km^2 yr^{-1}), and volume (VOL, 10^3 km^3 yr^{-1}) in the Northern (NH) or Southern (SH) Hemispheres, as determined by linear regression of model simulated annual change (ΔX) with respect to the corresponding annual surface air temperature change (ΔT) after abrupt $4 \times CO_2$.

	$\lambda_{AREA\text{-NH}}$ $10^6\,km^2\,K^{-1}\,yr^{-1}$	$\lambda_{VOL\text{-NH}}$ $10^3\,km^3\,K^{-1}\,yr^{-1}$	$\lambda_{AREA\text{-SH}}$ $10^6\,km^2\,K^{-1}\,yr^{-1}$	$\lambda_{VOL\text{-SH}}$ $10^3\,km^3\,K^{-1}\,yr^{-1}$
NorESM1-M, 2°	−2.39	−10.55	−0.86	−2.52

to temperature increases when other elements are kept unchanged, the feedback factors we present (e.g., for clouds) are termed gross feedback factors (Andrews et al., 2012). These factors can be influenced by simultaneous changes in other elements than the temperature (e.g., snow cover). See Gettelman et al. (2012) for estimates of proper feedback factors.

The Equilibrium Climate Sensitivity (ECS) is defined as the change in global mean near-surface air temperature when a new climate equilibrium is reached after an abrupt increase of the atmospheric CO_2 concentrations introduced to a climate already in equilibrium. To calculate the ECS from first principles requires climate model simulations over several thousand years (Boer and Yu, 2003). ECS is, therefore, frequently approximated as the difference, ΔT_{eq}, between equilibrium near surface air temperatures obtained from two runs over a few decades, but with a model version where the deep ocean model is replaced by a thermodynamic slab. Bitz et al. (2012) used a slab ocean model for which the deep ocean heat fluxes were calibrated with data from runs with the full CCSM4. With 1° atmospheric resolution they estimated $\Delta T_{eq} = 3.20$ K after doubling of CO_2, while 3.13 K was estimated for the 2° version. This is close to the value 3.14 K which was found for the previous CAM3-based version of CAM-Oslo coupled to a slab ocean (Kirkevåg et al., 2008a).

Estimates of ΔT_{eq} for NorESM1-M with a slab ocean are not available, but two other approximations of ECS are estimated for the full NorESM1-M. Both methods use simultaneous values of surface air temperature change ($\Delta T(t)$) and TOA radiation imbalance ($\Delta R(t)$) estimated at the time

t after the abrupt quadrupling of atmospheric CO_2 concentrations.

Gregory et al. (2004) proposed to use a linear regression between $\Delta R(t)$ and $\Delta T(t)$, assuming negligible contributions from time-varying feedbacks. The slope of the regression line is the overall feedback parameter $\lambda = -\mathrm{d}\Delta R/\mathrm{d}\Delta T$ (in units of $\mathrm{Wm^{-2}\,K^{-1}}$), the intercept at $\Delta T = 0$ approximates the instantaneous forcing R_f, while the intercept ΔT_reg at $\Delta R = 0$ approximates the ECS. In reality, this estimate of R_f disregards rapid adjustments during the first year of the simulation and it, therefore, underestimates the true instantaneous forcing of the quadrupled CO_2 (Andrews et al., 2012).

Murphy (1995) proposed to use the remaining TOA radiative imbalance $\Delta R(t)$ at the time t to approximate ECS. This approximation, termed the effective climate sensitivity and denoted $\Delta T_\mathrm{eff}(t)$, is:

$$\Delta T_\mathrm{eff}(t) = \frac{\Delta T(t) R_\mathrm{f}}{R_\mathrm{f} - \Delta R(t)}. \quad (1)$$

Assuming the same linear relationship between $\Delta T(t)$ and $\Delta R(t)$, ΔT_eff should not depend on time. However, slow feedback processes, for example involving the deep ocean, may cause changes to occur over decades and centuries (Senior and Mitchell, 2000). Furthermore, chaotic fluctuations in the climate response may lead to high-frequency variations in $\Delta R(t)$. Figure 1a shows results for both $\Delta T(t)$ (black dots for years 1–150) and ΔT_eff (red dots for years 111–150), where we assume $R_\mathrm{f} = 7.0\,\mathrm{Wm^{-2}}$ as estimated by Kay et al. (2012).

The two approximations to ECS are $\Delta T_\mathrm{reg}(4\times CO_2) = 5.74\,\mathrm{K}$ from the regression, with feedback parameter $\lambda \cong 1.101\,\mathrm{Wm^{-2}\,K^{-1}}$, and $\Delta T_\mathrm{eff}(4\times CO_2) = 5.71\,\mathrm{K}$ using Eq. (1) with values averaged over the last 40 of the 150 yr of the abrupt $4\times CO_2$ experiment (black cross in Fig. 1). The numbers in Table 1 are these divided by 2 since the effect of CO_2 doubling are more standard in the literature (e.g., Andrews et al., 2012). Notice that the forcing approximated by the regression (see Fig. 1a) is only $6.32\,\mathrm{Wm^{-2}}$ due to the fast adjustments during the first year of the integration. Furthermore, slow deep-oceanic feedbacks may delay the response and, thus, render the linear regression inaccurate. For example, a regression for years 1–76 yields a smaller approximation of the ECS (5.18 K), indicating that there may be slow feedback mechanisms at work. Andrews et al. (2012) indicate that short-wave radiative effects of clouds over oceans may cause nonlinearity over the first decades.

As shown in Table 1, our approximate ECS estimates for doubled CO_2 are close, but slightly larger than Bitz et al. (2012) obtained for CCSM4. For both NorESM1-M and CCSM4, the estimates of ΔT_reg are in close agreement with the estimated ΔT_eff. In relation to the other 14 models studied by Andrews et al. (2012) NorESM1-M is amongst the least sensitive. Figure 1b and the numbers in Table 2 show that clouds tend to stabilise the response as the long-wave response is positive but small, and the short-wave response is negative. Of the 15 models studied by Andrews et al. (2012), 9 produce a negative gross cloud feedback, and the spread in values are large. NorESM1-M is close to the average. There is a much better agreement between models for clear-air feedback, all with values close to those given in Table 2 (Andrews et al., 2012).

A simple measure of climate sensitivity associated with gradual changes in the external forcing is the Transient Climate Response (TCR). TCR can be estimated from the gradual $4\times CO_2$ experiment as the globally averaged difference in surface air temperature (ΔT_TCR) between the time of doubled atmospheric CO_2 (averaged over years 60–80) and the corresponding years in the piControl. An effective response that approximately takes into account the remaining TOA radiative imbalance can also be estimated by applying Eq. (1). We have estimated ΔT_TCR to be 1.39 K and $\Delta T_\mathrm{TCR,eff}$ to be 2.32 K, and compared them with values calculated for CCSM4 by Bitz et al. (2012) (Table 1). While the approximate values for ECS were close to each other, the TCR for NorESM1-M is considerably smaller than for CCSM4. As discussed below, this feature of the TCR for NorESM1-M can be related to the model's strong AMOC which contributes to an efficient flux of heat into the oceans.

As documented by Bentsen et al. (2012), the average maximum strength of the AMOC at 26.5° N in piControl is 30.8 Sv ($\mathrm{Sv} = 10^6\,\mathrm{m^3\,s^{-1}}$). Gent et al. (2011) reports the maximum AMOC strength in CCSM4 to be above 24 Sv, which is also strong compared to many other models. Figure 1c shows how AMOC responds to the abrupt (blue) and gradual (red) CO_2 increase in the model, and Fig. 1d shows, for the gradual $4\times CO_2$ experiment, that the deep ocean is particularly efficiently heated at high latitudes where dense water is created and sinks. While AMOC is reduced by 8–10 Sv over the first couple of decades and then remains almost constant in the abrupt experiment, the reduction is slower and almost linear with time in the gradual experiment. Figure 1e and f show the heat flux at different ocean depths averaged over the entire globe and illustrates how efficient the net downward radiative heat flux at the top of the model penetrates downwards in the world oceans.

By the time of CO_2 doubling, AMOC is reduced with about 3–5 Sv in the gradual experiment. The heat fluxes into the deep ocean shown in Fig. 1e and f reduce the fraction of the net heat flux at the top of the model that is available for further increase in surface temperatures, evaporation of water and melting of ice. An efficient heat transport into the deep oceans, thus, reduces the traditional measures of climate sensitivity. It can be seen from Fig. 1f that a slab ocean model with 200 m thickness of the mixed layer would require almost 50 yr spin-up to reach a quasi-equilibrium state for the $4\times CO_2$ climate. The transfer of heat into the deep ocean is a much slower and spatially heterogeneous process.

Despite that AMOC is stronger in the experiment with gradual CO_2-increase, the heat transport into the deep ocean may appear more efficient in the abrupt experiment. This is

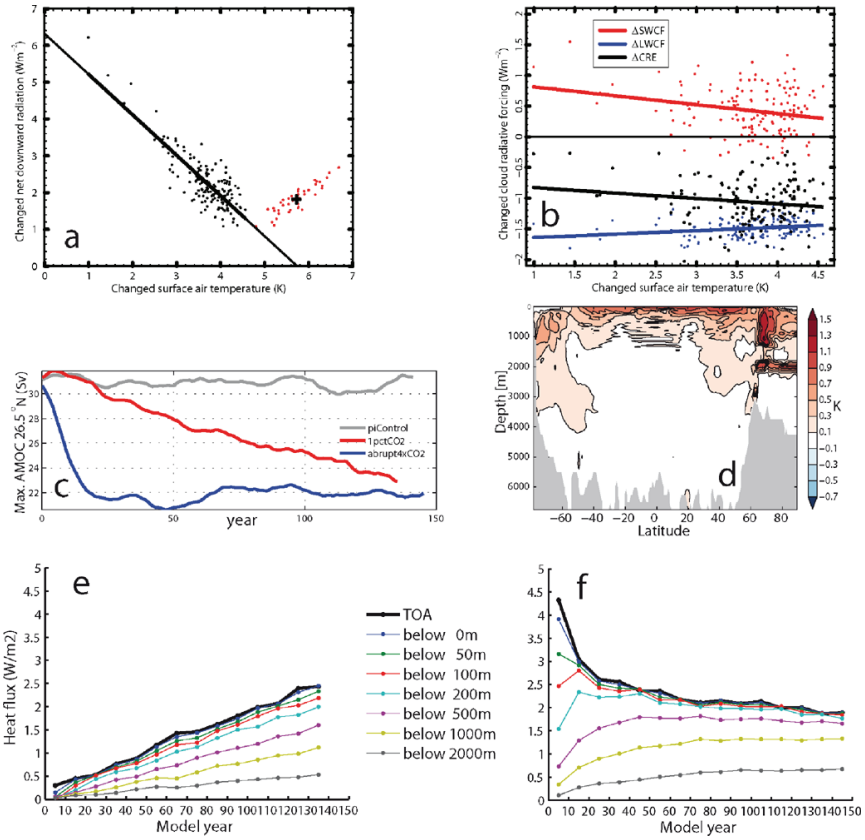

Fig. 1. Aspects of climate sensitivity and gross feedback effects in NorESM1-M based on the experiments "abrupt $4 \times CO_2$" and "gradual $4 \times CO_2$". **(a)** Model simulated change in yearly TOA net downward radiation (Wm^{-2}) as a function of changed global surface air temperature (K) (black dots) and effective temperature response, $\Delta T_{\mathrm{eff}}(n)$ (red dots, $n = 111, \ldots, 150$), for the abrupt $4 \times CO_2$ experiment. The black line is the linear regression with a slope $\lambda = 1.101\ Wm^{-2}\ K^{-1}$ and intercept $\Delta T_{\mathrm{reg}}(4 \times CO_2) = 5.74$ K with the x-axis. The black cross is the average for the red dots with $\Delta T_{\mathrm{eff}}(4 \times CO_2) = 5.71$ K. **(b)** Calculated changes in TOA long wave (blue), short wave (red) and net (black) downward cloud radiation (Wm^{-2}), as a function of changed global surface air temperature for the abrupt $4 \times CO_2$ experiment. The slopes of the linear regression lines are given in Table 2. **(c)** The maximum AMOC (Sv) at 26.5° N as a function of time for piControl (grey), abrupt $4 \times CO_2$ (blue) and gradual $4 \times CO_2$ (red). **(d)** Changed temperature zonally averaged for global oceans for the gradual $4 \times CO_2$ experiment at the time of CO_2 doubling. **(e)** The global TOA radiation heat flux as a function of time in the gradual $4 \times CO_2$ experiment along with the globally averaged downward flux of heat through depth levels in the world oceans. **(f)** Same as **(e)**, but for the abrupt $4 \times CO_2$ experiment.

an artefact caused by the exponential increase in atmospheric CO_2 (1 % increase per year) starting from pre-industrial levels. These annual forcing increments add to the TOA imbalance, and the increments penetrate into the deep ocean with a characteristic time which is influenced by the strength of the AMOC. As the AMOC strength decreases gradually, the downward heat transport at high latitudes also decreases. The deep ocean heating will, therefore, continue several decades even without further CO_2 increase after the doubling (when the TCR is estimated), but the efficiency will gradually decrease as AMOC steadily reduces its strength before stabilising at a smaller value. This is due to the heating and freshening of the upper ocean layers at high latitudes. This slow reduction of the deep ocean heating efficiency is different from the abrupt experiment which establishes a new quasi-stable AMOC already after a few decades. We hypothesise that $\Delta T_{\mathrm{TCR,eff}}$ at the time of CO_2-doubling underestimates the true equilibrium temperature after CO_2-doubling, due to this multi-decadal nonlinear contribution to the feedbacks.

The results from linear regressions between corresponding changes in selected variables characterising the global climate and the change in surface air temperature for the abrupt $4 \times CO_2$ experiment, are summarised in Tables 3 and 4. Table 3 shows positive gross feedback factors for the hydroclimatic variables, i.e., how much they change with a unit (K) increase in temperature. The factor for global precipitation increase is equivalent to ca. $2.7\,\%\,K^{-1}$, which probably is on the high side (e.g., Trenberth, 2011). The factor is about 6 times larger over the oceans than over continents, but almost all of the response over the ocean is due to recycling of oceanic evaporation. The slight surplus of $0.02 \times 10^3\,km^3\,K^{-1}$ for oceanic evaporation over precipitation equals the deficit over the continents. This number results from a small imbalance between terms that are several orders of magnitude larger, and the implied uncertainty is shown as an interval in Table 3. Nevertheless, based on the abrupt $4 \times CO_2$ experiment, the model predicts a more intense water cycle with a small, but uncertain increase in the atmospheric lifetime of water vapour with increased temperatures.

Corresponding factors for change in yearly mean sea-ice volume and area in each of the hemispheres are given in Table 4. The sensitivity parameters are all negative and the sensitivity is considerably higher in the Arctic than in the Antarctic. In the Arctic, melting of sea-ice is in particular associated with the surface albedo feedback effect, which also involves changes in the snow cover.

4 Time trends of interactive forcing agents

The only prescribed aerosol concentrations in the model are stratospheric sulphate from explosive volcanoes in the historical period (Ammann et al., 2003). Other aerosol components are calculated from prescribed emission data, or, for sea-salt, from emissions calculated as a function of wind speed and ocean temperature. Kirkevåg et al. (2013) present and evaluate the aerosol module, including estimates of direct and indirect aerosol forcing. We emphasise that a correct simulation of forcing of anthropogenic aerosols since 1850 depends on the amount and properties of the background of aerosols in 1850 of natural and anthropogenic (biomass burning and early industrialisation) origins, as well as the associated cloud droplet properties (Hoose et al., 2009). It should be noted that there were considerable anthropogenic aerosols already in 1850. In a few places, emissions from forest fires and also from natural secondary organics from areas that used to be forested were larger in 1850. The model calculates mass concentrations of sulphate, black carbon (BC) and particulate organic matter (POM) which includes the secondary organics (SOA), in addition to the major natural components sea-salt and mineral dust. The aerosols interact directly with solar radiation, and a prognostic equation for the liquid water droplet number in stratiform clouds uses activation of cloud condensation nuclei (CCN) from the modelled distribution of aerosol size and composition (Storelvmo et al., 2006).

Figure 2 shows the historic and future scenario developments of the average global loadings of particulate sulphate, BC, and POM since 1850 as simulated by NorESM1-M. Both natural and anthropogenic aerosols are included, but the major part of the long-term trends since 1850 are due to anthropogenic activities involving fossil fuel combustion and to some extent biomass burning. POM has a relatively larger fraction of natural aerosols because of biogenic emissions from oceans and from land vegetation. All the RCP scenarios, and RCP2.6 for BC in particular, peak during the first decades of the 21st century before decaying to slightly higher levels than in 1850 towards the end of the century. The globally averaged aerosol optical depth and the absorption component both show the natural part in the historical period. They include the contribution of stratospheric sulphate from known explosive volcanoes since 1850, and the scattering effect of the volcanic aerosols is considerable for 1–3 yr in each case. This also demonstrates that the sustained impacts of the anthropogenic aerosols are due to the continuous replenishment from human activity. The decaying loadings and optical depths in the 21st century, therefore, follow immediately from assumed changes in emissions. For most greenhouse gases this is not the case, because of their long residence time in the earth system.

Figure 3 shows the calculated TOA long-wave, short-wave and net radiative imbalances in the period from 1850 to 2300. While a negative trend is simulated for both the long-wave and short-wave from 1850 to 1970, the net radiative flux has a trend close to zero. The trends become positive after ca. 1970 and increase for the future RCP scenarios. The net TOA imbalance is ca. $0.6\,Wm^{-2}$ by the first decade of the 21st century, but the year-to-year variations are substantial. The effect of the change after 1970 is seen in the global mean near surface temperature and in the global precipitation rate. Bentsen et al. (2012) discuss the realism of this and other results for the historical period.

5 Historical single forcing simulations

As an element in attributing climate change and variability since 1850 to possible causes, a few selected single forcing simulations are made as a part of the CMIP5 protocol. We have only run single realisations for each of these forcing simulations, which is insufficient to estimate statistical significance with respect to attribution of climate variations. However, they contribute to the multi-model ensemble in CMIP5 for IPCC AR5. Here we discuss three such experiments. In "GHG only", all but the prescribed greenhouse gas concentrations are kept constant at the 1850-level; in "Aerosol only" all but aerosol emissions are as in 1850; and in "Natural forcing only", only the natural contributions from solar activity and eruptive volcanoes are varied after 1850.

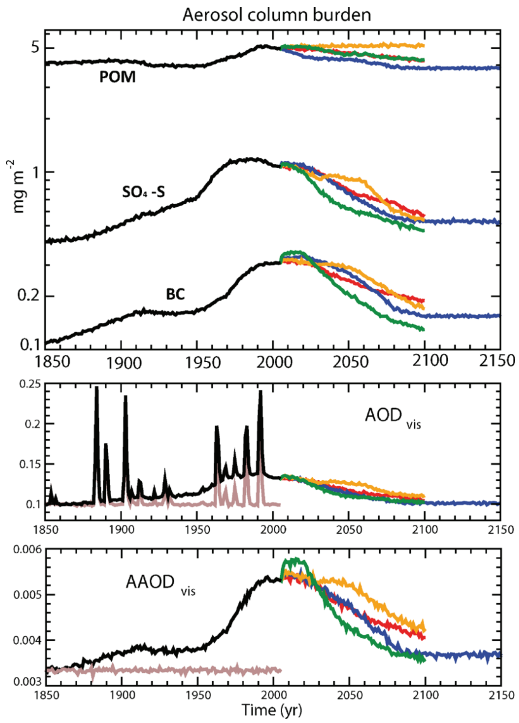

Fig. 2. Globally and annually averaged aerosol column burdens for particulate organic matter (POM), particulate sulphate as S (SO_4-S), and black carbon (BC) (upper panel), aerosol optical depth (AOD) (middle panel), and aerosol optical depth for absorption (AAOD) (lower panel) from 1850 onwards, calculated online in NorESM1-M. Curves for Historic1 from 1850 to 2005 are black. For scenario projections, green are RCP2.6 for 2005–2100, blue are RCP4.5 for 2005–2300 (negligible variations after 2150), orange are RCP6.0 for 2005–2100, and red are RCP8.5 for 2005—2100. The brown curves are contributions to AOD and AAOD in Historic1 by natural aerosols only, including prescribed stratospheric sulphate from explosive volcanoes.

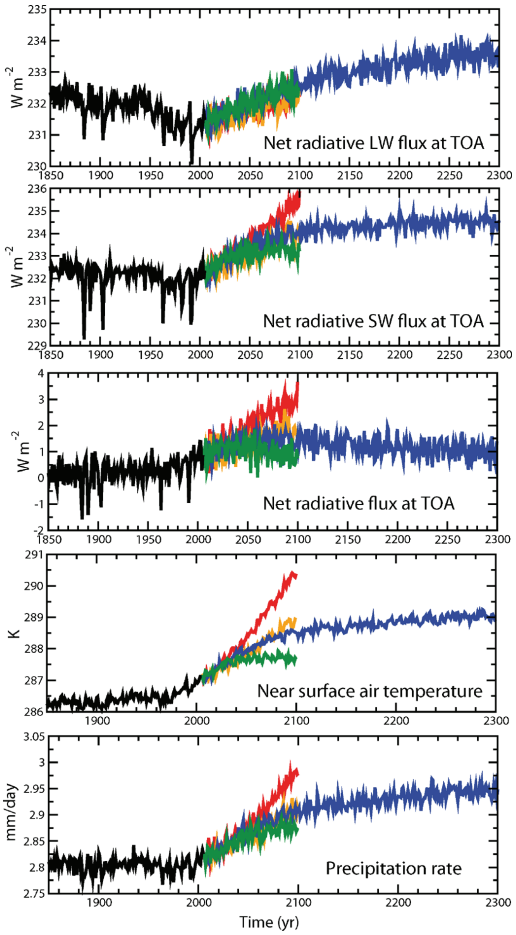

Fig. 3. From the top panel and downwards, the figure shows the net global long-wave (positive upwards), short-wave (positive downwards), and total (positive downwards) radiative flux at the top of the atmosphere during the NorESM1-M simulations for 1850 to 2300. The next two panels show diagrams for the global surface air temperature and average daily precipitation. Black: Historic1, green: RCP2.6, blue: RCP4.5, orange: RCP6.0, and red: RCP8.5.

Figure 4 shows results for surface air temperature and precipitation in the individual forcing experiments. For temperature it appears that the simulated warming since the 1970s cannot be reproduced with natural forcing only. Furthermore, the greenhouse gases alone will lead to an exaggerated warming estimate, while aerosols significantly dampen the warming exerted by GHG. For global precipitation the picture is much less clear, and the regional variations in the simulated precipitation changes are crucial. Even if the global trend in the annual precipitation is positive, there are considerable reductions in some continental regions.

The maps in Fig. 4 show that regional responses to GHG forcing and aerosol forcing have many similar geographical patterns, but with opposite sign. Given that the spatial forcing patterns of GHG and aerosols are very different, the similarity in the response pattern demonstrates that internal dynamics (Palmer, 1999; Branstator and Selten, 2009) and geographically determined feedbacks (Boer and Yu, 2003) determine the nature of the climate response, rather than the forcing pattern itself. Kirkevåg et al. (2008b) found similar results with a model coupled to a slab ocean.

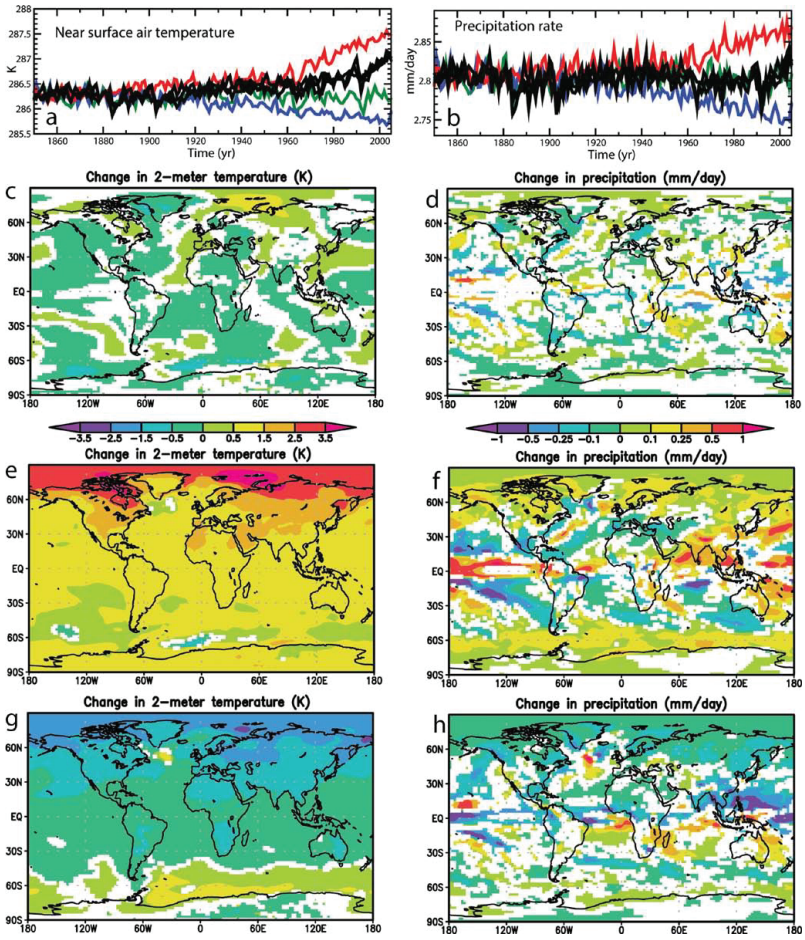

Fig. 4. NorESM1-M single forcing simulations of the historical period 1850–2005 and for the period 1976–2005 compared to piControl. Response in annual mean surface air temperature (left panels **a**, **c**, **e**, **g**) and average daily precipitation amounts (right panels, **b**, **d**, **f**, **h**). The graphs in the top panels (**a** and **b**) show global annual values from 1850 to 2005 for Historic1, 2, and 3 with full forcing (black), with natural forcing only (green), GHG-forcing only (red), and aerosol-forcing only (blue). The maps in the six panels below show changes between piControl and 1976–2005 for natural forcing only (**c** and **d**), GHG-forcing only (**e** and **f**), and aerosol forcing only (**g** and **h**). White patches indicate areas where changes are not significant at the 95 % confidence level (two-sided, Student t-test with respect to variance of annual values in piControl).

Figure 4 also shows that there are only small and patchy regional changes of temperature and precipitation in the run with only natural forcing included. Even though regionally the changes are diagnosed as significant at 5 % level compared to the unforced variance of annually averaged values, the trends appear unsystematic, where positive and negative values are approximately equally likely. This contrasts with the systematic trends in the runs with GHG-forcing only and aerosol-forcing only.

There are important exceptions for the precipitation response, however, which has the same sign for GHG forcing and aerosol forcing in some areas. This kind of apparent mutual reinforcement may occur by chance due to internal variability, and firm conclusions based on single realisations of the experiment are not possible. To some extent, random reinforcements or cancellations can be checked by adding the spatial response of each single forcing experiment and compare this sum with the response of a single experiment that employs the sum of the two forcing components. In areas

where the two fields differ considerably, chaotic internal variations may dominate over systematic mutual reinforcements or cancellations. Since random patterns in the two single-forcing experiments may also behave similarly by chance, however, a more confident conclusion requires several ensemble members.

The maps in Fig. 5 show the added annual precipitation responses of the GHG-only and the aerosol-only (c) and its difference from the total response in the Historic1 run (d). The difference in Fig. 5d is influenced by chaotic internal variability as well as impacts of minor forcing agents originating from volcanic eruptions, and changes in solar activity and surface albedo due to changed land cover. Amongst these, only the impacts of the sum of volcanoes and solar activity (natural forcing) are investigated in separate CMIP5-runs for the historic period, and the sum of the response to those, GHG-only, and aerosols-only are shown in Fig. 5e, whilst Fig. 5f show the difference between that sum and Historic1. The minor differences between Fig. 5d and f indicate that the differences in (d) are dominated by the sum of the response to land cover driven surface albedo changes and unforced, internal variability (chaos) and not by a response to the natural forcing. Unfortunately, we cannot quantify how large fraction of this is pure chaotic variability.

Any trend signals that, according to colours in Fig. 5c, may exist in areas that are not white in Fig. 5d are likely to be partly or fully masked by internal variability or land-cover induced albedo changes. On the other hand, areas which are white in both (c) and (d) probably experience systematically vanishing trends, for example due to cancellation between the effects of GHG and aerosols. Systematic non-zero trends are indicated where areas are coloured in (c) but white in (d), or the coloured values in (d) are considerably smaller than those in (c).

Based on this, the NorESM1-M results indicate significant increases in extra-tropical precipitation over oceans, whilst precipitation in sub-tropical areas and in some northern hemispheric continental temperate regions is reduced. In the tropics, vanishing precipitation trends dominate except for a few regions to the south (Africa and Oceania), where trends are positive.

The impact of GHG forcing on the tropical and subtropical precipitation patterns shown in Fig. 4 (right middle panel) relates to an intensified Hadley circulation with increased precipitation close to the equator and reduced in the adjacent subtropics in both hemispheres. The changes over oceans west of South America and Africa are not statistically significant at the 5 % level. There are also extended dry zones towards the middle latitudes. Whilst the impacts of aerosols in general tend to counteract the GHG-driven changes at low latitudes (Fig. 4 lower right panel), the larger cooling by anthropogenic aerosols in the Northern than in the Southern Hemisphere leads to a southward displacement of the Hadley cell and the associated strong precipitation in the ITCZ. This result was reported, for example, by Rotstayn and Lohmann (2002), Kristjansson et al. (2005), and Kirkevåg et al. (2008b) using slab ocean models. The reduced and displaced Hadley circulation caused by anthropogenic aerosols may lead to partial reinforcements of the considerably more symmetric strengthening caused by the GHG.

Since aerosols predominantly influence solar radiation, the asymmetric response is particularly pronounced during the NH summer. This can be seen by comparing Fig. 5a and b. The subtropical drying appears more pronounced in the Northern Hemisphere than in the Southern, while the moistening of the tropics is more pronounced in the southern flank of the ITCZ. As discussed in the companion paper by Bentsen et al. (2012), we relate the effects of aerosols to an improved precipitation pattern in NorESM1-M with a reduced split of the ITCZ over low latitudes in the Pacific Ocean compared to CCSM4 (Gent et al., 2011).

6 Climate projections based on RCP-scenarios

In accordance with the timing of the prescribed developments of concentrations and emissions in the RCP-scenarios, the first ensemble member of the historical period is extended with 4 climate projections to year 2100. RCP4.5 is, furthermore, extended to year 2300. Results discussed here are given in Tables 5 and 6, and Figs. 6–10.

6.1 Surface temperatures and sea-ice

Figure 6 shows calculated surface air temperatures at reference height relative to the mean 1850–1899 averaged both globally and over the polar region north of 65° N. By the end of the 21st century, the global mean ranges from ca. +1.2 K for RCP2.6 to ca. +4.0 K for RCP8.5 and the polar region mean from ca. +3.5 K to 9.7 K, with a notable downward trend for RCP2.6. The global numbers in Table 5 are smaller as they represent changes for two 30-yr periods separated by 95 yr (1976–2005 to 2071–2100).

The year-to-year variability is also considerably larger for the NH polar region than globally. The signal-to-noise ratio is not quantified, but it is smaller in the polar region due to the large natural variability in the region (Bentsen et al., 2012). Together with the fact that NorESM1-M underestimates the observed trends north of 60° N, this hampers a firm conclusion concerning the quality of modelled climate trends in the Arctic.

Figure 7 shows a comparison of NorESM1-M surface air temperature relative to the 1850–1899 average, with statistics from 15 CMIP5 models (one being NorESM1-M, Andrews et al., 2012). The selected results are for the RCP2.6 and RCP8.5 scenarios and are global means (left) and averages over land areas (right). NorESM1-M values are within one standard deviation away from the multi-model mean, but persistently lower than the average. This is in accordance with the relatively small climate sensitivity found in Sect. 3. A full explanation will require a separate study of the properties of all the models. Candidate explanations should for example

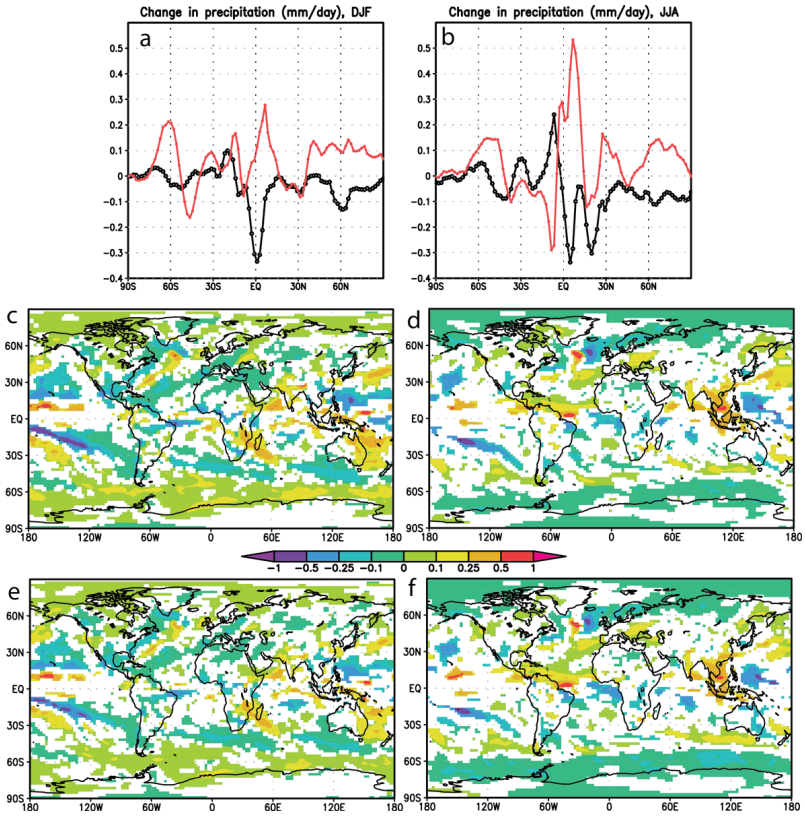

Fig. 5. Model simulated change in average daily precipitation during 1976–2005 relative to piControl for the historical forcing experiments "GHG only" and "aerosol only". Upper panels: zonally averaged changes in daily precipitation amounts for December-January-February **(a)** and June-July-August **(b)**. Red: GHG only; black: aerosol only. Lower panels: the sum of the annual changes in the GHG only and the aerosol only experiments **(c)**; the difference between the sum in **(c)** and the total changes in the Historic1 experiment **(d)**; the sum of the annual changes in the GHG only, the aerosol only, and the natural only experiments **(e)**; the difference between the sum in **(e)** and the total changes in the Historic1 experiment **(f)**. White patches indicate areas where changes are not significant at the 95 % confidence level (two-sided, Student t-test with respect to variance of annual values in piControl). Units are mm day^{-1} in all panels.

take into account that not all the CMIP5-models include the negative forcing contributions from both the direct and the indirect aerosol effect which NorESM1-M does. Furthermore, NorESM's gross cloud radiative feedback is negative, and the model's strong AMOC may transfer heat into the deep oceans more efficiently than many other models. Figure 7 also shows that both the inter-model spread and the size of the warming are considerably larger over land than globally, a feature which is also seen when comparing the changes in SST to those of global temperatures in Table 5. The simulated SST changes account for 55–60 % of the changes in global surface air temperatures. This is well known, e.g., from IPCC reports (Trenberth et al., 2007). It can be attributed as a manifestation of the cold-ocean warm-land (COWL) pattern (Wallace et al., 1996), caused by the low heat capacity of the continents compared to the oceans where heat is mixed in deep water masses.

The geographical distribution of the simulated annual temperature changes for 2071–2100 relative to 1976–2005 for RCP2.6 and RCP8.5 are given in Fig. 8a and b. The temperature increase is considerably larger in RCP8.5 than for RCP2.6. The patterns of COWL and the Arctic amplification are seen for both scenarios. The Arctic sea-ice extent is also projected to decrease by 2100 for all scenarios (see Fig. 9c). The reduction is particularly large for the annual minimum sea-ice extent in the Arctic. The Arctic sea-ice in September has almost disappeared by ca. 2100 for the RCP8.5 scenario. For the other scenario projections, some sea-ice always

Table 5. Simulated changes in selected global annual data with NorESM1-M from the period 1976–2005 (Historic1) to 2071–2100 based on the four projected representative concentration pathways (RCP) scenarios. The hydro-climatic quantities marked with a star (*) are estimated using the fact that $E_{\mathrm{GLOBAL}} = P_{\mathrm{GLOBAL}}$ in the model. The rightmost columns contain total values simulated for 1976–2005 (Historic1), and the difference between this and piControl.

	RCP8.5 – Historic1	RCP6.0 – Historic1	RCP4.5 – Historic1	RCP2.6 – Historic1	Historic1 1976–2005	Historic1 – piControl
$T_{2\,\mathrm{m}}$/K	+3.07	+1.86	+1.65	+0.94	286.78	+0.50
SST/K	+1.76	+1.06	+0.95	+0.59	282.92	+0.34
$\mathrm{AREA}_{\mathrm{SeaIce}}/10^6\,\mathrm{km}^2$	−6.24	−3.48	−2.97	−1.43	20.76	−1.14
$P_{\mathrm{GLOBAL}}/1000\,\mathrm{km}^3\,\mathrm{yr}^{-1}$	+27	+17	+17	+12	521	0
$E_{\mathrm{OCEANS}}/1000\,\mathrm{km}^3\,\mathrm{yr}^{-1}$	+25	+15	+14	+10	442	+1
$(E\text{-}P)_{\mathrm{OCEANS}}/1000\,\mathrm{km}^3\,\mathrm{yr}^{-1}$	+8	+4	+2	+1	43	+1
$P^*_{\mathrm{OCEANS}}/1000\,\mathrm{km}^3\,\mathrm{yr}^{-1}$	+17	+11	+12	+9	399	0
$P^*_{\mathrm{LAND}}/1000\,\mathrm{km}^3\,\mathrm{yr}^{-1}$	+10	+6	+5	+3	122	0
$E^*_{\mathrm{LAND}}/1000\,\mathrm{km}^3\,\mathrm{yr}^{-1}$	+2	+2	+3	+2	79	−1

Table 6. Simulated changes in annual total precipitation (P, $\mathrm{mm\,yr}^{-1}$) and annual total runoff (R, $\mathrm{mm\,yr}^{-1}$) with NorESM1-M in Europe, Northern Europe, and the Mediterranean region, from the period 1976–2005 (Historic1) to 2071–2100 based on the four projected representative concentration pathways (RCP) scenarios. The rightmost columns contain total values simulated for 1976–2005 (Historic1), and the difference between this and piControl.

		RCP8.5 – Historic1	RCP6.0 – Historic1	RCP4.5 – Historic1	RCP2.6 – Historic1	Historic1 1976–2005	Historic1 – piControl
Europe	$P_{\mathrm{EUR}}/\mathrm{mm\,yr}^{-1}$	+32.3	+12.0	+25.5	+42.1	862.1	−19.8
	$R_{\mathrm{EUR}}/\mathrm{mm\,yr}^{-1}$	−11.8	−16.5	−10.1	+5.7	316.4	−2.0
North Europe	$P_{\mathrm{N\text{-}EUR}}/\mathrm{mm\,yr}^{-1}$	+81.9	+61.2	+53.5	+18.9	723.1	+43.3
	$R_{\mathrm{N\text{-}EUR}}/\mathrm{mm\,yr}^{-1}$	+24.1	+21.8	+11.6	−10.3	468.4	+40.6
Mediterranean region	$P_{\mathrm{MED}}/\mathrm{mm\,yr}^{-1}$	−79.7	−36.3	−5.8	+20.6	611.5	−41.1
	$R_{\mathrm{MED}}/\mathrm{mm\,yr}^{-1}$	−25.3	−12.2	−3.6	+3.9	90.3	−9.77

remains. The response in the Southern Hemisphere is considerably smaller. The simulated response from 1976–2005 to 2071–2100 in the total global and annual mean sea-ice area is given for each RCP scenario in the bottom row in Table 5. In relative numbers the reduction varies from ca. 7 % (RCP2.6) to ca. 30 % (RCP8.5).

6.2 Precipitation

The climatology of precipitation and dry spells has strong impacts on the natural environment as well as human society. Changes in annual total amounts as well as the intensity of precipitation events are important in this connection. As discussed by Bentsen et al. (2012) NorESM1-M overestimates the global precipitation by the end of the 20th century by ca. $0.14\,\mathrm{mm\,d}^{-1}$ [$(2.81–2.67)\,\mathrm{mm\,d}^{-1}$] compared to the GPCP data (Adler et al., 2003), where the overestimations are particularly pronounced in the tropics. However, Trenberth (2011) mentions that GPCP values may underestimate warm rain in the extra-tropics and refers to increased

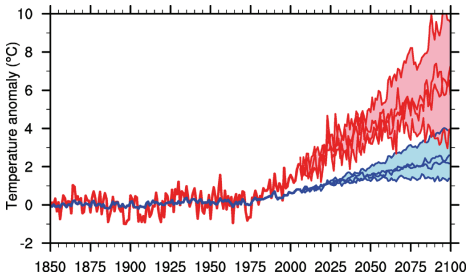

Fig. 6. Model simulated development from 1850 to 2100 in surface air temperature relative to the 1850–1899 average for Historic1 until 2005 followed by a range defined by the four RCP scenario projections. Blue: global data, red: the NH polar area north of 65° N. The diagram can be compared with Fig. 25 in Bentsen et al. (2012).

estimates of 5 % over the ocean. NorESM1-M also has a slightly too intense hydrological cycle, since oceanic evaporation is about 4 % larger than estimates from synthesized observational data (Trenberth et al., 2011). Opposed to many other global climate models with too fast recycling of water vapour, NorESM1-M slightly overestimates the atmospheric residence time of oceanic water vapour, and the atmospheric transfer of water vapour from ocean to land is overestimated by about 8 % compared to the estimate of Trenberth et al. (2011).

Figure 8 shows projections of relative change (%) in annual precipitation amounts by 2071–2100 relative to 1976–2005 for the extreme scenarios RCP2.6 and RCP8.5. In general the patterns are the same, but RCP8.5 has larger anomalies. Some increases occur over arid regions giving very large relative changes, for example, over central parts of northern Africa. Otherwise, there are strong increases over the tropical Pacific Ocean paired with strong decreases in the subtropics. There is also reduced precipitation in the Mediterranean region and in southern parts of North America. Otherwise there are mainly precipitation increases, including the polar latitudes in both hemispheres. Many of these features are more pronounced in the seasonal maps for RCP8.5. Drying in the northern hemispheric continents is more pronounced in NH summer, whilst in the NH winter the precipitation increase is more ubiquitous.

Figure 9a and b show the simulated time development of the difference between evaporation and precipitation (E-P) and evaporation (E) integrated over the global oceans. The oceanic E-P is the net water vapour transported from ocean to land in the atmosphere, while the oceanic E is a measure of the intensity of the hydrological cycle. Both quantities increase in the simulations of the RCP scenarios. The budget changes in Table 5 indicate that all gross quantities, except for one, increase with the size of the forcing by 2071–2100 compared to 1976–2005. The global annual precipitation amounts increase by 2.3–5.2 %, the oceanic evaporation by 2.3–4.5 %, the net atmospheric transfer from ocean to land by 2–18 %, and the precipitation on land by 2.5–8.2 %, where the low numbers are for RCP2.6 and the high for RCP8.5.

The quantity that does not increase is evaporation from land which, thus, in practice is preserved while both the net flux of vapour from ocean to land and the precipitation over land increase. Evaporation from the land surface is strongly influenced by direct water availability in the upper soil and by plant transpiration which provides access to water in deeper soil layers. Both these would normally be expected to increase with increased precipitation. Since the model does not predict this to happen for the total land evaporation, the soil is being allowed to dry out more by either having longer dry spells between precipitation events or by increasing the spatial scale of dry sub-regions. In both cases, the average intensity of precipitation over land must increase, since the predicted precipitation increase will take place over smaller fractions of space or time. Thus, we can hypothesize that in

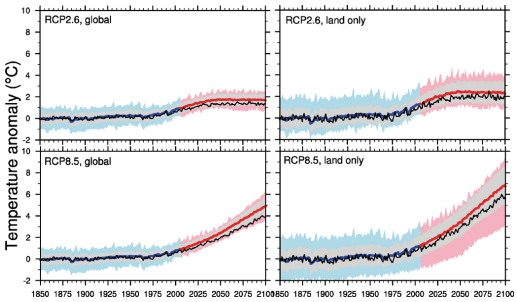

Fig. 7. Model calculated annual surface air temperature anomalies relative to the 1850–1899 average for RCP2.6 (upper panels) and RCP8.5 (lower panels), averaged globally (left panels) and over land areas (right panels). Black lines: NorESM1-M; blue and red lines: ensemble mean over 15 other models contributing to CMIP5, grey shading: one standard deviation on each side of the ensemble mean; blue and red shading: range defined by max and min values amongst the 15 models.

NorESM1-M future climate change scenarios there is an increase in both the precipitation intensity and space-time fraction of dry spells. Such effects were deduced for a warmer climate by Trenberth et al. (2003) and further elaborated by Trenberth (2011). The relevance of dry spells in diagnosing the intensity of the hydrological cycle was thoroughly discussed and analysed by Giorgi et al. (2011).

Table 6 analyses the possible future situation in Europe for the RCP scenarios. The table clearly shows that the NorESM1-M simulations produce a striking difference between increased precipitation in Northern Europe and more dry conditions in Southern Europe towards 2100. According to the simulations in Historic1, such a development may already have occurred.

6.3 AMOC and ocean temperatures

We have already discussed the possible regulating role of the AMOC for the impacts of radiative forcing on near surface air temperature, SST, surface evaporation and melting of sea-ice. This 3-D current is regarded as a part of the global ocean conveyer belt. A common view is that the upward closing branch is a large scale balance between upwelling and diapycnal mixing (e.g., Munk and Wunsch, 1998). AMOC is driven by wind stress and by thermohaline forcing. The latter occurs when cold and saline water is produced at high latitudes and becomes negatively buoyant and sinks.

Under anthropogenic climate change, increased precipitation and melting of the cryosphere may stabilise the vertical water column at high latitudes and lead to a reduced AMOC (e.g., Hofmann and Rahmstorf, 2009). We have already seen that NorESM1-M simulates increased precipitation in the northern North Atlantic Ocean and reduced precipitation in

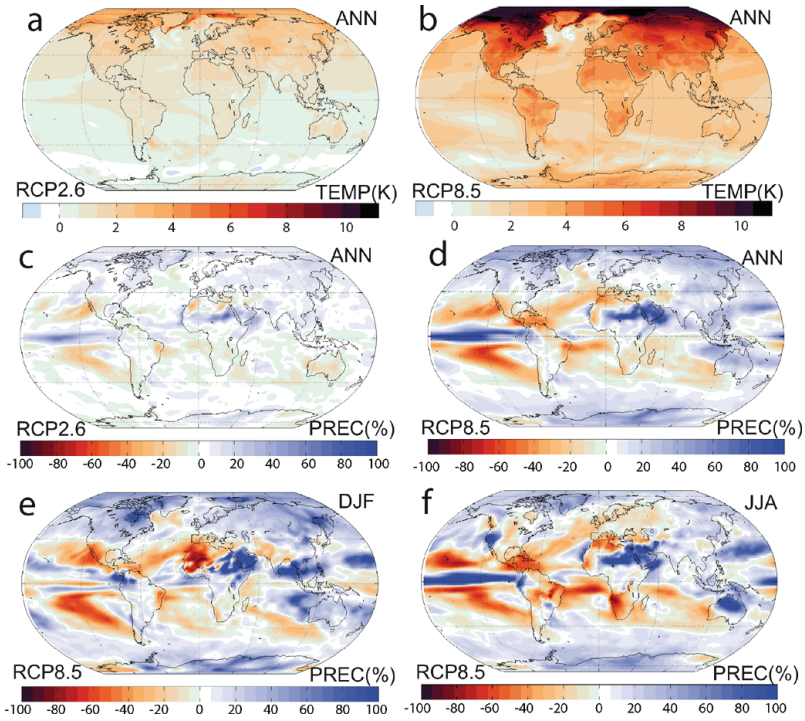

Fig. 8. Model simulated change in mean surface air temperature (K) **(a, b)** and percentage change in precipitation **(c, d, e, f)** from 1976–2005 to 2071–2100. Annual averages for RCP2.6 (**a** and **c**) and for RCP8.5 (**b** and **d**); RCP8.5 precipitation for **(e)** Dec-Jan-Feb and **(f)** Jun-Jul-Aug.

the subtropics under RCP scenarios (Fig. 8). Observational studies indicate that surface water has become fresher in areas relevant for deep water formation already during the recent decades (Curry and Mauritzen, 2005). A slower AMOC may be associated with reduced poleward transport of heat in the upper ocean and cause colder climate regionally over the northern North Atlantic Ocean, the Arctic, and in Northwest Europe. Persistent wind stress in the storm-track regions combined with increased subtropical surface salinity may compensate if more saline water is transported northwards by the surface wind driven currents (Bethke et al., 2006).

Figure 10 (upper panel) shows the time series of maximum AMOC strength at 26.5° N in the NorESM1-M runs piControl, Historic1, 2 and 3, and the 4 RCP scenarios. The piControl time series has a mean value of 30.8 Sv and a small but significant (p-value < 0.01) linear trend of -0.6 Sv over 500 yr (Bentsen et al., 2012). The historical experiments do not deviate significantly from the long-term evolution of the piControl experiment, which shows considerable amplitudes due to unforced internal variability. However, they all show a decreasing AMOC strength after about 1980. In the moving averaged time series, two of the historical members end at an AMOC strength near the minimum value encountered during the whole piControl integration.

The reduction seen in the RCP experiments is considerably larger than the trend and variability of the piControl. When comparing the mean AMOC strength of the years 2091–2100 in the scenario experiments to the mean strength of the control, the reductions are 3.6 Sv for RCP2.6, 5.1 Sv for RCP4.5, 5.6 Sv for RCP6.0, and 9.9 Sv for RCP8.5. The relative reductions are, thus, approximately 12 %, 17 %, 18 %, and 32 %, respectively. In the SRES A1B scenario experiment of 16 models participating in CMIP3, Schneider et al. (2007) found a mean reduction of maximum AMOC strength at 30° N of about 4 Sv from year 2000 to 2100. This amounts to an average decline of about 25 %. The SRES A1B scenario is closest to the RCP6.0 scenario in terms of estimated radiative forcing towards year 2100 (Houghton et al., 2001; van Vuuren et al., 2011). The NorESM1-M simulation based on the RCP4.5 scenario, which was extended to year 2300 with constant aerosol emissions and greenhouse gas concentrations

after year 2100, shows a rather stable AMOC strength of 25–26 Sv after year 2100.

The zonal mean temperature change for years 2071–2100 of NorESM1-M RCP8.5 compared to corresponding years of the piControl experiment is shown in the two bottom panels in Fig. 10. In the upper 200 m, the warming is in excess of 2 K most places except where sea-ice is present and constrains the temperature at the freezing temperature. The warming is in general reduced with depth, and below 3000 m the warming signal is weak, particularly in the global average shown in the right panel of Fig. 10. At high latitudes, the warming penetrates deeper. A generally stronger warming signal is seen for the Atlantic Ocean in the left panel of Fig. 10 compared to the global ocean. Also, for the Atlantic Ocean, the upper ocean temperature increase is efficiently communicated to the ocean interior at high latitudes.

The overturning circulation of the Atlantic seems to carry a warming signal southward in the Atlantic at 2000–3000 m depth. Given that AMOC strength is reduced by a third by 2100, further penetration of heat to the deep ocean will be considerably reduced, although it will remain strong in this model. A larger fraction of the greenhouse gas heating in the RCP8.5 scenario will nevertheless remain in the atmosphere and contribute to enhance the globally averaged surface warming. However, a considerably reduced heating (possibly cooling) may occur regionally at high latitudes adjacent to where the negatively buoyant water normally is formed in the Atlantic Ocean. In order to study such consequences, the RCP8.5-based simulation should be prolonged. Some caution should also be taken with regard to these results since NorESM1-M probably overestimate the strength of AMOC in the first place.

7 Changes in regional flow patterns

The climate of the mid-latitudes is closely linked to large-scale cyclones that develop and propagate in the westerly jet-stream systems. In particular, extreme precipitation and flooding are linked to storminess and transport in the associated warm conveyor belt (Stohl et al., 2008; Gimeno et al., 2011). Extra-tropical cyclones are also important vehicles for the atmospheric meridional transport of heat, humidity and momentum between the low and high latitudes, as well as the maintenance of the jet-streams themselves (e.g., Bratseth, 2001, 2003). Absence of cyclones associated with persistent blocking events is likewise important for the occurrence of droughts. Furthermore, the changed occurrence of flow regimes or prevalent intrinsic weather modes can be claimed to be a regional manifestation of global climate change (Corti et al., 1999; Branstator and Selten, 2009). In this section, we address these aspects of the NorESM1-M simulation results, emphasising the Northern Hemisphere (NH) and ENSO.

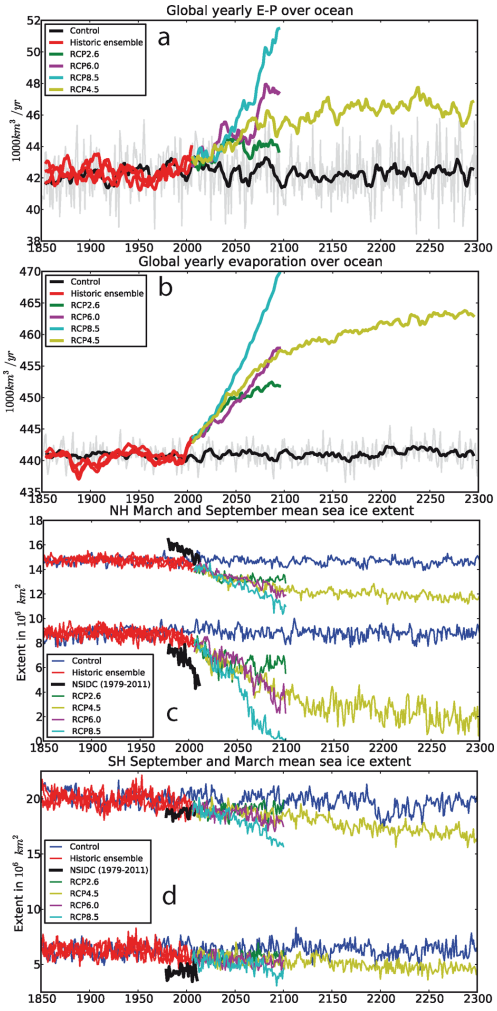

Fig. 9. Decadal moving average annual evaporation minus precipitation **(a)** and evaporation **(b)** from the oceans, and the northern **(c)** and southern hemispheric **(d)** March and September sea-ice extent during the NorESM1-M simulations for 1850 to 2300. Black in **(a)** and **(b)** and blue in **(c)** and **(d)**: the piControl, red: 1850–2005 Historic1, 2, and 3; dark green: RCP2.6 2005–2100; light green: RCP4.5 2005–2300; magenta: RCP 6.0 2005–2100; cyan: RCP8.5 2005–2100. Black curves in **(c)** and **(d)** are sea-ice extents estimated from observations (NSIDC, Fetterer et al., 2009).

7.1 NH storminess

The climatological storminess in the Northern Hemisphere (NH) extra-tropics simulated with NorESM1-M is diagnosed using the standard deviation of 2.5–6 days band-pass filtered

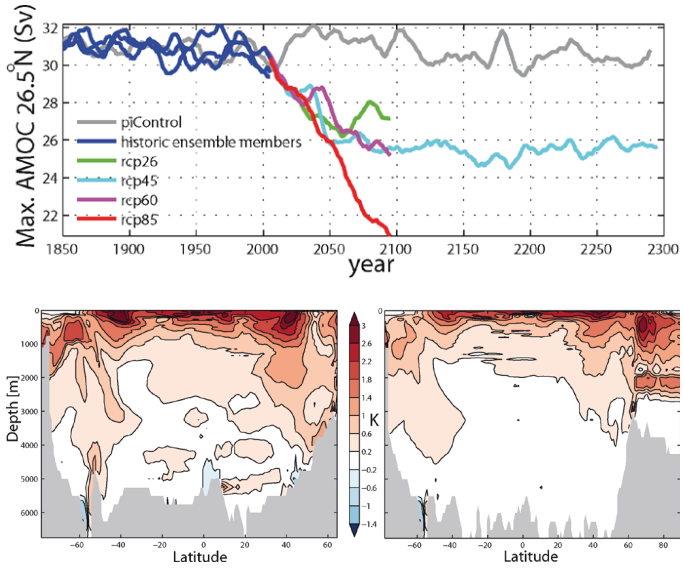

Fig. 10. The top panel shows decadal moving averages of the annual max AMOC at 26.5° N, where grey is piControl, blue are Historic1, 2, and 3, green is RCP2.6, turquoise RCP4.5, violet RCP6.0, and red is RCP8.5. The bottom two panels show annual and zonal mean NorESM1-M simulated ocean temperature change for years 2071–2100 with RCP8.5 compared to piControl. Left: the Atlantic Ocean, right: global oceans.

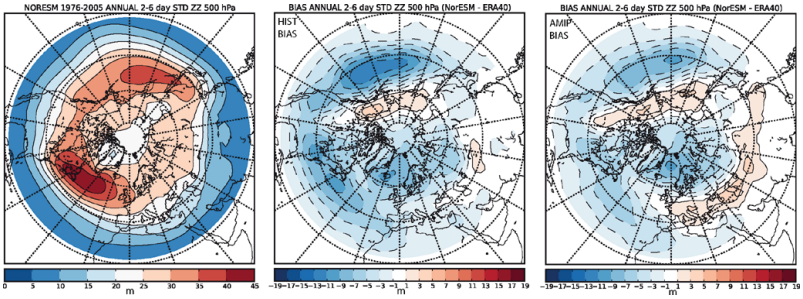

Fig. 11. Diagnosis of NH extra-tropical storminess in NorESM1-M simulations of 1976–2005 (Historic1) by applying a band-pass frequency filter, emphasising periods from 2.5 to 6 days, to the 500 hPa geopotential height (left). The middle panel shows bias error when compared to the ERA40 reanalysis data for 1976–2002 (Uppala et al., 2005), and the right panel shows the corresponding bias for the period 1979–2005 of the AMIP simulations with NorESM1-M run without coupling to the ocean model, but with SST-fields prescribed from observations.

500 hPa geopotential height. The band-pass filter is the same as used by Blackmon (1976), which has been shown to retain baroclinic waves consistent with theoretical and modelling studies (e.g., Chang et al., 2002 and references therein). Although this field represents baroclinic wave activity we will refer to it here as a measure of storm track activity. Figure 11 shows the annual mean storm tracks for the NorESM1-M historical simulation compared to the ERA-40 reanalysis (Uppala et al., 2005). Many of the main characteristics of the NH storm tracks are well simulated, although the amplitude of the band-pass filtered variability overall are slightly too weak. Note that this amplitude bias is significantly reduced for the AMIP run of the NorESM1-M model with prescribed SSTs based on observations. Parts of the bias in the fully coupled NorESM1-M can, thus, be attributed to systematic errors in the simulated SST field. Another notable bias is found over the North-Atlantic Ocean where the storm track is too zonal and lacks the characteristic poleward tilt in the

ERA-40 data. This bias is very similar to that reported for the CAM3 model (Hurrell et al., 2006), and the bias appears to be intrinsic to the atmospheric model component, since it is virtually unchanged in the AMIP run of the NorESM1-M.

Figure 12 shows the projected changes for 2071–2100 compared to 1976–2005 for the RCP8.5 scenario. The annual mean change is dominated by a slight general weakening of the band-pass filtered variability except over the northern North-Atlantic Ocean where a poleward shift in the storminess is apparent. This poleward shift is prominent mainly during summer and autumn. Although the shift is statistically significant at the 5 % level relative to the variational spread in the time series, Fig. 12 also includes the spread between the 3 historical NorESM1-M simulations for the period 1976–2005. This sample is of course too small to adequately represent the model's internal variability as an ensemble, but the amplitude of the poleward shift as well as the more general weakening can, at least, be seen to exceed this ensemble spread. A poleward shift of mid-latitude storm tracks has also been diagnosed in many other climate model simulations as a response to anthropogenic greenhouse-gas forcing (e.g., Yin, 2005).

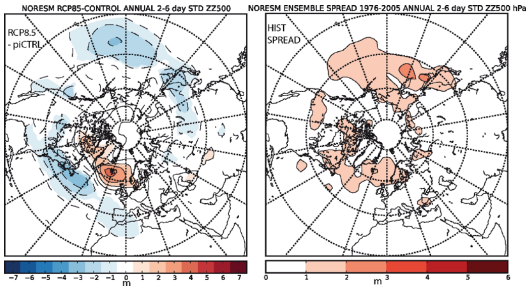

Fig. 12. NorESM1-M simulated change from 1976–2002 to 2071–2100 in NH extra-tropical storminess, diagnosed as described in Fig. 11, using the RCP8.5 projection scenario (left). Colours indicate significant changes on the 95 % confidence level. The right panel shows the standard deviation in the storminess amongst the three ensemble-members Historic1–3 for 1976–2005, revealing that the significant changes diagnosed in the left panel are considerably larger for the main maxima.

7.2 NH blocking

Whilst storminess is associated with frequent occurrence of precipitation and possibly flooding, the blocking phenomenon is closely connected with persistent anticyclones, which tend to suppress precipitation at mid-latitudes for periods of up to several weeks. Incidents of extensive droughts can be associated with blocking, and the ability of climate models to simulate and project the climatic occurrence of droughts at mid-latitudes will be influenced by their ability to simulate blocking. Many blockings will also include a cold cyclone with low static stability and heavy convective storms.

To diagnose atmospheric blocking, we use the index originally proposed by Lejanäs and Økland (1983) and later modified by Tibaldi and Molteni (1990) (TM). The TM index uses a persistent reversal of the gradient of the 500 hPa geopotential height around a central latitude (50° N) as an indicator of blocked flow. The central latitude is allowed to vary by approximately 3.8° (2 grid points in the NorESM) to include small latitudinal shifts in the block. The blocks were further required to last for at least 5 days and be present at 7.5° consecutive longitudes.

Pelly and Hoskins (2003) have shown that a fixed central blocking latitude suitable for detecting blocks over the North Atlantic leads to spurious detection over the North Pacific. We, therefore, also calculate a "vTM" index where the central latitude varies with the longitude of the climatological storm track. The central latitude is defined as the maximum of the standard deviation of the 2.5–6 days band-pass filtered geopotential height anomalies at 500 hPa. To account for the seasonal cycle of the storminess, the central latitude for a given month is calculated as the climatological 3-month average centred on that month.

Figure 13 shows the seasonal blocking frequency for the NorESM1-M Historic1 simulation for 1976–2005 compared to the ERA-40 reanalysis for 1979–2002. The variable latitude "vTM" index is shown. For all seasons the model largely fails to adequately simulate blocking over the North-Atlantic Ocean and western Europe in NH winter and spring. This is consistent with the too zonal propagation of storms in this sector (Fig. 11). This common deficiency amongst climate models (e.g., D'Andrea et al., 1998) may be partly attributed to the coarse resolution, as the investigation of Jung et al. (2012) suggests that around 40 km resolution is needed. Matsueda et al. (2009) even found that a horizontal resolution of 20 km was required to accurately simulate the frequency of Euro-Atlantic blocking, and that higher resolution generally improves the representation in this sector. Further to the east, over the Eurasian continent, blocking is better simulated but exaggerated. Similar results are seen when blocking is defined at 50° N fixed latitude, although the bias is smaller in spring (not shown). For blocking in the NH summer and fall, the Euro-Atlantic blocking is better reproduced, but still underestimated.

Over the Pacific Ocean the simulated blocking frequency is closer to the observed, which is consistent with the conclusion by Matsueda et al. (2009) that the required horizontal resolution is coarser in the Pacific sector than in the Atlantic. It should be noted that there is some evidence that blocking deficits also can be reduced, even with relatively coarse resolution, by improving the SST field and reducing the time mean bias in the westerlies (Scaife et al., 2011).

The projected changes in blocking frequency during 2071–2100 for the RCP8.5 scenario compared to 1976–2005

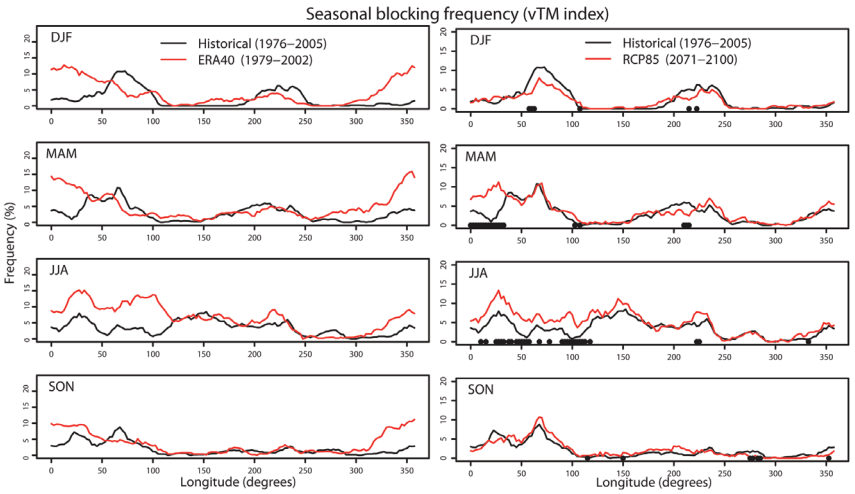

Fig. 13. Northern hemispheric seasonal blocking statistics for the Tibaldi and Molteni (1990) (vTM) index diagnosed relative to the latitudes of the seasonally averaged position of the westerlies (Pelly and Hoskins, 2002). Left panels are for the simulated NorESM1-M Historic1 for 1976–2005 compared to ERA40 statistics for 1976–2002, and right panels are projections for 2071–2100 with the RCP8.5 scenario compared to the period 1976–2005 (Historic1) with NorESM1-M. Dots signify longitudes where differences are significant at the 95 % confidence level.

are shown in Fig. 13. Using again the "vTM" index an increased blocking frequency is apparent for the sector 0–100° E for the summer months as well as in the sector 0–40° E during spring. We emphasise, however, that since there are large systematic biases in blocking frequency for the same sectors, these projections must be interpreted with great caution. The projected changes diagnosed using the index with fixed 50° N latitude (not shown), show considerably smaller changes than "vTM", which may be due to the simultaneous pole-ward shift in the position of the westerly air currents. This contradicts the use of fixed latitudes for the blocking index. Such sensitivity to choice of index has also been reported by Barnes et al. (2012), and adds to the uncertainties connected with blocking simulation in climate models. The projected increase in blocking frequency can be linked to the reduced precipitation in the region except for Northern Europe.

7.3 NH EOF-analysis

In order to describe the low frequency variability in the NorESM1-M, an EOF (empirical orthogonal function) analysis has been applied to monthly mean 500 hPa geopotential height anomalies during extended winter seasons (DJFM) from 1976 to 2005, where the DJFM-months define the year associated with each season. The three historical ensemble members for the mentioned period define the climatology about which the anomalies are calculated.

To calculate the EOFs (see e.g., Bjørnsson and Venegas, 1997; Hannachi et al., 2007; Monahan et al., 2009) the anomalies for each historical ensemble member are detrended by calculating deviations from a 5 yr moving average, and a common seasonal cycle for the simulated 1976–2005 period estimated by subtracting separate averages for each month (3×30 values are averaged per month). The EOFs, thus, represent spatial structures of the 500 hPa geopotential height fields associated with non-seasonal variations up to a few years, similar to the analysis of Corti et al. (1999) which was further extended by Molteni et al. (2006), based on NCEP re-analysis data (Kalnay et al., 1996).

The detrended, non-seasonal monthly anomalies are formally organised into a matrix $\mathbf{A}$, where the rows are the $3 \times 30 \times 4$ spatial anomaly patterns and the columns are the monthly values of the anomaly in each point in space. The EOFs are the eigenvectors (w.r.t. the standard Euclidian inner product) of the covariance matrix, $\mathbf{C} = \mathbf{A}^T\mathbf{A}$, i.e., $\mathbf{CR} = \boldsymbol{R}^T\Lambda$, where Λ is the diagonal matrix containing the eigenvalues, λ_i of $\mathbf{C}$. The column vectors in $\boldsymbol{R}$ are the mutually orthogonal eigenvectors $\boldsymbol{eof}_i$ of $\mathbf{C}$. Each eigenvalue measures the fraction of the total variance that the corresponding EOF pattern accounts for.

The associated principal components (PC) are time-series of the projections of $\mathbf{A}$ onto the EOFs: $\boldsymbol{PC}_i = \mathbf{A}^T \cdot \boldsymbol{eof}_i$. In addition to calculating the PCs for the three historical simulations for the DJFM-winters 1976–2005, the time-series of the projections of the non-detrended anomaly data on each EOF have been estimated for the GHG only (GHG), aerosol

only (AER), and natural forcing only (NAT), as well as the projected scenario RCP8.5. Note that all anomalies are calculated w.r.t. the 1976–2005 climatology for the three historical ensemble members before projection onto the EOFs.

One reason for using EOF-based flow regime analysis in the context of climate change, is that internal dynamics in the climate system may determine the patterns of climate response to external forcing rather than the structure of the forcing itself (Palmer, 1999; Branstator and Selten, 2009; Iversen et al., 2009), although this view needs to be extended to account for local internal feedbacks in the climate system, which can be particularly strong in connection with Arctic snow and sea-ice (Boer and Yu, 2003).

The obtained projections onto selected EOFs for scenario simulations can, therefore, be directly compared with the PCs of the three historical ensemble members. If systematic differences are found, these can potentially be attributed to the differences in external conditions, whilst differences between the historical ensemble members' PCs will reflect internal variability. At present, we have not estimated any probability density functions for projection coefficients; a method whose validity is under some discussion (Stephenson et al., 2004; Molteni et al., 2006).

The validity of potential results described above will not be convincing if the EOFs for the modelled fields differ considerably from "observed" EOFs from re-analysis data (e.g., Corti et al., 2003). One additional purpose of an analysis like this is, therefore, to investigate to what extent selected atmospheric flow regime patterns are reproduced in NorESM1-M. Hence, we have also calculated EOFs to the NCEP reanalysis data for the same extended winter seasons of 1976–2005, in the same way as was done by Corti et al. (1999) and Molteni et al. (2006), but for a shorter period.

Figure 14 shows the 500 hPa geopotential height pattern for the 4 leading EOFs from the de-trended monthly data for the three ensemble members of the historical simulations with NorESM1-M. Each EOF is scaled to represent one standard deviation of its principal component. They are then compared to the two leading EOFs calculated in the same way for the reanalysis data from NCEP for the same 30 winters (Kalnay et al., 1996). The first EOF for both the reanalysis and the model represents the Arctic Oscillation (AO) (Thompson and Wallace, 2000), or alternatively the Northern Annular Mode (NAM). The shapes are slightly different in NorESM1-M with a maximum centred in the central Arctic, while the NCEP data has a centre displaced over to the Atlantic sector, but both have secondary maxima of the opposite sign in southern Europe, north-eastern North America, and the northern Pacific Ocean.

The second EOF of NorESM1-M differs significantly from that of the NCEP data. Both EOFs are combinations of patterns reminiscent of the Pacific North American (PNA) (Wallace and Gutzler, 1981) and North Atlantic Oscillation (NAO) (Barnston and Livezey, 1987). However, while the NCEP EOF2 is dominated by the latter in strong combination

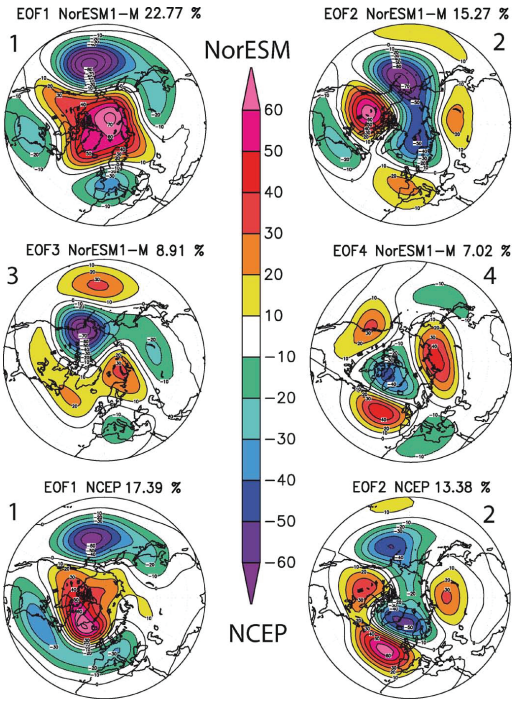

Fig. 14. First and second rows show the 500-hPa-geopotential height associated with the 4 leading EOF-vectors for detrended, monthly average anomalies of the 500 hPa geopotential height for December–March over the years 1976–2005, based on the three ensemble members (Historic1, 2, and 3) simulated with NorESM1-M. Seasonal variations are removed by calculating anomalies relative to the 30-yr average for each month, while trends are removed by subtracting the 5-yr moving average. The third row shows the corresponding maps of the 2 leading eof-vectors calculated in the same way for the same 30 yr using the NCEP re-analysis data (Kalnay et al., 1996).

with the cold-ocean-warm-land (COWL) (Wallace et al., 1996), the NorESM1-M EOF2 is dominated by the PNA with little resemblance of the COWL pattern. Furthermore, the NAO resemblance in NorESM1-M's EOF2 is weak and displaced towards east over Europe. The COWL pattern only turns up convincingly in EOF4 for NorESM1-M, and in this case combined with a NAO pattern which is considerably more correctly positioned than in EOF2. It appears that a suitable combination ("rotation") of EOF2 and EOF4 from NorESM1-M can be made to better resemble EOF2 from NCEP than any of them do separately. Such a combination was, for example, made by Corti et al. (2003) for results from a simpler climate model. The third EOF of NorESM1-M resembles the EOF4 of NCEP (not shown).

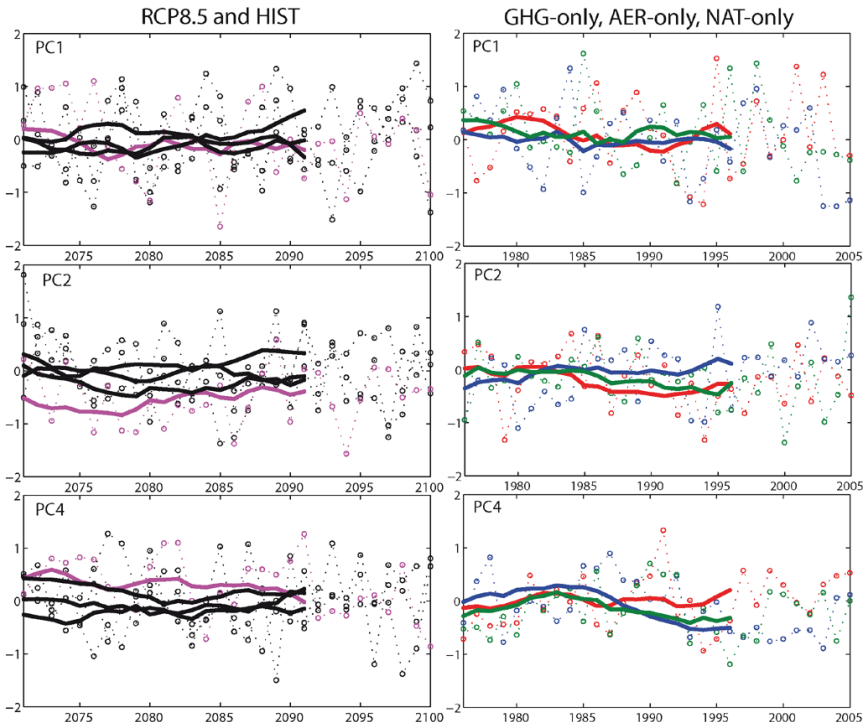

Fig. 15. The left column shows components of the non-detrended geopotential height anomalies for each 4-month season (DJFM) of the 3 historical ensemble members for 1976–2005 (black dashed lines and circles), and for the simulated climate projection for each 4-month season of the years 2071–2100 (denoted on the x-axes) using the RCP8.5 scenario with NorESM1-M (magenta dashed lines and circles). Thick lines are 10-yr forward moving averages. Right column shows similar components for the experiments with GHG-only (red), Aerosol-only (blue), and Natural forcing only (green) for 1976–2005.

Another difference between NorESM1-M and NCEP is revealed by the eigenvalues associated with the EOFs, i.e., the "explained variance" of each EOF as shown by the percentages above each EOF in Fig. 14. The low-order EOFs from the NorESM1-M data "explain" a larger portion than the corresponding low-order NCEP EOFs.

As a separate test we have also calculated EOFs over a sector of the Northern Hemisphere (80° W–40° E and 20° N–80° N) for both NorESM1-M and NCEP data (not shown). In this case, the first sectorial EOF explains approximately the same amount of the variance in NorESM1-M (33.9 %) and NCEP (33.4 %). However, the patterns are very similar to the hemispheric leading EOFs over the sectors. Thus, the NAO-pattern in NorESM1-M's EOF1 is displaced towards the east compared to NCEP. The patterns of the second EOFs are considerably more similar with explained fractions of variance of 18.0 % (NCEP) and 15.4 % (NorESM1-M). This pattern is dominated by a strong monopole over the central North Atlantic with a weaker monopole of the opposite sign over central Europe, and does not appear to have a clear counterpart in the hemispheric EOFs or to any established regional flow regime patterns.

To summarise the EOF analysis, the model's Arctic Oscillation is slightly too strong with an associated NAO-like pattern displaced towards the east over Europe, and it has too much variability. Furthermore, relative to COWL and the geographically correct NAO-pattern, the model produces too strong variability associated with the correctly placed PNA pattern. A sectorial EOF-analysis gives similar results for the leading EOF as the hemispheric analysis with respect to the displaced NAO-like pattern, probably because COWL is a truly hemispheric pattern.

These differences between the EOFs of NCEP and NorESM1-M can be associated with systematic errors in the storminess and the blocking occurrence over the North Atlantic Ocean and Europe mentioned in Sects. 7.1 and 7.2. The eastward displacement of parts of the NAO-pattern is, in particular, associated with the too zonal storminess pattern and

the under-representation of blocking in the European–North Atlantic region.

Figure 15 shows the time series of the decomposition of monthly 500 hPa geopotential height anomalies from NorESM1-M on the respective EOF1, EOF2 and EOF4 with the sign shown in Fig. 14. The data are from the three historical ensemble members and the RCP8.5 scenario for the years 2071–2100. These data include the inter-annual (and longer) trends and the systematic differences between the historical and the scenario, but not the seasonal variations. Since all the anomalies are calculated with respect to the same climatology, defined by the three historical ensemble members for 1976–2005, a given value of the component identifies an exact monthly state, irrespective of the data source. The main curves in the diagrams are the 10-yr moving averages of the components. If a coloured curve lies outside of the range of the three historical ensemble members, this may indicate that the scenario assumption (RC8.5) leads to systematic differences from internal natural variability.

For PC1, this is clearly not the case, and neither for PC3 (not shown). For PC2 and PC4, however, there are indications of systematic differences, although less clear for the latter. One possible interpretation is that in the RCP8.5 climate towards the end of the 21st century, positive phase PNA may occur less frequently or the negative phase PNA may occur more often. Furthermore, but with less confidence, positive phase NAO may occur more often or negative phase NAO less frequently. More investigations of the significance of this and on probability density functions for the different combinations of PCs are ongoing.

Finally, Fig. 15 also includes the components of anomalies associated with the historical single forcing experiments. Even though there are some signs of opposite results for the GHG and the aerosol experiments, none of these are outside the ranges of natural variability defined by the three ensemble members with all forcing components included.

7.4 ENSO

The "El Niño Southern Oscillation" phenomenon is a dominant mode of interannual climate variability based in the tropical Pacific which is associated with far reaching atmospheric tele-connections (Trenberth, 1997). The amplitude (Trenberth and Shea, 1987; Wang, 1995), the frequency of occurrence, and the pattern structure (An and Wang, 2000) are modulated on multi-decadal timescales. Nevertheless, it is a well recognised pattern of variability with large impacts on the weather over the western equatorial South America. It also has considerable remote impacts (Trenberth et al., 1998) showing up as a pattern in the NH extra-tropical troposphere reminiscent of the PNA internal mode of variability although the patterns of the ENSO-response and the PNA are different (Straus and Shukla, 2002). The annual global mean surface air temperature is influenced by the ENSO phase.

Bentsen et al. (2012) show that for the NINO3.4 index NorESM1-M simulates variability on shorter time-scales (2–4 yr) than the HadISST observations (3–7 yr, Rayner et al., 2003). It has not been investigated to what extent this is dominated by model errors or if it can be related to inter-decadal modes of variability (An and Wang, 2000). However, the recent analysis by Kim and Yu (2012) indicates that both modes of the ENSO variability are represented in the NorESM1-M simulations, as one of the 9 out of 20 CMIP5 models.

Figure 16 shows the time series of the NINO3.4 index for HadISST data, and from NorESM1-M, the piControl, the Historic1 and the RCP8.5. It is possible to identify a more frequent occurrence of ENSO events in the piControl and Historic1 simulations compared to HadISST. A difference between the time series for RCP8.5 and either Historic1 or piControl is less evident even though both amplitudes and return periods appear slightly reduced in the scenario. To the extent that it is correct to associate warm-phase ENSO with a positive PNA pattern, this result is consistent with the EOF-analysis in Sect. 6.3.

The spectra in Fig. 16b also indicate such changes. There are two peaks in the piControl, a primary peak around 3 yr and a secondary around 6–7 yr. Except for RCP4.5, the two peaks are less distinct in the scenarios. For RCP4.5 the two peaks appear distinct with a smaller difference between them, but both peaks occur at shorter periods than in piControl. There are also signs of less energy on periods longer than a decade for all RCPs except RCP6.0.

Further investigations with a larger number of ensemble members are required to establish the significance of these changes. The significant biases in the model simulations also reduce the confidence in the changes, even though they are internally consistent and the preliminary study by Guilyardi et al. (2012) confirms that NorESM1-M is one of the two out of 14 CMIP5 models which simulate significantly reduced ENSO variability (in that case, the NINO3 index) for the abrupt $4\times CO_2$ experiment, and close to significantly reduced for the gradual experiment.

8 Summary and conclusions

This paper presents a wide range of results of simulations with the new global climate model NorESM1-M. The companion paper by Bentsen et al. (2012) presents the basic features of the model, together with validation studies, while we have presented and discussed different aspects of the model's properties concerning the climate sensitivity and response to prescribed changes that lead to radiative forcing. We believe that the results from CMIP5 experiments with NorESM1-M, which are only discussed to some extent in this paper, are valuable contributions to the development of climate system science, as well as to the total evaluation of possible human induced climate change. The

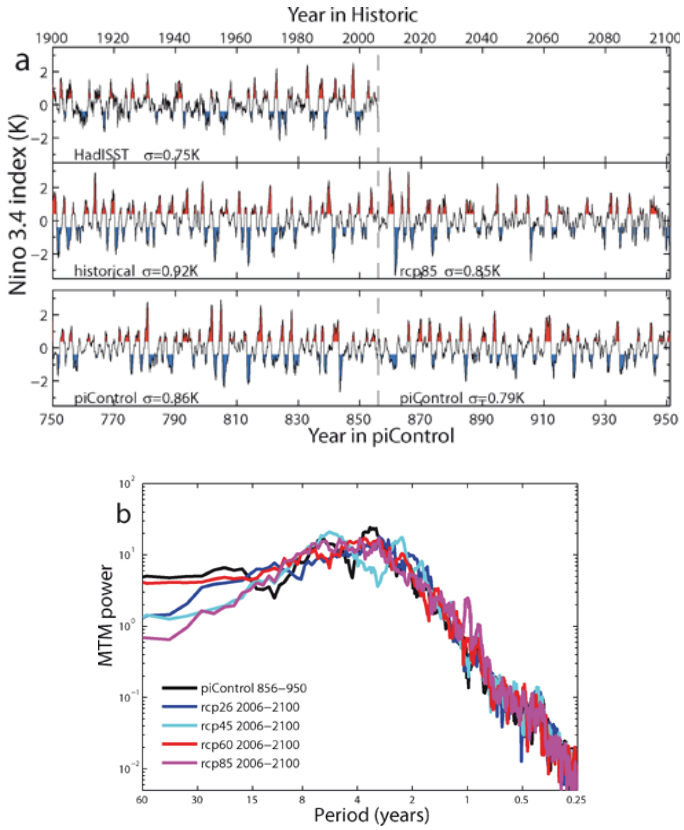

Fig. 16. Panel **(a)** shows time series of detrended monthly SST anomalies of the NINO3.4 region (5° S–5° N, 170–120° W). The anomalies are found by subtracting the monthly means for the whole time series. Red (blue) colours indicate that anomalies are larger (smaller) than +0.4 K (−0.4 K), see Trenberth (1997) for recommendations. Upper time series shows Hadley Centre Sea Ice and Sea Surface Temperature data set (HadISST; Rayner et al., 2003) for years 1900–2005; middle time series consist of NorESM1-M Historic1 for years 1900–2005 continued with NorESM1-M RCP8.5 for years 2006–2100; lower time series displays NorESM1-M piControl for years 750–950. Panel **(b)** shows power spectra of the NINO3.4 index (the SST anomalies normalised with its standard deviation) using the multi-taper method of Ghil et al. (2002) with resolution $p = 4$ and number of tapers $t = 7$. Data sources are NorESM1-M piControl years 856–950 (black), and NorESM1-M RCP2.6 (blue), RCP4.5 (cyan), RCP6.0 (red), and RCP8.5 (magenta) for years 2006–2100.

data are open for anyone to download and analyse from http://cmip-pcmdi.llnl.gov/cmip5/index.html.

The clouds in the NorESM1-M tend to dampen the response to GHG forcing ($-0.09\,\mathrm{Wm^{-2}\,K^{-1}}$), as the longwave cloud response is considerably smaller than the negative short-wave response. The clear-sky response is negative ($-1.02\,\mathrm{Wm^{-2}\,K^{-1}}$), in close agreement with other models (Andrews et al., 2012). The model has a strong Atlantic meridional overturning circulation (AMOC) of 30.8 Sv averaged over the piControl simulation period. This contributes to an efficient transport of heat into the deep oceans and reduces the heat available for increasing the surface temperature and to melt ice and snow. Exceptions are seen adjacent to major deep water formation regions, such as in the Atlantic sector of the Arctic and in Northwest Europe, where strong convergence of warm water in the upper ocean levels may occur. The two estimates we have made of the equilibrium climate sensitivity are both slightly lower than 2.9 K for a long-term adjustment to an abrupt doubling of CO_2. The transient climate sensitivity is estimated at slightly less than 1.4 K for gradual CO_2-increase until doubling. We argue that the latter may be an underestimate since very slow feedback processes may occur in response to a reduction of AMOC, which will gradually decrease the efficiency of deep ocean heat uptake. Nevertheless, NorESM1-M is amongst the least sensitive global climate models (Andrews et al., 2012).

We have also seen that the projections of global temperature increase based on RCP scenarios are substantially smaller than in most other global climate models contributing to CMIP5, although inside one standard deviation below the ensemble mean. In addition to the low climate sensitivity, NorESM1-M also includes the predominant cooling of aerosols, both the direct effect and the indirect effects of pure water clouds, although their magnitude in the present model version is quite moderate (Kirkevåg et al., 2013). The geographical distribution of the projected warming in the scenarios shows the well-known pattern of a stronger warming over the continents than the oceans, and a considerable amplification in the Arctic. The response in sea-ice is projected to be considerably larger in the Arctic than the Antarctic, and the extent in September is reduced to less than half by 2100 for three of the four RCP scenarios. For RCP8.5 this annual minimum is reduced to zero. Even though the winter maximum in March is relatively much less reduced, this will mean that the major extent of the winter Arctic sea-ice is generated during the same season.

For precipitation the largest response in the RCP scenarios towards the end of the 21st century is simulated at low latitudes, with an increase in the tropics and a decrease in the subtropics. In the extra-tropics and the high latitudes, precipitation is projected to increase, but in the NH summer the subtropical drying is extended northwards to mid-latitudes, including southern parts of North America and Europe. Projections of gross budget numbers in the atmospheric water cycle indicate intensification of all components except the evaporation from land. This reflects that the occurrences of both dry spells and high precipitation intensities increase over land, while widespread medium precipitation intensities probably occur less frequently.

The increased precipitation and melting in the Arctic will influence the thermohaline forcing of the deep water formation and, thus, the strength of the AMOC. All the RCP-scenarios are projected to lead to significantly reduced AMOC. In RCP8.5, AMOC is reduced by ca. one third by 2100, and in RCP4.5, which was run to 2300 with a stabilisation scenario after 2100, the AMOC levels off at about 15–17 % lower intensity. Since NorESM1-M probably overestimates the AMOC strength, there are doubts about the reliability of these results.

Extra-tropical precipitation climatology and, in particular, the occurrence of extreme precipitation and droughts, are associated with anomalies in storminess and blocking occurrence. The model is found to generally underestimate the variability in the zones of extra-tropical storminess, and a considerable part of this bias is linked to errors in the SST-simulations. The regional patterns of storminess are also too zonal over the North Atlantic Ocean. This is consistent with the underestimated frequency of blocking over the North Atlantic Ocean and western Europe. Other recent investigations indicate that this can be related to too coarse horizontal resolution (Jung et al., 2012). Under RCP scenarios, NorESM1-M generally projects a northward displacement of the storminess. For the most extreme scenario (RCP8.5), an increased blocking occurrence is found in the European-Atlantic sector in spring and further extended over Eurasia during summer.

The leading EOF of the 500 hPa geopotential height during winter, representing the northern annular mode (NAM), has some pattern errors that can be associated with the systematic errors of the storminess. Furthermore, while the second EOF is dominated by a pattern reminiscent of the Pacific North American (PNA) pattern, the main influence of the North Atlantic Oscillation (NAO) turns up in the fourth EOF. From NCEP re-analysis data, the second EOF contains the main pattern of the NAO in addition to PNA. Under the RCP8.5 scenario towards 2100, there are indications that the average NAO index will increase (more positive and fewer negative events) and the average PNA index will decrease (more negative and fewer positive). The first result is consistent with the changes in storminess, while changes in blocking are insignificant in winter. The reduced PNA can be associated with the reduced amplitude of the projected NINO3.4 index, even though both the change in ENSO and the relation between ENSO and PNA are associated with low confidence.

Two of the single forcing experiments for the historical period have been addressed: the GHG only and the aerosol only. The response pattern in surface air temperature by 1976–2005 compared to the pre-industrial control run is similar, but with opposite sign. This is to a large extent also true for precipitation, but there are important exceptions at low latitudes. The model simulates a southward displacement of ITCZ due to aerosol forcing, and in particular during NH summer. This change may partly cancel and partly reinforce changes caused by GHG alone. Reinforcements are simulated in the northern hemispheric subtropics with reduced precipitation and increased droughts, and at the southern flank of the ITCZ in the Pacific Ocean with increased precipitation. In consequence, the double ITCZ systematic error seen in many models (also CCSM4, Gent et al., 2011) is reduced in NorESM1-M partly due to the impact of aerosols (see Bentsen et al., 2012).

Acknowledgements. This work has been supported by the Research Council of Norway through the EarthClim (207711/E10) and NOTUR/NorStore projects, the Center for Climate Dynamics at the Bjerknes Centre, and through the European Commission FP7 projects PEGASOS (FP7-ENV-2010-265148) and ACCESS (FP7-ENV-2010-265863). The development of both versions of NorESM1 has been possible because of the granted early access to the later public versions of the CCSM4 and CESM1. We are particularly grateful to P. J. Rasch, A. Gettelman, J. F. Lamarque, S. Ghan, M. Vertenstein, B. Eaton, M. Flanner, and others, for invaluable advice on numerous scientific and technical issues, and the support by the CESM programme directors during the development period, P. Gent and J. Hurrel. We are grateful for contributions during the development of NorESM1 by K. Alterskjær, A. Ekman, C. Heinze, C. Hoose, Ø. Hov, D. Nilsson, O. H. Otterå, D. Olivié,

C. Roelandt, M. Simonsen, H. Struthers, T. Storelvmo, J. Berger, J. Su, and J. Tjiputra.

Section 7.3 in this paper is intended to be part of a Ph.D. thesis at the University of Oslo (M. Sand) in agreement with all the co-authors.

Edited by: O. Marti

References

Adler, R. F., Huffman, G. J., Chang, A., Ferraro, R., Xie, P., Janowiak, J., Rudolf, B., Schneider, U., Curtis, S., Bolvin, D., Gruber, A., Susskind, J., and Arkin, P.: The Version 2 Global Precipitation Climatology Project (GPCP) Monthly Precipitation Analysis (1979-Present), J. Hydrometeor., 4, 1147–1167, 2003.

Ammann, C. M., Meehl, G. A., Washington, W. M., and Zender, C.: A monthly and latitudinally varying volcanic forcing dataset in simulations of 20th century climate, Geophys. Res. Lett., 30, 1657, doi:10.1029/2003GL016875, 2003.

An, S.-I. and Wang, B.: Interdecadal change of the structure of the ENSO mode and its impact on the ENSO frequency, J. Clim., 13, 2044–2055, 2000.

Andrews, T., Gregory, J. M., Webb, M. J., and Taylor, K. E.: Forcing, feedbacks and climate sensitivity in CMIP5 coupled atmosphere-ocean climate models, Geophys. Res. Lett., 39, L09712, Doi:10.1029/2012gl051607, 2012.

Assmann, K. M., Bentsen, M., Segschneider, J., and Heinze, C.: An isopycnic ocean carbon cycle model, Geosci. Model Dev., 3, 143–167, doi:10.5194/gmd-3-143-2010, 2010.

Barnes, E. A., Slingo, J., and Woollings, T. J.: A methodology for the comparison of blocking climatologies across indices, models and climate scenarios, Climate Dyn., 38, 2467–2481, doi:10.1007/s00382-011-1243-6, 2012.

Barnston, A. G. and Livezey, R. E.: Classification, Seasonality and Persistence of Low-Frequency Atmospheric Circulation Patterns, Mon. Weather Rev., 115, 1083–1126, doi:10.1175/1520-0493(1987)115¡1083:CSAPOL¿2.0.CO;2, 1987.

Bentsen, M., Bethke, I., Debernard, J. B., Iversen, T., Kirkevåg, A., Seland, Ø., Drange, H., Roelandt, C., Seierstad, I. A., Hoose, C., and Kristjánsson, J. E.: The Norwegian Earth System Model, NorESM1-M – Part 1: Description and basic evaluation, Geosci. Model Dev. Discuss., 5, 2843–2931, doi:10.5194/gmdd-5-2843-2012, 2012.

Bethke, I., Furevik, T., and Drange, H.: Towards a more saline North Atlantic and a fresher Arctic under global warming, Geophys. Res. Lett., 33, L21712, doi:10.1029/2006GL027264, 2006.

Bitz, C. M., Shell, K. M., Gent, P. R., Bailey, D. A., Danabasoglu, G., Armour, K. C., Holland, M. M., and Kiehl, J. T.: Climate Sensitivity of the Community Climate System Model, Version 4, J. Climate, 25, 3053–3070, doi:10.1175/JCLI-D-11-00290.1, 2012.

Bjørnsson, H. and Venegas, S. A.: A manual for EOF and SVD analyses of climate data, McGill University, CCGCR Report No. 97-1, Montréal, Québec, 52 pp., 1997.

Blackmon, M. L.: A climatological spectral study of the 500 mb geopotential height of the Northern Hemisphere, J. Atmos. Sci., 33, 1607–1623, 1976.

Boer, G. J. and Yu, B.: Climate sensitivity and response, Clim. Dynam., 20, 415–429, doi:10.1007/s00382-002-0283-3, 2003.

Branstator, G. and Selten, F.: "Modes of Variability" and Climate Change, J. Climate, 22, 2639–2658, doi:10.1175/2008JCLI2517.1, 2009.

Bratseth, A. M.: Eddy Acceleration of the Mean Flow in the Atmosphere, J. Atmos. Sci., 58, 3328–3339, 2001.

Bratseth, A. M.: Zonal-mean transport characteristics of ECMWF re-analysis data, Q. J. R. Meteorol. Soc., 129, 2331–2346, doi:10.1256/qj.02.90, 2003.

Chang, E. K. M., Lee, S., and Swanson, K. L.: Storm Track Dynamics, J. Climate, 15, 2163–2183, 2002.

Corti, S., Molteni, F., and Palmer, T. N.: Signature of recent climate change in frequencies of natural atmospheric circulation regimes, Nature, 398, 799–802, 1999.

Corti, S., Gualdi, S., and Navarra, A.: Analysis of the mid-latitude weather regimes in the 200-year control integration of the SINTEX model, Annals Geophys., 46, 27–37, 2003.

Curry, R. and Mauritzen, C.: Dilution of the Northern North Atlantic Ocean in Recent Decades, Science, 308, 1772–1774, doi:10.1126/science.1109477, 2005.

D'Andrea, F., Tibaldi, S., Blackburn, M., Boer, G., Déqué, M., Dix, M. R., Dugas, B., Ferranti, L., Iwasaki, T., Kitoh, A., Pope, V., Randall, D., Roeckner, E., Strauss, D., Stern, W., Van den Dool, H., and Williamson, D.: Northern Hemisphere atmospheric blocking as simulated by 15 atmospheric general circulation models in the period 1979–1988, Climate Dynam., 14, 385–407, 1998.

Fetterer, F., Knowles, K., Meier, W., and Savoie, M.: Sea Ice Index. Boulder, CO: National Snow and Ice Data Center, Digital media, 2009.

Flanner, M. G. and Zender, C. S.: Linking snowpack microphysics and albedo evolution, J. Geophys. Res., 111, D12208, doi:10.1029/2005JD006834, 2006.

Furevik, T., Bentsen, M., Drange, H., Kindem, I. K. T., Kvamstø, N. G., and Sorteberg, A.: Description and evaluation of the bergen climate model: ARPEGE coupled with MICOM, Clim. Dynam., 21, 27–51, doi10.1007/s00382-003-0317-5, 2003.

Gent, P. R., Danabasoglu, G., Donner, L. J., Holland, M. M., Hunke, E. C., Jayne, S. R., Lawrence, D. M., Neale, R. B., Rasch, P. J., Vertenstein, M., Worley, P. H., Yang, Z.-L., and Zhang, M.: The Community Climate System Model Version 4. J. Climate, 24, 4973–4991, doi:10.1175/2011JCLI4083.1, 2011.

Gettelman, A., Kay, J. E., and Shell, K. M.: The Evolution of Climate Sensitivity and Climate Feedbacks in the Community Atmosphere Model, J. Climate, 25, 1453–1469, doi:10.1175/JCLI-D-11-00197.1, 2012.

Ghil M., Allen, R. M., Dettinger, M. D., Ide, K., Kondrashov, D., Mann, M. E., Robertson, A., Saunders, A., Tian, Y., Varadi, F., and Yiou, P.: Advanced spectral methods for climatic time series, Rev. Geophys., 40, 3.1–3.41, doi:10.1029/2000RG000092, 2002.

Gimeno, L., Nieto, R., Drumond, A., Durán-Quesada, A. M., Stohl, A., Sodemann, H., and Trigo, R. M.: A Close Look at Oceanic Sources of Continental Precipitation, Eos Transactions AGU, 92, 193–195, 2011.

Giorgi, F., Im, E.-S., Coppola, E., Diffenbaugh, N. S., Gao, X . J., Mariotti, L., and Shi, Y.: Higher Hydroclimatic Intensity with Global Warming, J. Climate, 24, 5309–5324, doi:10.1175/2011JCLI3979.1, 2011.

Gregory, J. M., Ingram, W. J., Palmer, M. A., Jones, G. S., Stott, P. A., Thorpe, R. B., Lowe, J. A., Johns, T. C., and Williams, K. D.: A new method for diagnosing radiative forcing and climate sensitivity, Geophys. Res. Lett., 31, L03205, doi:10.1029/2003GL018747, 2004.

Guilyardi, E., Bellenger, H., Collins, M., Ferrett, S., Cai, W., and Wittenberg, A.: A first look at ENSO in CMIP5, CLIVAR Exchanges No. 58, 17, 29–32, available at: http://www.gfdl.noaa.gov/~atw/yr/2012/guilyardi_etal_2012_clivex.pdf last access: February 2012, 2012.

Hannachi, A., Jolliffe, I. T., and Stephenson, D. B.: Empirical orthogonal functions and related techniques in atmospheric science: A review, Internat. J. Clim., 27, 1119–1152, 2007.

Hofmann, M. and Rahmstorf, S.: On the stability of the Atlantic meridional overturning circulation, P. Natl. Acad. Sci. USA, 106, 20584–20589, 2009.

Hoose, C., Kristjánsson, J. E., Iversen, T., Kirkevåg, A., Seland, Ø., and Gettelman, A.: Constraining cloud droplet number concentration in GCMs suppresses the aerosol indirect effect, Geophys. Res. Lett., 36, L12807, doi:10.1029/2009GL038568, 2009.

Houghton, J. T., Ding, Y., Griggs, D. J., Noguer, M., van der Linden, P. J., Dai, X., Maskell, K., and Johnson, C. A.: Climate Change 2001: The Scientific Basis. Contribution of Working Group I to the Third Assessment Report of the Intergovernmental Panel on Climate Change. Cambridge University Press. 881 pp. 2001.

Hurrell, J. W., Hack, J. J., Phillips, A. S., Caron, J., and Yin, J.: The Dynamical Simulation of the Community Atmosphere Model Version 3 (CAM3), J. Climate, 19, 2162–2183, 2006.

Iversen, T. and Seland, Ø.: A scheme for process-tagged SO_4 and BC aerosols in NCAR-CCM3: Validation and sensitivity to cloud processes, J. Geophys. Res., 107, 4751, doi:10.1029/2001JD000885, 2002.

Iversen, T. and Seland, Ø.: Correction to "A scheme for process-tagged SO4 and BC aerosols in NCAR-CCM3. Validation and sensitivity to cloud processes", J. Geophys. Res., 108, 4502, doi:10.1029/2003JD003840, 2003.

Iversen, T., Kristiansen, J., Jung, T., and Barkmeijer, J.: Optimal atmospheric forcing perturbations for the cold-ocean warm-land pattern, Tellus A, 60, 528–546, doi:10.1111/j.1600-0870.2008.00310.x, 2008.

Jiang, J. H., Su, H., Zhai, C., Perun, V., Del Genio, A. D., Nazarenko, L. S., Donner, L. J., Horowitz, L. W., Seman, C. J., Cole, J., Gettelman, A., Ringer, M. A., Rotstayn, L. D., Jeffrey, S. J., Wu, T., Brient, F., Dufresne, J.-L., Kawai, H., Koshiro, T., Masahiro, W., L'Écuyer, T. S., Volodin, E. M., Iversen, T., Drange, H., dos Santos Mesquita, M., Read, W. G., Waters, J. W., Tian, B., Teixeira, J., and Stephens, G. L.: Evaluation of cloud and water vapor simulations in CMIP5 climate models using NASA "A-Train" satellite observations, J. Geophys. Res., 117, D14105, doi:10.1029/2011JD017237, 2012.

Jung, T., Miller, M. J., Palmer, T. N., Towers, P., Wedi, N., Achuthavarier, D., Adams, J. M., Altshuler, E. L., Cash, B. A., Kinter III, J. L., Marx, L., Stan, C., and Hodges, K. I.: High-Resolution Global Climate Simulations with the ECMWF Model in Project Athena: Experimental Design, Model Climate, and Seasonal Forecast Skill, J. Climate, 25, 3155–3172, doi:10.1175/JCLI-D-11-00265.1, 2012.

Kalnay, E., Kanamitsu, M., Kistler, R., Collins, W., Deaven, D., Gandin, L., Iredell, M., Saha, S., White, G., Woollen, J., Zhu, Y., Leetmaa, A., Reynolds, R., Chelliah, M., Ebisuzaki, W., Higgins, W., Janowiak, J., Mo, K. C., Ropelewski, C., Wang, J., Jenne, R., and Joseph, D.: The NCEP/NCAR 40-Year Reanalysis Project, B. Am. Meteorol. Soc., 77 437–471, 1996.

Kay, J. E., Holland, M. M., Bitz, C. M., Blanchard-Wrigglesworth, E., Gettelman, A., Conley, A., and Bailey, D.: The influence of local feedbacks and northward heat transport on the equilibrium Arctic climate response to increased greenhouse gas forcing, J. Climate, 25, 5433–5450, doi:10.1175/JCLI-D-11-00622.1, 2012.

Kim, S. T. and Yu, J.-Y.: The Two Types of ENSO in CMIP5 Models, Geophys. Res. Lett., 39, L11704, doi:10.1029/2012GL052006, 2012.

Kirkevåg, A. and Iversen, T.: Global direct radiative forcing by process-parameterized aerosol optical properties, J. Geophys. Res., 107, 4433, doi:10.1029/2001JD000886, 2002.

Kirkevåg, A., Iversen, T., Seland, Ø., Debernard, J. B., Storelvmo, T., and Kristjánsson, J. E.: Aerosol-cloud-climate interactions in the climate model CAM-Oslo, Tellus A, 60, 492–512, doi:10.1111/j.1600-0870.2008.00313.x, 2008a.

Kirkevåg, A., Iversen, T., Kristjánsson, J. E., Seland, Ø., and Debernard, J. B.: On the additivity of climate response to anthropogenic aerosols and CO2, and the enhancement of future global warming by carbonaceous aerosols, Tellus A, 60, 513–527, doi:10.1111/j.1600-0870.2008.00308.x, 2008b.

Kirkevåg, A., Iversen, T., Seland, Ø., Hoose, C., Kristjánsson, J. E., Struthers, H., Ekman, A. M. L., Ghan, S., Griesfeller, J., Nilsson, E. D., and Schulz, M.: Aerosol-climate interactions in the Norwegian Earth System Model – NorESM1-M, Geosci. Model Dev., 6, 207–244, doi:10.5194/gmd-6-207-2013, 2013.

Kristjánsson, J. E.: Studies of the aerosol indirect effect from sulphate and black carbon aerosols, J. Geophys. Res., 107, 4246, doi:10.1029/2001JD000887, 2002.

Kristjánsson, J. E., Iversen, T., Kirkevåg, A., Seland, Ø., and Debernard, J.: Response of the climate system to aerosol direct and indirect forcing: Role of cloud feedbacks, J. Geophys. Res., 110, D24206, doi:10.1029/2005JD006299, 2005.

Lamarque, J.-F., Bond, T. C., Eyring, V., Granier, C., Heil, A., Klimont, Z., Lee, D., Liousse, C., Mieville, A., Owen, B., Schultz, M. G., Shindell, D., Smith, S. J., Stehfest, E., Van Aardenne, J., Cooper, O. R., Kainuma, M., Mahowald, N., McConnell, J. R., Naik, V., Riahi, K., and van Vuuren, D. P.: Historical (1850–2000) gridded anthropogenic and biomass burning emissions of reactive gases and aerosols: methodology and application, Atmos. Chem. Phys., 10, 7017–7039, doi:10.5194/acp-10-7017-2010, 2010.

Lean, J., Rottman, G., Harder, J., and Kopp, G.: SORCE contributions to new understanding of global change and solar variability, Sol. Phys., 230, 27–53, 2005.

Lejanäs, H. and Økland, H.: Characteristics of Northern Hemisphere blocking as determined from a long series of observational data, Tellus A, 35, 350–362, 1983.

Matsueda, M., Mizuta, R., and Kusunoki, S.: Future change in wintertime atmospheric blocking simulated using a 20-km-mesh atmospheric global circulation model, J. Geophys. Res., 114, D12114, doi:10.1029/2009JD011919, 2009.

Medhaug, I. and Furevik, T.: North Atlantic 20th century multidecadal variability in coupled climate models: sea surface temperature and ocean overturning circulation, Ocean Sci., 7, 389–404, doi:10.5194/os-7-389-2011, 2011.

Meehl, G. A., Covey, C., McAvaney, B., Latif, M., and Stouffer, R. J.: Overview of the coupled model intercomparison project, B. Am. Meteorol. Soc., 86, 89–93, doi:10.1175/BAMS-86-1-89, 2005.

Meehl, G. A., Washington, W. M., Arblaster, J. M., Hu, A., Teng, H., Tebaldi, C., Sanderson, B., Lamarque, J.-F., Conley, A., Strand, W. G., and White III, J. B.: Climate System Response to External Forcings and Climate Change Projections in CCSM4, J. Climate, 25, 3661–3683, doi:10.1175/JCLI-D-11-00240.1, 2012.

Molteni, F., Kucharski, F., and Corti, S.: On the predictability of flow-regime properties on interannual to interdecadal timescales, in: Predictability of Weather and Climate, edited by: Palmer, T. and Hagedorn, R., Cambridge University Press, 365–389, 2006.

Monahan, A. H., Fyfe, J. C., Ambaum, M. H. P., Stephenson, D. B., and North, G. R.: Empirical orthogonal functions: the medium is the message, J. Climate, 22, 6501–6514, 2009.

Munk, W. and Wunsch, C.: Abyssal recipes II: energetics of tidal and wind mixing, Deep-Sea Res. I, 45, 1977–2010, 1998.

Murphy, D. M.: Transient response of the Hadley Centre coupled ocean-atmosphere model to increasing carbon dioxide: Part III. Analysis of global-mean response using simple models, J. Climate, 8, 495–514, doi:10.1175/1520-0442(1995)008¡0496:TROTHC¿2.0.CO;2, 1995.

Myhre, G., Samset, B. H., Schulz, M., Balkanski, Y., Bauer, S., Berntsen, T. K., Bian, H., Bellouin, N., Chin, M., Diehl, T., Easter, R. C., Feichter, J., Ghan, S. J., Hauglustaine, D., Iversen, T., Kinne, S., Kirkevåg, A., Lamarque, J.-F., Lin, G., Liu, X., Lund, M. T., Luo, G., Ma, X., van Noije, T., Penner, J. E., Rasch, P. J., Ruiz, A., Seland, Ø., Skeie, R. B., Stier, P., Takemura, T., Tsigaridis, K., Wang, P., Wang, Z., Xu, L., Yu, H., Yu, F., Yoon, J.-H., Zhang, K., Zhang, H., and Zhou, C.: Radiative forcing of the direct aerosol effect from AeroCom Phase II simulations, Atmos. Chem. Phys., 13, 1853–1877, doi:10.5194/acp-13-1853-2013, 2013. .

Neale, R. B., Richter, J. H., and Jochum, M.: The impact of convection on ENSO: From a delayed oscillator to a series of events, J. Climate, 21, 5904–5924, 2008.

Neale, R. B, Richter, J. H., Conley, A. J., Park, S., Lauritzen, P. H., Gettelman, A., Williamson, D. L., Rasch, P. J., Vavrus, S. J., Taylor, M. A., Collins, W. D., Zhang, M., and Lin, S.-J.: Description of the NCAR Community Atmosphere Model (CAM 4.0), NCAR Technical Note, NCAR/TN-485+STR, April 2010.

Neale, R. B., Richter, J. H., Park, S., Lauritzen, P. H., Vavrus, S. J., Rasch, P. J., and Zhang, M.: The mean climate of the Community Atmosphere Model (CAM4) in forced SST and fully coupled experiments, J. Climate, submitted, 2012.

Otterå, O. H., Bentsen, M., Bethke, I., and Kvamstø, N. G.: Simulated pre-industrial climate in Bergen Climate Model (version 2): model description and large-scale circulation features, Geosci. Model Dev. Discuss., 2, 507–549, doi:10.5194/gmdd-2-507-2009, 2009.

Otterå, O. H., Bentsen, M., Drange, H., and Suo, L.: External focing as a metronome for Atlantic multidecadal variability, Nat. Geosci., 3, 688–694, doi:10.1038/NGEO955, 2010.

Palmer, T. N.: A nonlinear dynamical perspective on climate prediction, J. Climate, 12, 575–591, doi:10.1175/1520-0442(1999)012¡0575:ANDPOC¿2.0.CO;2, 1999.

Pelly, J. L. and Hoskins, B. J.: A new perspective on blocking, J. Atmos. Sci., 60, 743–755, 2003.

Rasch, P. J. and Kristjánsson, J. E.: A comparison of the CCM3 model climate using diagnosed and predicted condensate parameterisations, J. Climate, 11, 1587–1614, 1998.

Rasch, P. J., Coleman, D. B., Mahowald, N., Williamson, D. L., Lin, S.-J., Boville, B. A., and Hess, P.: Characteristics of atmospheric transport using three numerical formulations for atmospheric dynamics in a single GCM framework, J. Climate, 19, 2243–2266, 2006.

Rayner, N. A., Parker, D. E., Horton, E. B., Folland, C. K., Alexander, L. V., Rowell, D. P., Kent, E. C., and Kaplan, A.: Global analyses of sea surface temperature, sea ice, and night marine air temperature since the late nineteenth century, J. Geophys. Res., 108, 4407, doi:10.1029/2002JD002670, 2003.

Richter, J. H. and Rasch, P. J.: Effects of convective momentum transport on the atmospheric circulation in the Community Atmosphere Model, version 3, J. Climate, 21, 1487–1499, 2008.

Rotstayn, L. D. and Lohmann, U.: Tropical rainfall trends and the indirect aerosol effect, J. Climate, 15, 2103–2116, 2002.

Samset, B. H., Myhre, G., Schulz, M., Balkanski, Y., Bauer, S., Berntsen, T. K., Bian, H., Bellouin, N., Diehl, T., Easter, R. C., Ghan, S. J., Iversen, T., Kinne, S., Kirkevåg, A., Lamarque, J.-F., Lin, G., Liu, X., Penner, J. E., Seland, Ø., Skeie, R. B., Stier, P., Takemura, T., Tsigaridis, K., and Zhang, K.: Black carbon vertical profiles strongly affect its radiative forcing uncertainty, Atmos. Chem. Phys., 13, 2423–2434, doi:10.5194/acp-13-2423-2013, 2013.

Scaife, A. A., Copsey, D., Gordon, C., Harris, C., Hinton, T., Keeley, S., O'Neill, A., Roberts, M., and Williams, K.: Improved Atlantic winter blocking in a climate model, Geophys. Res. Lett., 38, L23703, doi:10.1029/2011GL049573, 2011.

Schneider, B., Latif, M., and Schmittner, A.: Evaluation of Different Methods to Assess Model Projections of the Future Evolution of the Atlantic Meridional Overturning Circulation, J. Climate, 20, 2121–2132, 2007.

Seland, Ø., Iversen, T., Kirkevåg, A., and Storelvmo, T.: Aerosol-climate interactions in the CAM-Oslo atmospheric GCM and investigations of associated shortcomings, Tellus A, 60, 459-491, 2008.

Senior, C. A. and Mitchell, J. F. B.: The time-dependence of climate sensitivity, Geophys. Res. Lett., 27, 2685–2688, doi:10.1029/2000GL011373, 2000.

Stephenson, D. B., Hannachi, A., and O'Neill, A.: On the existence of multiple climate regimes, Q. J. Roy. Meteor. Soc., 130, 583–605, 2004.

Stohl, A., Forster, C., and Sodemann, H.: Remote sources of water vapor forming precipitation on the Norwegian west coast at 60° N: A tale of hurricanes and an atmospheric river, J. Geophys. Res., 113, D05102, doi:10.1029/2007JD009006, 2008.

Storelvmo, T., Kristjánsson, J. E., Ghan, S., Kirkevåg, A., Seland, Ø., and Iversen, T.: Predicting cloud droplet number in CAM-Oslo, J. Geophys. Res., 111, D24208, doi:10.1029/2005JD006300, 2006.

Straus, D. M. and Shukla, J.: Does ENSO force the PNA?, J. Climate, 15, 2340–2358, 2002.

Struthers, H., Ekman, A. M. L., Glantz, P., Iversen, T., Kirkevåg, A., Mårtensson, E. M., Seland, Ø., and Nilsson, E. D.: The effect of sea ice loss on sea salt aerosol concentrations and the radiative balance in the Arctic, Atmos. Chem. Phys., 11, 3459–3477, doi:10.5194/acp-11-3459-2011, 2011.

Struthers, H., Ekman, A. M. L., Glantz, P., Iversen, T., Kirkevåg, A., Seland, Ø., Mårtensson, E. M., Noone, K., and Nilsson, E. D.: Climate-induced changes in sea salt aerosol number emissions: 1870 to 2100, J. Geophys. Res., 118, 670–682, doi:10.1002/jgrd.50129, 2013.

Subramanian, A. C., Jochum, M., Miller, A. J., Murtugudde, R., Neale, R. B., and Waliser, D. E.: The Madden Julian Oscillation in CCSM4, J. Climate, 24, 6261–6282, doi:10.1175/JCLI-D-11-00031.1, 2011.

Taylor, K. E., Stouffer, R. J., and Meehl, G. A.: An overview of CMIP5 and the experiment design, B. Am. Meteorol. Soc., 90, 485–498, doi:10.1175/BAMS-D-11-00094.1, 2012.

Thompson, D. W. J. and Wallace, J. M.: Annular modes in the extratropical circulation, Part I: month-to-month variability, J. Climate, 13, 1000–1016, 2000.

Tibaldi, S. and Molteni, F.: On the operational predictability of blocking, Tellus A, 42, 343–365, 1990.

Tjiputra, J. F., Roelandt, C., Bentsen, M., Lawrence, D. M., Lorentzen, T., Schwinger, J., Seland, Ø., and Heinze, C.: Evaluation of the carbon cycle components in the Norwegian Earth System Model (NorESM), Geosci. Model Dev., in press, 2013.

Trenberth, K. E.: The definition of El Niño, B. Am. Meteorol. Soc., 78, 2771–2777, 1997.

Trenberth, K. E.: Changes in precipitation with climate change, Climate Res., 47, 123–138, doi:10.3354/cr00953, 2011.

Trenberth, K. E. and Shea, D. J.: On the evolution of the Southern Oscillation, Mon. Weather Rev., 115, 3078–3096, 1987.

Trenberth, K. E., Branstator, G. W., Karoly, D., Kumar, A., Lau, N.-C., and Ropelewski, C.: Progress during TOGA in understanding and modeling global teleconnections associated with tropical sea surface temperatures, J. Geophys. Res., 103, 14291–14324, doi:10.1029/97JC01444, 1998.

Trenberth, K. E., Dai, A., Rasmussen, R. M., and Parsons, D. B.: The changing character of precipitation, B. Am. Meteorol. Soc., 84, 1205–1217, 2003.

Trenberth, K. E., Jones, P. D., Ambenje, P., Bojariu, R., Easterling, D., Klein Tank, A., Parker, D., Rahimzadeh, F., Renwick, J. A., Rusticucci, M., Soden, B., and Zhai, P.: Observations: surface and atmospheric climate change, in: Climate Change 2007: The Physical Science Basis, Intergovernmental Panel on Climate Change 4th Assessment Report, edited by: Solomon, S., Qin, D., Manning, M., Chen, Z., Marquis, M., Averyt, K. B., Tignor, M., and Miller, H. L., Cambridge University Press, Cambridge, 235–336, 2007.

Trenberth, K. E., Fasullo, J. T., and Mackaro, J.: Atmospheric Moisture Transports from Ocean to Land and Global Energy Flows in Reanalyses, J. Climate, 24, 4907–4924, doi:10.1175/2011JCLI4171.1, 2011.

Uppala, S. M., Kallberg, P. W., Simmons, A. J., Andrae, U., Bechtold, V. D., Fiorino, M., Gibson, J. K., Haseler, J., Hernandez, A., Kelly, G. A., Li, X., Onogi, K., Saarinen, S., Sokka, N., Allan, R. P., Andersson, E., Arpe, K., Balmaseda, M. A., Beljaars, A. C. M., Van De Berg, L., Bidlot, J., Bormann, N., Caires, S., Chevallier, F., Dethof, A., Dragosavac, M., Fisher, M., Fuentes, M., Hagemann, S., Holm, E., Hoskins, B. J., Isaksen, L., Janssen, P. A. E. M., Jenne, R., McNally, A. P., Mahfouf, J. F., Morcrette, J. J., Rayner, N. A., Saunders, R. W., Simon, P., Sterl, A., Trenberth, K. E., Untch, A., Vasiljevic, D., Viterbo, P., and Woollen, J. T.: The ERA-40 re-analysis, Q. J. Roy. Meteorol. Soc., 131, 2961–3012, 2005.

Yin, J. H.: A consistent poleward shift of the storm tracks in simulations of 21st century climate, Geophys. Res. Lett., 32, L18701, doi:10.1029/2005GL023684, 2005.

van Vuuren, D. P., Edmonds, J., Kainuma, M., Riahi, K., Thomson, A., Hibbard, K., Hurtt, G. C., Kram, T., Krey, V., Lamarque, J.-F., Masui, T., Meinshausen, M., Nakicenovic, N., Smith, S. J., and Rose, S. K.: The representative concentration pathways: an overview, Climatic Change, 109, 5–31, doi:10.1007/s10584-011-0148-z, 2011.

Wallace, J. M. and Gutzler, D. S.: Teleconnections in the geopotential height field during the Northern Hemisphere winter, Mon. Weather Rev., 109, 784–812, 1981.

Wallace, J. M., Zhang, Y., and Bajuk, L.: Interpretation of interdecadal trends in Northern Hemispheric surface air temperature, J. Climate, 9, 249–259, 1996.

Wang, B.: Interdecadal changes in El Nino onset in the last four decades, J. Climate, 8, 267–285. 1995.

Wang, Y.-M., Lean, J. L., and Sheeley Jr., N. R.: Modeling the Sun's magnetic field and irradiance since 1713, Astrophys. J., 625, 522–538. 2005.

Zhang, G. J. and McFarlane, N. A.: Sensitivity of climate simulations to the parameterisation of cumulus convection in the Canadian Climate Centre general circulation model, Atmos. Ocean., 33, 407–446, 1995.

IV